NTNU – Trondheim
Norwegian University of
Science and Technology

A Comparative Study of Control Structures Applied in Gas Lift Systems to Prevent Casing Heading

Henrik Hjelseth Hansen

Master of Science in Engineering Cybernetics
Submission date: June 2012
Supervisor: Morten Hovd, ITK
Co-supervisor: Sigurd Skogestad, IKP

Norwegian University of Science and Technology
Department of Engineering Cybernetics

Problem Description

The severe slugging multiphase flow regime, that occurs during the casing heading instability in gas lift systems, is undesired as it may be damaging to the equipment and reduces the average production rate. Automatic control is a possible solution to prevent the instability and to optimize the production. It has been successfully applied, with different control structures, both in research and on full scale tests. A mathematical comparison to investigate which control structure that is most suited for disturbance rejection and stabilization of the casing heading was initiated in the project fall assignment. The goal for this thesis is to complete that work through the following objectives:

Objectives

- Complete the development of the low order gas lift model. The model should be able to sufficiently reproduce the system behavior during the casing heading phenomenon.
- Learn how to use the advanced OLGA flow simulator and the OLGA gas lift case. The OLGA simulator should be regarded as the real flow process in this assignment.
- Compare and adjust the low order model to fit the response of the OLGA flow simulator.
- Perform an controllability analysis on the fitted low order model. The result of the analysis should reveal the most promising control structures.
- Implement and test the most promising control structures in a simulation study. Simulations should be performed on both the low order model and on the OLGA simulator. Evaluate the robustness of the controllers against non-linearity and uncertainty.
- Establish communication between the OLGA flow simulator and MATLAB. This connection should be used to test controllers developed in Matlab on the OLGA simulator.

Preface

This master thesis was written during the spring of 2012 as a part of the study program leading to a M.Sc. in Engineering Cybernetics at the Norwegian University of Science and Technology (NTNU). It is a continuation of my project work in the fall of 2011 on modeling and stabilizing the casing heading instability phenomenon that may occur during gas lift operations. The project made the basic work on developing a new low order nonlinear mathematical model for describing the flow in a riser consisting of an annulus and tubing, which is a normal setup in gas lift systems. A controllability analysis of the new model, the version of the model at this point, was also conducted to investigate the possible control structures which can be used in automatic control of the system. With the knowledge acquired from the project assignment, the main objective for this thesis has been to further develop the low order model, and to implement, test and compare different controllers and control configurations to prevent the casing heading instability. Further the robustness properties of the controllers are evaluated as they are also tested on the advanced OLGA flow simulator.

This thesis has provided me with a deeper understanding of some of the relevant flow assurance problems that are focused on in the oil industry today. I have had great benefits of learning from these problems and I am sure this experience will be useful in future work.

I would like to thank my supervisors for this project: Professor *Sigurd Skogestad* at the Process System Engineering group. He has been helpful and positive trough the whole project. I would also like to thank my co- supervisor Ph.D. student *Esmaeil Jahanshahi*, for his continuous support and help. Esmaeil is very enthusiastic about his work and since we have been working closely together during this project he has been a real motivation for me to perform at my utmost. I would also like to thank my co-supervisor Professor *Morten Hovd* at the Department of Engineering Cybernetics. Morten was kind to evaluate results and discuss the use of an estimator, an unscented Kalman filter, which is presented later in this thesis. Further I would like to thank Professor *Bjarne Foss* at the Department of Engineering Cybernetics for helpful feedback on the estimator. I have also been in contact with the Statoil research center at Rotvoll. At Statoil I would like to thank *Gisle Otto Eikrem* and *John-Morten Godhavn* for meeting with me to discuss some of the challenges that they are working on today. It was also very helpful that Gisle provided me with an OLGA gas lift case model, which contained realistic parameter values to be used in a gas-lift system. This was much appreciated. At last I would like to thank my fellow students at NTNU for a good supportive working environment, my family for their continuous support and *Adele* for her patience during my work.

Henrik Hjelseth Hansen
Trondheim, June 2012.

Abstract

Gas lift is an artificial lift technique which is intended to be used in oil and gas production systems to enhance the oil recovery rate. The technique is used in production systems which suffers from insufficient production rates because of inadequate reservoir pressure. The principle is to inject extra gas, from an external source, into the fluid mixture flowing out of the reservoir. This reduces the weight of the fluid column, which in turn enables the reservoir pressure to lift the mixture of fluids up to the surface. Thus, the restriction in production rate, resulting from insufficient reservoir pressure, is resolved.

The casing heading instability cycle is a phenomenon which may occur in such gas lift systems at certain pressure and flow conditions. In such a case, a blocking constraint leads to an accumulation of gas that is building up a high pressure in the container storing the extra gas. Eventually the pressure is able to overcome the blocking constraint which further leads to a production flow blow out at the surface. This process repeats itself over a period of several hours. The resulting flow regime may be damaging to the receiving surface equipment. It also leads to a decrease in the average production rate, which is highly undesirable.

In this thesis a new low order mathematical model to describe the casing heading instability is presented. The model is further compared and fitted to a gas lift case implemented in the advanced OLGA flow simulator, which is regarded as the real flow process in this thesis. A controllability analysis is performed on the newly fitted model, and the results of the analysis are used to investigate which control structures that seems reasonable for stabilizing the casing heading instability. The most promising control strategies are further tested in simulations, both on the low order model and on the advanced flow simulator. The results from the analysis, which is further confirmed in simulations, show that out of the measurement candidates that were considered in this thesis, the bottom hole pressure, i.e., the pressure measured in the well or near the depth of the producing formation, is the single best measurement to use for both disturbance rejection and stabilization of the system. However, this measurement is known to be unreliable, if at all available, because of its location in a harsh environment. Another control structure which showed promising results both in analysis and simulations is therefore concluded as the better choice. This is a cascaded control structure, which only relies on realistically available top side pressure measurements. It proved successful in stabilizing the system.

Sammendrag

Gass løft er en kunstig løfte metode som kan brukes i olje og gass produksjonssystemer for å øke produksjonsraten. Teknikken brukes gjerne i produksjonssystemer som lider av lave produksjonsrater som resultat av utilstrekkelig trykk i reservoaret. Prinsippet går ut på å injisere ekstra gass, fra en ekstern kilde, inn i fluidblandingen som flyter ut av reservoaret. På den måten vil vekten av fluidkolonnen som reservoartrykket skal løfte opp til overflaten reduseres. Ved å injisere nok gass vil den gjennomsnittlig vekten av fluidblandingen reduseres til et punkt der reservoartrykket igjen er tilstrekkelig til å løfte fluidene opp til overflaten. Dermed er restriksjonen i produksjonraten, som konsekvens av utilstrekkelig reservoartrykk, løst.

Casing heading ustabilitet syklusen er et fenomen som kan oppstå i slike gas løft systemer under visse trykk og flytbetingelser. I et slikt tilfelle, vil en trykkrestriksjon føre til at flyten fra annulus til tubing blir stoppet opp. Videre bygges det da opp et høyt trykk i annulus ettersom at gass akkumuleres i dette volumet. Når trykket på et tidspunkt blir høyt nok til å overkomme trykkrestriksjon som blokkerer flyten, så vil det resultere i en utblåsning av olje og gass på overflaten, ettersom at et stort volum av gass flyter fra annulus inn i tubingen og løfter ut hele fluidblandingen. Denne prosessen kan repetere seg selv med en periodetid på flere timer. Det resulterende flytregimet kan virke ødeleggende på utstyret som befinner seg på overflaten. Videre fører det også til en redusert gjennomsnittlig produksjonsflyt, som er svært lite ønskelig.

I denne oppgaven blir det presentert en ny lavordens matematisk modell for å beskrive denne ustabiliteten. Modellen blir så sammenliknet og tilpasset til en gass løft case som er implementert i den mer avanserte OLGA flytsimulatoren, som anses for å være den virkelige flytprosessen i denne oppgaven. En kontrollabilitetsanalyse blir videre utført på den nye lav-ordensmodellen. Resultatene av analysen blir brukt til å undersøke hvilke målinger som passer seg best i en kontrollstruktur som kan brukes til å stabilisere systemet. De mest lovende resultatene fra analysen blir videre testet gjennom simulering av både den nye modellen, samt i OLGA flytsimulatoren.

Resultatene fra analysen, som ble videre bekreftet gjennom simuleringer, viser at ved bruk av en enkelt måling i en kontrolstruktur, er det trykket i bunnen av tubingen, nært reservoaret, som er den beste kandidaten for stabilisering av systemet. Imidlertid er det kjent at denne målingen er usikker, om i det hele tatt tilgjengelig, ettersom den befinner seg i et tøft miljø med høyt trykk og temperatur. En annen kontrollstruktur som også viste seg lovende i både analysen og gjennom simuleringer, er en kaskadestruktur av tilgjengelige topptrykkene i annulus og tubing. Dette oppsettet klarte både å stabilisere systemet og motvirke forstyrrelser. Det konkluderes derfor med å anbefale denne kontrollstrukturen, med mindre en har bunntrykket tilgjengelig.

Contents

List of Figures

List of Tables

List of Abbreviations

SISO:	Single Input Single Output
SIMO:	Single Input Multiple Output
MIMO:	Multiple Input Multiple Output
UKF:	Unscented Kalman Filter
EKF:	Extended Kalman Filter
CV:	Controlled Variable
MV:	Manipulated Variable
LQR:	Linear Quadratic Regulator
LQG:	Linear Quadratic Gaussian control
PI:	*Proportional Integral*
PID:	*Proportional Integral Derivative*

Chapter 1

Introduction

The following chapter is inspired by my previous work with gas lift systems, conducted during my project assignment in the fall of 2011 at NTNU, which is presented in [1].

1.1 Motivation

The dependency of energy for today's society to function as normal is absolute. Availability of energy is so hardwired into our everyday living that it seems impossible to imagine how the world would evolve without it. As the human population is increasing rapidly, so is the energy demand. It is expected to be an 1.9% annual increase in the worlds total energy demand up to the year 2030, and the majority of that demand, about 90%, is anticipated to be met by hydrocarbons, which is found naturally in crude oil[1]. Unfortunately our oil reserves are limited, and the methods used to recover oil from the reservoirs we do have, are not optimal. This may result in large portions of reservoirs that is left untapped, as it is not economically profitable to produce the leftover oil from the reservoir. The importance of optimizing reservoir production and enhancing oil recovery to fully utilize our every oil reservoir is evident. Thus, we need to ensure that research continue to emphasize on reducing the risk and lowering the costs that is associated with hydrocarbon recovery.

One class of methods that is developed to enhance oil recovery from reservoirs is called artificial lift techniques. In reservoirs which have inadequate pressure to push the oil up to the surface on its own, these techniques are essential for extending the lifetime of the oil well and boosting oil production rates, thereby increasing the utilization of the reservoirs. These techniques are used on more than 90% of the approximately one million currently producing oil wells in the world today, [2]. There are four different artificial lift methods which are used in the oil industry: road pumping, electric submersible pumping, subsurface hydraulic pumping and gas-lift, [3]. Out of these four techniques, gas-lift is the most economic and widely used lift technique for mature offshore oil wells. It is currently being used on approximately 30 thousand wells today, [2]. This is mainly because of its minimal use of surface well equipment, justified by the fact that the gas that is used in the lift process usually is available from high-pressure gas wells or a compression system

[1] Data taken from [2]

already accessible on location, [3]. The gas-lift technique is explained in detail in section (1.2).

Even though gas-lift has the advantageous that it may boost production and help to retrieve more of the resources in the reservoirs, it may unfortunately also make the system unstable under certain pressure and flow conditions. One of the instabilities that may occur in gas-lift systems is called the casing heading instability, and this is the focus of this report. The resulting unstable multiphase flow regime is called slug flow, or severe slugging, and will be further explained in section (2.2), and is depicted in figure (2.2.2). This flow regime lowers the average oil production rates and may be damaging to the upstream receiving facilities. This is elaborated in section (2.6.2).

Needles to say, in the oil and gas industry, a major concern is to stabilize the transportation of oil and gas in pipelines, at operating points which optimizes production. The mixture of oil and gas flowing through the pipes is called multiphase flow, as it consists of several phases. In this project only two phases are considered, which is gas and liquid. Stabilizing this multiphase flow in the pipe, and ensuring that the fluids flows as intended, is referred to as flow assurance. There is rapid development in the field of flow assurance and the discipline is progressing fast [4].

1.2 Explanation of The Gas Lift Technique

The extraction rate of oil from an offshore well is dependent on the pressure in the reservoir. The reservoir pressure can be considered as the driving force of the system, as it is the force which pushes the oil up through the pipeline. Higher pressure leads to higher production rates. During the lifetime of an oil well the reservoir pressure will decrease as the well matures and fluids are extracted from the reservoir. When the reservoir pressure is decreased below a certain point, the well will no longer be able to produce oil on its own. The gas lift technique may then be used to inject extra gas into the pipeline to reduce the average density of the fluid mixture. This will reduce the average weight of the fluids, thus enabling the reservoir pressure to once again push the oil up the pipe. How this process works will now be explained in detail.

A reservoir is a subsurface body of rock which, because of sufficient porosity and permeability, is able to store and transmit fluids, [5]. The reservoir pressure, also referred to as the formation pressure, is the result of the natural forces that surround and trap the fluids within the pores of the reservoir. It is these forces which prevents the fluids from escaping. More information on reservoirs can be found in [6]. When a well, i.e., a hole, is drilled into a reservoir, the fluids are presented with a flow path through which they may escape. Provided that there is a positive pressure drop from the reservoir in the bottom to the receiving end at the top, the fluids will start to flow into pipeline, up the tubing, through the production choke and finally arrive at the receiving facilities, which is usually a separator. See figure (1.2.1), which is a modification of the figure presented in [7]. This means that to be able to produce oil, the pressure in the reservoir has to overcome the back pressure from both the fluid column in the tubing and the surface facilities. If, however, the reservoir pressure is too low, the oil will not be able to flow up the tubing, so the system can not produce oil on its own. Applying gas lift to the system however, may change the situation.

Figure 1.2.1: The Gas Lift Riser Model

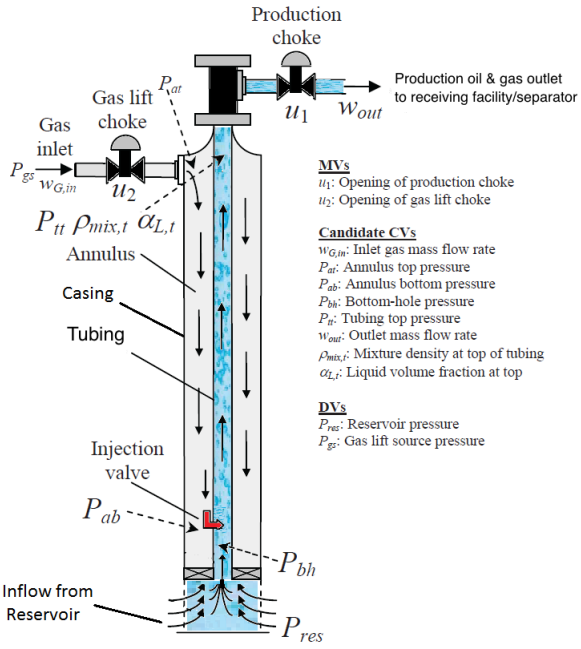

Introducing gas lift to a system is done by providing an extra gas source from which lift-gas can be injected. The lift-gas is routed from the new gas source at the surface, through a container, usually an annulus around the tubing in the riser, and into to tubing, preferably near the bottom, again see figure (1.2.1). The supplied lift-gas will infiltrate the fluid in the tubing and consequently reduce the average density of the fluid mixture. Reduction of the mixture density causes the weight of the fluid column in the tubing to decrease, which in turn decreases the pressure which the reservoir has to overcome for the system to produce oil. By injecting a sufficient amount of lift-gas, the weight of the mixture in the tubing will be reduced to the point where it is possible for the formation pressure to lift the column of fluids. The system is then able to produce oil. Gas lift is therefore an effective technique for boosting oil production in wells that have inadequate natural reservoir pressure. It may also be used in systems which suffers from low production rates, even though the reservoir pressure is sufficient to produces oil on its own. Gas lift will then enhance the average production rate.

Even though the intention of applying the gas lift technique is to increase the production rate, it may sometimes have the exact opposite effect. This is because of unfortunate system constraints which may result in an unstable system at certain pressure and flow conditions. Unstable flow causes severe pressure and flow oscillations that reduces the average production rate and may also be damaging to the equipment. This is elaborated in section (2.6.2). One type of instability that may occur in gas lift systems is named the casing heading instability, and is explained in detail in chapter 2. Preventing and stabilizing the casing heading instability, through the use of automatic control, is the focus of this thesis.

1.3 Scope and Emphasis

This master thesis is a direct continuation from my introductory study on gas lift systems, performed in my project assignment, [1], on NTNU in the fall of 2011. In that project the main part of a new low order model, designed to be able to reproduce the casing heading instability in gas lift systems, was developed. The scope of this thesis has been to complete the model by comparing it to a more advanced flow simulator, OLGA. The reason for making a simplified model of the casing heading is that this low order model can, in contrast to the OLGA model, be used as a basis for controller development, analysis, estimators and design. With the new model at hand, the scope is further to use it as a basis in a controllability analysis to compare how suitable different measurements candidates are to be used for automatic control. An important objective has been to test the most promising measurements candidates from the analysis, in simulations. These simulations are performed on both the low order model and the OLGA flow simulator. Several simplifications are made in this thesis which should be considered when selecting a control structure for the real facilities. E.g., the different control structures are compared and judged purely by their ability to stabilize the system, and performance in ease of control. The different control structures are not considered from an economic point of view in this assignment. The main simplification done in this thesis is that the OLGA flow simulator is regarded as the real flow process. It is important to emphasize that OLGA is also just a flawed model of the reality. As a consequence, even though results show promising on the simulator, they may not be valid for the real systems.

1.4 Outline of Thesis

This thesis is outlined in the following way: Chapter 2 presents the nature of the casing heading instability cycle and explains different ways to prevent it. Further it is motivated for the use of automatic control to stabilize the system and it is justified as an effective way to optimize the production costs. Chapter 3 further presents the advanced flow simulator, OLGA, which is regarded at the real flow process in this thesis. In chapter 4 the new low order model for describing the casing heading phenomenon is presented. This is mainly a rendering of the modeling work conducted in my fall project, [1]. However some new changes is added to the model, including a new friction factor term. Chapter 5 uses the tuning parameters in the new model to fit its response to the more advanced OLGA flow simulator. This serves as a validation of the low order model and justifies it to be used as a basis for control design and simulation studies, regarding the casing heading instability. A controllability analysis of the fitted new model is further performed in chapter 6, to investigate which control structures that seems reasonable to implement. Chapter 7 discusses the real life availability of the measurements in gas lift systems. It is concluded that to use the most promising measurement candidate from the analysis, in realistic simulation study, an estimator should be introduced to the system. The unscented Kalman filter is chosen, and it is explained how it functions. In chapter 8, the controllers used in this thesis are presented. Further, in chapter 9 and 10, the most promising control structures are tested in simulations, both on the low order model and on the OLGA simulator, respectively. Finally in chapter 11, a control structure is recommended and the results are concluded. The appendices contains the constants used in the model and estimator, calculated bounds from the controllability analysis, some of the MATLAB implementations codes, as well as a conference paper based on some of the results from the fall project and this thesis. The paper was accepted to the 2012 International Symposium

on Advanced Control of Chemical Processes, (ADCHEM 2012).

Chapter 2

The Casing Heading Instability

2.1 Description of The Instability Cycle

As early as in 1953 a paper, [8], was written in which there was mentioning of observed instabilities in gas-lifted wells, under certain flow and pressure conditions. It was stated that during these unsteady flow conditions, a sudden pressure drop in the tubing would be followed by a sudden surge of gas flowing from the annulus into the tubing. It was also noted that the inflow volume of gas was dependent on the pressure and volume of the gas in the annulus. This resulted in a cyclic behavior, because when the pressure in the annulus dropped below a certain point, the gas ceased to flow into the tubing, until the pressure in the annulus was built back up. The worst consequence of this was that the well would stop producing oil while the pressure in the annulus was building up, which because of its volume, could take considerable time. These observations are the fundamentals of the casing heading instability. Casing heading is basically a compressibility problem resulting from the gas-density's dependency on the pressure in the respective volumes. The instability is caused by the accumulation of gas within the annulus. The reason for the name casing heading is due to the fact that the pressure in the top of the annulus often is referred to as the casing head pressure, which is oscillating during the instability.

The casing heading instability cycle is thoroughly explained and described in greater detail in more present literature. The following description of the phenomenon is based on what is presented in [7], [9] and [1].

In a gas-lift system with one production tubing within its casing volume, a single injection point in which the lift gas can flow from the annulus to the tubing, a constant feed rate of gas into the annulus, there is uncontrolled gas passage between the annulus and tubing and there is a one-way flow restriction from the annulus to the tubing, the casing heading instability cycle can be described in the following way:

1. The compressed gas which enters at the top of the annulus flows down the annulus, through the single injection point near the bottom of the annulus, and into the tubing. When the gas enters the tubing the pressure in the tubing will decrease as a result of the reduction in mixture density of the oil and gas. The decrease of pressure in the tubing acts as a reinforcing loop as it causes an acceleration of the flow of gas from the annulus into the tubing.

2. The gas which has entered the tubing from the annulus infiltrates the liquid and reduces the average mixture density in the tubing. In this way the reservoir pressure is able to push the oil out of the tubing, which is what is intended. However, the accelerated inflow rate of injection-gas has led to an excessive amount of gas in the tubing, more than what is necessary to produce oil in a stable manner. This causes a rapid state change in the liquid-gas fraction in the tubing. The fluid mixture weight is highly reduced, and the reservoir pressure is now more than adequate to push the content content of the tubing. The result is a blowout through the production choke in the top of tubing, caused by the gas pushing a major part of the liquid up and out, to the receiving facility.

3. Immediately after the blowout, the annulus has practically no gas mass left, i.e., it was emptied during the blowout. Now there is a negative pressure difference over the injection orifice from the annulus to the tubing, that is, the pressure in the annulus is lower than the pressure in the tubing at the injection point. This blocking constraint prevents the gas from flowing from the annulus into to the tubing. As a consequence, the annulus is filling up with gas, and the tubing is filling up with liquid.

4. At one point the annulus will once again contain an amount of gas corresponding to a pressure, upstream the injection orifice, high enough for the gas to overcome the blockage constraint. At this instant, the gas will once again start to flow from the annulus into the tubing. A new cycle has begun.

2.2 Demonstrating the Casing Heading Instability

The results of the casing heading instability are highly oscillating flows and pressures in the system. This is shown in figure (2.2.1), which is made with the advanced OLGA flow simulator. The OLGA simulator is further presented in chapter (3).

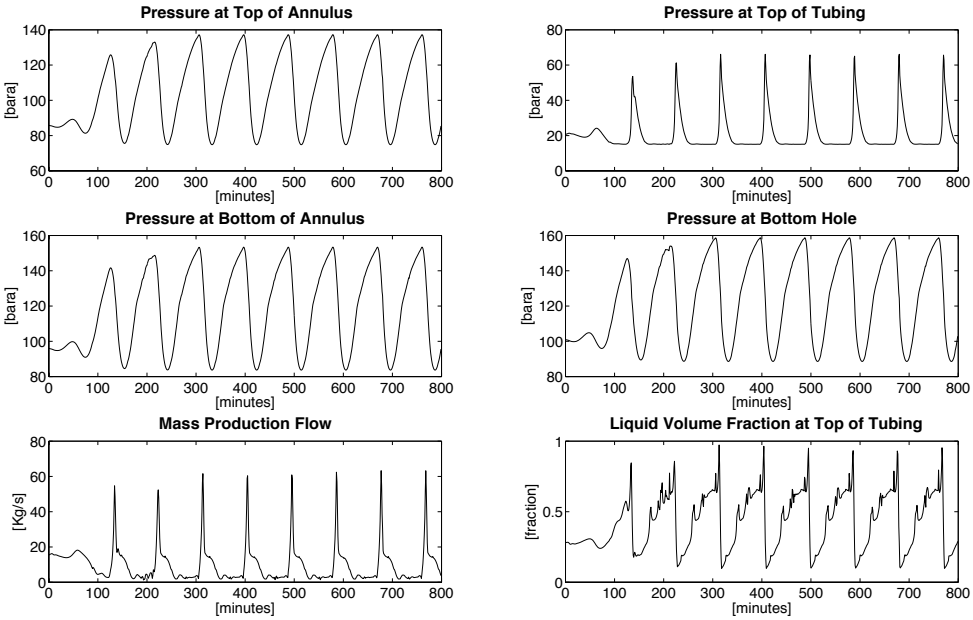

Figure 2.2.1: The Casing Heading Phenomenon

As can be seen in figure (2.2.1), the system behaves as the previously explained cycle, in section (2.1). The pressure in the annulus is building up to the point where it overcomes the pressure in the tubing at the injection point. Notice that the pressure in the annulus drops when a surge of gas flows from the annulus into the tubing. The tubing pressure decreases rapidly. This is immediately followed by a peak in the mass production flow, representing the blowout, as seen in the plot. Oscillations in flows and pressures are slow and can occur with a period time of several hours. The resulting unstable flow regime is named severe-slugging and can be described as an alternating flow of gas pockets and liquid slugs, see figure (2.2.2), taken from [4].

Figure 2.2.2: Vertical Slug Flow

Slug-flow is one of several different flow regimes which is possible in multiphase flow

systems. An extensive description of slug flow and the other types of multiphase flow regimes, as well at which conditions they may occur, is given in the book "*Multiphase Flow Assurance*" by *Ove Bratland,* [4].

2.3 Consequences of Casing Heading

Severe-slugging may be damaging to the receiving equipment downstream the production choke at the top of the tubing, i.e., the separator. Slug-flow is also a possible reason for why deposits, like wax or hydrates, sometimes build up inside the pipe over time. To understand why severe-slugging may cause deposit buildup, one must consider how long periods of alternating gas pockets and liquid slugs affects a pipeline. Fast temperature changes and pressure fluctuations, associated with the respective phases, is the foundation of chemical reactions that occurs at specific temperature and pressure conditions, [10]. Specifically, the combination of low temperature and high pressure, when water is in contact with natural gas, will often lead to formation of hydrates. Also, initiated production shutdown, to avoid the unstable flow regime, will contribute to hydrate formation. Deposits buildup is unwanted as it may throttle the line and also cause complete blockage [4]. This blockage which reduces or in the worst case stops the flow, is difficult to remove without shutting down the pipe for several hours, consequently halting the production. A more detailed presentation of the formation of deposits and its resulting pipe damage is presented in chapter 18 in [4]. Another highly undesirable consequence of the unstable flow-regime is that the average oil production rate is decreased, which is further shown in section (2.6.2).

2.4 Requirements for Casing Heading

The casing heading instability only occurs during certain pressure and flow conditions in the gas-lift systems. Necessary, but not sufficient conditions for casing heading to exist in a gas-lift system can be formulated as a pressure drop criteria. Keeping in mind that the pressure drop is what drives the flow, and that the pressure drop is a result of gravity and friction forces in the system, the criteria is given as follows. The pressure drop over the flow-path from the top of the annulus, down the annulus, over the injection-valve, to the top of the tubing and over the production choke, has to be gravity dominated, [11], [9]. That means the pressure drop due to gravity is higher than the pressure drop term resulting from friction forces acting on the system.

2.5 Remedies for Casing Heading

The casing heading instability may be avoided without the use of automatic feedback-control. One way to prevent the unstable flow regime is simply to choke back, i.e., reduce the opening, of the production choke, which is located on the top of the tubing, see figure (1.2.1). Even though choking back will cause the pressure in the tubing to increase, resulting in a stabilizing effect, it will also decrease the average production rate. The choking is often exaggerated to ensure a sufficient stability margin. Since control is not applied, the opening will remain constant and the average production flow will remain suboptimal. This is undesirable.

Increasing the amount of gas injected into the annulus, i.e., the amount of lift gas, will also have a stabilizing effect on the system. However, as will be shown in section (2.6.1), after increasing the injection-gas rate up to a certain point, this will also result in a reduction of the average production rate. In addition, the expense of compressing the extra amount of injection-gas has to bee considered in the overall production costs.

Interestingly, in earlier literature covering instabilities in gas-lift systems, such as [9], the recommended remedy to prevent the problem was to accurately fit the orifice geometry in the gas-lift injection valve. It was stated that to manually adjust the the surface chokes was probably the least efficient way to avoid the instability, as it resulted in either a significantly higher injection rate of gas, or lower production rate then intended. Later on however, the rise of automatic control to adjust the surface chokes was recognized as the recommended solution [7], and has been applied to gas-lift systems for quite a while. Apparently, sizing of the downhole injection-valve was for a while disregarded. However, in most recent literature covering innovations in gas-lift system, [2], sizing of the downhole orifice is once again praised as an actual solution. Where it is stated that to use a venturi-flow geometry in the gas lift injection vale between the annulus and the tubing, can significantly extend the maximum pressure limitations of gas-lift systems.

However, the approach investigated in this assignment is to apply automatic feedback control, for adjusting the production choke, on top of the tubing, or alternatively the gas lift choke, on top of the annulus, or a combination of the two.

2.6 The Benefits of Automatic Control

2.6.1 Optimal Production

As explained in section (2.5), the casing heading instability can be avoided without the use of automatic control. To justify the need for control, one must therefore consider if applying control may result in optimizing the production in some manner. To investigate the possible benefits of control, a comprehensive simulation study was performed using a gas lift setup in the advanced OLGA flow simulator. The OLGA model will be further presented in chapter (3), and the constants used in the gas lift setup case study is presented in appendix (B).

The simulation study was conducted in the following way: First a constant production valve opening of *10 percent* was selected. For the chosen valve opening, the OLGA model was simulated with different gas injection flow rates, ranging from *0.4* $[kg/s]$ to *3* $[kg/s]$, with an increment size of *0.1* $[kg/s]$ between each simulation. When a gas injection rate of *3* $[kg/s]$ was reached, it was reset to *0.4* $[kg/s]$, and the production valve opening was incremented with *10 percent*. With this new constant production valve opening, the simulations were repeated trough the whole range of the chosen gas injection rates. This process was repeated until the production valve opening reached *100 percent,* i.e. a fully open valve.

The simulations were performed with the steady state preprocessing option enabled in OLGA. With this option enabled, the initial simulation outputs is set to the steady-state

values at the operating point corresponding to the chosen inputs, regardless of whether the system is stable or unstable at this point. If the system is unstable, it will not be able to maintain the steady state production rate. However, by introducing automatic feedback control, it may be possible to stabilize the system at this operating point. The steady state value of the mass production flow rate was noted for each of the different combinations of gas-injection rates and valve-openings. It was also noted if the system was stable at the different operating points.

The result of the study is presented in figure (2.6.1). In the figure, the gas-injection rates are on the horizontal axis, and the mass production flow rates are on the vertical axis. Each of the continuous lines in the plot represent the response of a constant production valve opening. The red X on the line represents the point where the system changes from unstable to stable. This transition will occur when the gas injection rate becomes high enough. The stability transition point will also vary with the production valve opening, that is, increasing the opening of the production valve turns the system unstable. Consequently more injection gas is needed to stabilize the system when the production valve opening is increased.

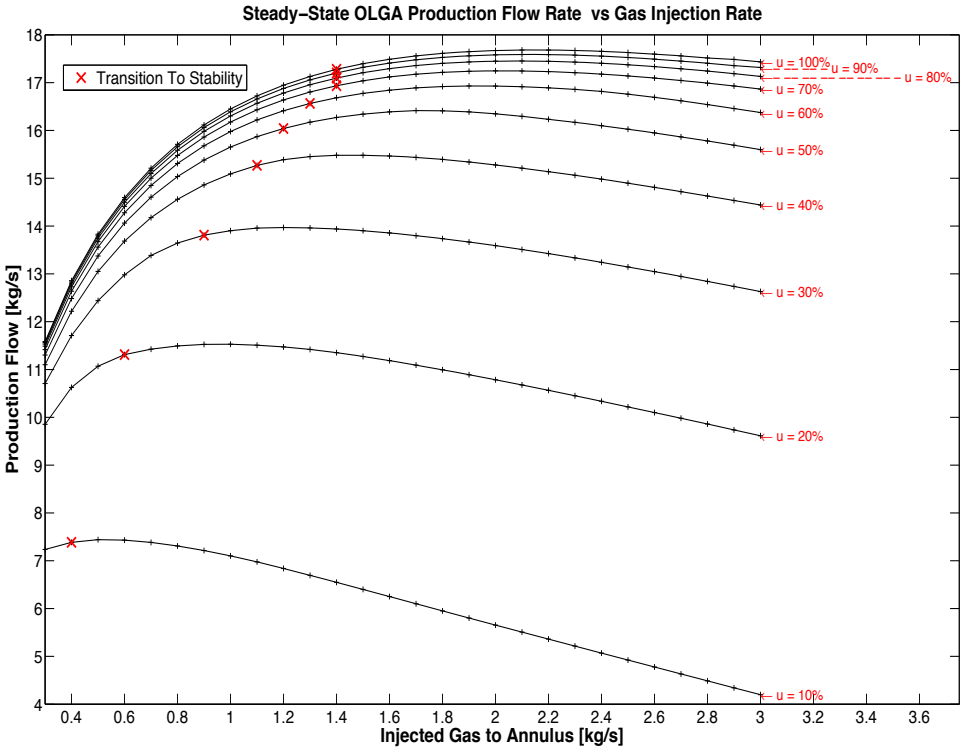

Figure 2.6.1: Production Rate subject to Gas Injection Rate

In the figure it can be seen that when increasing the gas injection rate, while maintaining the production valve opening constant, the result is an increase in the mass production rate. However, the figure also reveals that after the gas injection rate is increased up to a certain point, the mass production flow rate is decreasing when the gas injection rate is

further increased. With the objective to minimize the use of injection gas and maximizing the mass production rate, it can be seen that the optimal production conditions lies in an unstable operation region. For example, by examining the plotted line in the figure which represents a production choke opening of *40 percent*, there seems to be optimal to use a gas injection rate of approximately *0.8 [kg/s]*. The fact that this operating point is unstable can bee seen in the figure by noting that the red X which marks the transition to stability, is not yet reached, as it requires more injection gas to stabilize the system. Why this gas injection rate is optimal for the given production valve opening is justified as follows. Even though a further increase in the gas injection rate will lead to a small increase in the production rate, the gain in production is small. It is therefore not very cost effective, especially when considering the cost of retrieving and compressing the extra amount gas. The conclusion is therefore that the optimal gas injection rate for a given production valve opening is located at an unstable operating point. Unfortunately the steady state production rate at this optimal operating point can only be maintained through active stabilization of the system, which we hope to achieve by introducing a controller. This justifies the use of automatic control in gas-lift systems. It should however be noted that if the gas produced from the reservoir is at least *10 percent* of the total circulated gas rate, experience has shown that this produced gas is enough to support the gas lift system without the need of an additional external gas source, [3]. This would of course reduce the cost associated with the use of extra lift gas.

2.6.2 Compering Stable and Unstable Production Rates

In the previous subsection it was shown that, with the objectives to minimize the use of injection gas and maximizing the production flow, the optimal operating points is located in an unstable region. However, that conclusion was based on an argument in which only the steady state production values was considered. Thus it was implicitly assumed that the stable steady state production rate is higher than the unstable production rate at the same operating point. To investigate if this is true, a new simulation study was conducted with the OLGA flow simulator.

The study was performed in the following way. A constant gas injection rate of *0.8 [kg/s]* was selected. The system was then simulated, in turn, with the production valve opening ranging from almost closed (*10 percent opening)* to fully open (*100 percent opening).* The opening was incremented with *5 percent* between each simulation. As long as the specific combination of gas injection rate and production valve opening resulted in a stable system, the steady state production value was noted. When the combination resulted in a unstable system, the average of the unstable production, over a longer time period, was calculated. The results are presented in figure (2.6.2).

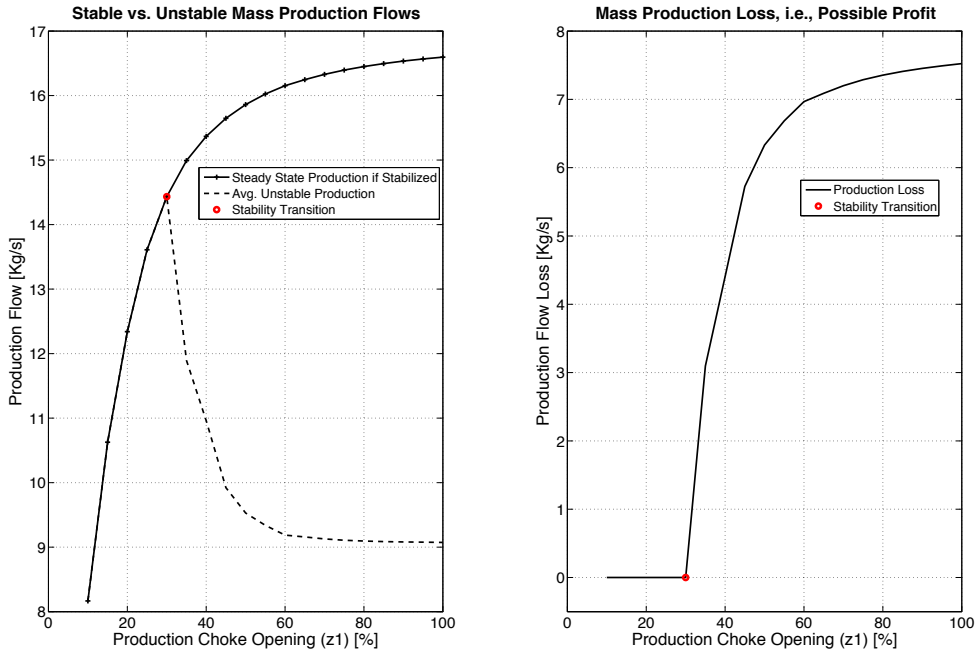

Figure 2.6.2: Stable vs Unstable Production

In the figure, to the left, both the steady state production rate and the average unstable production rate is plotted as a result of the different production valve openings. To the right, the difference between the two flow rates are shown. It can be seen that the production rate in the system is increasing while the production valve opening is increasing, as long as the system is stable. However, as soon as the system turns unstable, the average production rate is drastically decreasing. Note that the system turns unstable with a valve opening of approximately *30 percent*. This opening is lower than what was found to be the optimal operating point, which was at *40 percent,* with the specified gas injection rate. It is concluded that the unstable flow regime results in a lower average production than the stable flow regime. This proves that the conclusion reached in the end of section (2.6.1) is indeed true: it may be beneficial to introduce automatic control in gas lift systems due to the fact that it can possibly result in stabilizing the system at an operating point which maximizes production subject to minimizing the amount of injection gas.

2.7 Other Instabilities in Gas Lift Systems

Besides the casing heading instability, there are two other types of instabilities which is recognized in gas-lift systems: the formation-heading and the tubing-heading. Casing heading and formation-heading are close to identical. For more information on these types of instabilities, outside the scope of this thesis, see [12].

Chapter 3

Advanced Flow Simulator : The OLGA Model

The OLGA flow simulator is regarded as the real flow process in this work. This chapter therefore presents the simulator and describes the gas lift case setup which is used in this thesis.

3.1 What is OLGA

To perfectly describe a phenomenon as complex as multiphase flow is virtually impossible. Each single interaction between each specific part of an enormous system would have to be considered in the equations. Even in the hypothetical case that all the correct equations governing each relationship and causality in the system were taken into account, solving them would be extremely challenging and require tremendous calculation power. Nonetheless because of our need to be able to predict how flow systems, such as a gas lift system, are going to behave at different operating conditions, advanced flow simulators are continuously in development. A commercially available flow simulator model which is recognized to be one of the most accurate to this date, is the OLGA flow simulator, marketed by the SPT-group. The OLGA flow simulator can be used to simulate a specific setup composed by the user. The graphical interface can be used to combine pipelines, different process equipment and a network of wells. The user can build a system that is desired to simulate by combing a large selection of different options included into the software.

OLGA is widely applied in research, e.g., [7] and [13], and is also used in the industry. In the manual following the software it is claimed that *"OLGA is the industry standard tool for transient simulation of multiphase petroleum production",* [14]. However it is important to note that regardless of how advanced the OLGA flow simulator may be, it is also just another flawed model trying its best to replicate and predict the complex real behavior of a flow system. That is, the OLGA model is in no way guaranteed to produce the exact real behavior of a system. Hopefully however, the simulation results render an adequate description of the situation at hand.

From the start of its development in 1980, the OLGA model has gone through several

changes. With time, SINTEF and a number of oil companies have contributed with field data which has been incorporated in the software to improve the simulation accuracy and reduce uncertainty, [14]. OLGA was recently purchased by one of the worlds leading oilfield services providers, Schlumberger. This may contribute to further recognition and wider applications of the flow simulator. In this work it is the latest version of the simulator, OLGA 7, which is used.

3.2 OLGA Model Fundamentals

Unlike the low order model, which will be presented in chapter (4), the OLGA model is a three-fluid model with separate continuity equations for each phase. The low order model is only based on simple mass balances for gas and liquid that flows in and out of the defined system. The OLGA model on the other hand, accounts for interfacial mass transfer. Furthermore, the flow simulator uses three momentum equations. Two are used for the continuous liquid phases, i.e., one for water and one for oil. The third momentum equation is for the combination of gas with liquid drops, [15]. Needles to say, the OLGA flow simulator is much more advanced than the low order model that will be presented in the next chapter.

3.3 The Gas Lift Case In OLGA

The specific case study which is implemented and used in OLGA in this thesis, is a slightly modified version of the one provided by Gisle Otto Eikrem, at Statoil. It is assumed to use somewhat realistic parameter values made up from the Norwegian Petroleum Institute. All the specific settings and constants used in the case study are given in a system report generated by the OLGA software, located in appendix (B). The main parameters, however, are a vertical well with the length of 2048 meters. A tubing with a diameter of 0.124 meters. The reservoir pressure is 150 bara with a temperature of 108 degrees celsius and a productivity index of $2.47 \cdot 10^{-6}$ [kg/s/Pa]. The pressure in the inlet of the separator is 15 bara. While the temperature of the gas injected into the annulus is at 60 degrees celsius, at 160 bara and a constant injection rate of 0.8 [kg/s.]

3.4 OLGA Stability Map

To investigate how the gas lift setup in OLGA behaves during different operating conditions, it was decided to make a stability map of the system. By using the same data that was generated through the simulations performed to make the production figure (2.6.1) presented in section (2.6.1), the following figure is created.

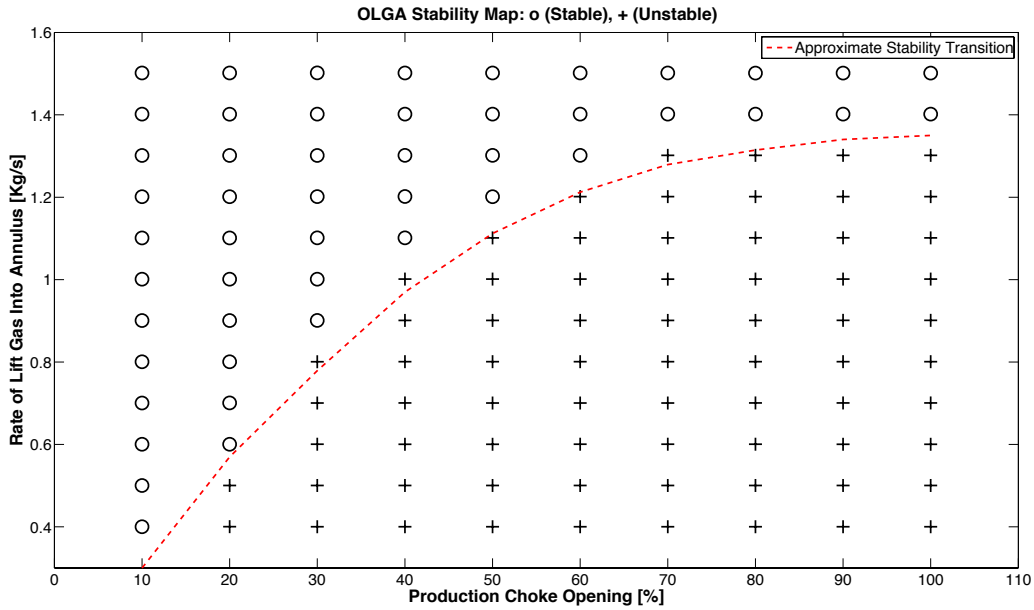

Figure 3.4.1: OLGA Stability Map

In figure (3.4.1) it is shown if the system is stable or unstable at different combinations of gas injection rates into the annulus and production choke opening. The circles *(o)* depicts stable operating points, and the *(+)* show the unstable operating points. An approximate transition between the stable and unstable region is also shown as a dotted red line. The map provides a good insight of the system behavior, and it can easily be seen when the system turns unstable. Note that the system behaves as expected. At combinations of low gas injection rates in relation to high production choke openings, results in an unstable system. As the gas injection rate is increased or alternatively, the production choke opening is decreased, the system moves towards the stable region. By a closer inspection of the plotted approximate stability transition line, it seems to be an almost linear relationship between the two variables. At least between production choke openings from *10* to *50* percent. In that region, a *10* percent increase in the production valve opening changes the stability transition line to a gas injection rate corresponding to an increase of approximately *0.2 [kg/s].*

Chapter 4

Low Order Model for Gas lift Systems

The reasons for developing a simplified model when we already have available a much more advanced flow simulator, i.e., the OLGA model, is justified as follows. The OLGA model consist of equations that are not directly available, it is more like a black box from which one can apply an input and get an output. With that in mind, it can not be used directly in a controllability analysis, or for model based controllers. Furthermore the OLGA model consist of much more equations, relationships and possibilities that what is used in this simple gas lift setup, since it is supposed to be used for many other different flow scenarios as well. It is however a great tool for testing results found in the low order model in a more realistic scenario.

This section derives the final version of the new low-order model to be used for gas lift systems. Most of what is presented in this chapter is more or less a direct rendering of what was presented in the fall project assignment, [1], where the main part of the model development was conducted. Still, some new modifications to the model are presented, such as a new friction term. The resulting non-linear model is implemented in Matlab and is solved with an numerical integrator. The implementation code of the model is given in appendix (D.0.2).

4.1 Basis and Foundation of the New Model

In the paper "Simplified Dynamical Models for Control of Severe Slugging in Multiphase Risers" [13], Jahanshahi and Skogestad presents a simple dynamical new low-order model for multiphase flow in risers. In the fall project, a modification of that model, to be used for gas lift systems, was developed. The model consists of three states, similar to what we refer to as the Eikrem model, presented in [16], and [7]. In contrast to the Eikrem model, the model proposed here also include a pressure drop term due to friction in the tubing. The state which involves the mass of the liquid in the tubing is also modified so that is also accounts for the liquid mass below the gas injection point. Another difference between the two models is also noted. In the Eikrem model, the mass production flow of gas and liquid is calculated from the weight fractions of the different phases in relation to total fluid weight in the whole tubing. In the model presented in here, and in the project assignment, an assumption made by Skogestad and Jahanshahi in [13], is used to

calculate the phase fractions and the density in the top of the tubing. The assumption is explained in more detail in section (4.3.6). Furthermore this model also accounts for gas flowing in from the reservoir.

4.2 Mass Balances in Model

The model consists of three states, which are; The mass of the gas in the annulus (x_1), the mass of the gas in the whole tubing (x_2) and the mass of the liquid in the whole tubing (x_3). The state equations which constitutes the model is simply the mass balances of the respective phases over the tubing volume and the annulus volume. A mass balance is the mass inflow to a respective volume, subtracted by the mass outflow from the same volume. The change in the mass of gas in the annulus, with respect to time, i.e., the time derivative of x_1, is given by the mass inflow rate of gas into the top of the annulus ($w_{G_a,in}$), subtracted by the mass outflow rate of gas ($w_{G_a,out}$). The outflow is the lift gas which flows through the gas lift injection valve into the tubing. The result is equation (4.2.1). By applying the same principle, the change in the mass of the gas in the tubing, is the mass flow rate of gas flowing into the tubing from the annulus, through the gas lift injection valve ($w_{G_a,out}$), added with the mass flow rate of gas flowing into the bottom of the tubing, from the reservoir ($w_{G_r,out}$), and finally subtracted by the mass rate of the gas flowing out of the top of the tubing ($w_{G_t,out}$), through the production choke. The result is equation (4.2.2). Since there is no liquid in the annulus, the change in the liquid mass in the tubing is simply the mass flow rate of liquid flowing in from the reservoir, ($w_{L_r,out}$), subtracted by the mass flow rate of liquid flowing out the top of the tubing, ($w_{L_t,out}$), through the production choke. The result is equation (4.2.3), which together with equation (4.2.1) and (4.2.2) describes the whole system.

$$\dot{x}_1 = \dot{m}_{G_a} = w_{G_a,in} - w_{G_a,out} \tag{4.2.1}$$

$$\dot{x}_2 = \dot{m}_{G_t} = w_{G_r,out} + w_{G_a,out} - w_{G_t out} \tag{4.2.2}$$

$$\dot{x}_3 = \dot{m}_{L_t} = w_{L_r,out} - w_{L_t,out} \tag{4.2.3}$$

4.3 Flows, Pressures, Phase fractions and Friction

As just shown, the low order model is defined by the mass flows in and out of the system. However, it is how the flows in the equations, (4.2.1)-(4.2.3), are calculated, which slightly differs from many other similar models of gas lift systems, proposed by different authors. It is the flow calculations which is the challenge.

4.3.1 Flow into Annulus

Firstly the flow from the external gas source into the top of the annulus, through the gas lift choke ($w_{G_a,in}$) is derived. Due to the fact that there is only gas inside the annulus, the pressure in the top of the annulus can be calculated with the ideal gas law, assuming that temperature inside the annulus (T_a) is constant. Assuming constant temperature is a reasonable as it is varying slowly. By using the fact that mass equals volume times mass density, the expression for the pressure in top of the annulus is therefore given as:

$$P_{at} = \frac{RT_a x_1}{M_G V_a} \tag{4.3.1}$$

where R is the ideal gas constant and M_G is the molar mass of the gas. Pressure in the bottom of the annulus near the gas injection point to the tubing, (P_{ab}) , is calculated in the same way as in the Eikrem model [7]. That is, it is given by adding the pressure drop from the gas column to the pressure at top of the annulus. The resulting expression is:

$$P_{ab} = P_{at} + \frac{x_1 g L_a}{V_a} \tag{4.3.2}$$

where g is the gravitational constant, L_a is the length of the annulus, and V_a is the volume of the annulus. A pressure drop term due to friction in the annulus is not considered in this model, only friction in the tubing in applied, and is derived in section (4.3.3). The gas density at the bottom of the annulus is therefore given from the pressure in the bottom of the annulus, through a rewrite of the ideal gas law, and can be expressed as:

$$\rho_{G,ab} = \frac{P_{ab} M_G}{R T_a} \tag{4.3.3}$$

Gas entering the annulus on the topside is assumed to come from an external gas source, a tank or a compressor, with pressure denoted P_{gs}. The density of the gas flowing into the annulus can be expressed in a way similar to that in equation (4.3.3), and is given as:

$$\rho_{G_a,in} = \frac{P_{gs} M_G}{R T_a} \tag{4.3.4}$$

Using the mass flow version of the general valve model presented in equation 4.1 in [17], the resulting gas mass flow into the annulus is therefore given as:

$$w_{G_a,in} = K_{gs} z_2 \sqrt{\rho_{G_a,in} \cdot max\{P_{gs} - P_{at}, 0\}} \tag{4.3.5}$$

where K_{gs} is a constant discharge coefficient, the valve parameter, and z_2 is the gas-lift choke opening fraction. A linear valve characteristic is used. $P_{gs} - P_{at}$ is the pressure drop across the restriction. When the pressure in the top of the annulus is greater than the pressure in the external gas source, the will be no gas flow into the annulus.

4.3.2 Pressure in The Tubing at The Gas Injection Point

On page 4 in [18], a saturated oil reservoir is defined as a reservoir were the initial pressure is equal to the bubble-point pressure of the reservoir, i.e., the reservoir is fully in liquid state but it is about to vaporize. Assuming a saturated oil reservoir and high pressure in the bottom of the tubing, we conclude that the distance between the gas injection point in the tubing and the bottom hole of the well, denoted L_{bh}, is filled with fluid in pure liquid phase. The volume of the gas in the tubing is calculated by using the total volume of the tubing, subtracted by volume occupied by the liquid. The volume occupied by the liquid, above the gas injection point, is calculated in the following way:

$$V_{L_t} = \frac{m_{L_t}}{\rho_L} - S_{bh} L_{bh} = \frac{x_3}{\rho_l} - S_{bh} L_{bh} \tag{4.3.6}$$

where S_{bh} is the surface area of the bottom hole, and ρ_L is the density of the liquid, which is assumed constant. Using equation (4.3.6), the density of the gas at the top of the tubing is the sum of the mass of gas and liquid divided by the volume, and is calculated as:

$$\rho_{G,tt} = \frac{m_{G_t}}{V_t - V_{Lt}} = \frac{x_2}{V_t - \frac{x_3}{\rho_L} + S_{bh} L_{bh}} \tag{4.3.7}$$

where V_t is the total volume of the tubing, including the bottom hole part. This expression can be used together with the ideal gas law to calculate the pressure in the top of the tubing:

$$P_{tt} = \frac{\rho_{G,tt} R T_t}{M_G} \tag{4.3.8}$$

where T_t is the temperature in the tubing, which is assumed constant. The average mixture density inside the tubing is

$$\bar{\rho}_{mix} = \frac{x_2 + x_3 - \rho_L S_{bh} L_{bh}}{V_t} \tag{4.3.9}$$

The pressure in the tubing at the gas injection point can now be calculated similar to what was done in equation (4.3.2) , by adding the pressure drop from the fluid column in the tubing to the pressure at top of the annulus, i.e.,

$$P_{tb} = P_{tt} + \bar{\rho}_{mix} g L_t + F_t \tag{4.3.10}$$

where L_t is the length from the top of the tubing to the gas injection point. F_t is the pressure drop term over the same distance, due to friction in the tubing, which will be derived in section (4.3.3).

4.3.3 Friction

Calculating the pressure drop due to friction in the tubing was one of the main challenges in the fall project work. In the riser model proposed by Jahanshahi and Skogestad [13], which this model is based on, the friction is calculated in an expression that is based on the flow rate through the tubing. But in a gas lift system, the flow rate of gas into the tubing, from the annulus, is dependent on the pressure at the gas injection point in the tubing. This pressure is again dependent on the pressure drop due to friction. To avoid this mutual dependence, it is proposed to define an average flow rate from the reservoir to the tubing, $\bar{w}_{res}$, which will be an constant in the model, and can be used as an tuning parameter for the friction term.

To be able to include friction in the model, it is necessary to introduce the term *superficial vel*ocity. In single phase flow the volumetric flow rate divided by the the pipe cross-sectional area is often used as the average velocity at a particular point in time, i.e., the instantaneous average velocity. In that way the average velocity directly reflects the volumetric flow rate. However, in multiphase flow systems, the fraction of the pipe cross-sectional area occupied by one particular phase will vary in time and space. That means that the flow is no longer proportional to the velocity at a given point. Instead we may define the average phase velocity by using the fraction of the cross-sectional area occupied by the particular phase. For a more detailed definition of superficial velocities, see section 1.5.3 in [4]. Using the previously defined average flow rate from the reservoir ($\bar{w}_{res}$), and with a cross section in the tubing equal to πr^2, the average superficial velocity of the liquid phase in the tubing is expressed as

$$\bar{U}_{sl,t} = \frac{(1 - \alpha^m_{G,tb})\bar{w}_{res}}{\rho_L \pi r^2} \tag{4.3.11}$$

where r is the radius of the the tubing, and $\alpha^m_{G,tb}$ is the gas mass fraction at the bottom of the tubing. Defining the mass gas-oil-ratio (GOR) as the ratio between the mass gas

rate and the mass liquid rate flowing in from the reservoir, i.e., ($GOR = \frac{\dot{w}_{G_r,out}}{\dot{w}_{L_r,out}}$), the gas mass fraction at the bottom of the tubing can be expressed as

$$\alpha^m_{G,tb} = \frac{GOR}{GOR+1} \tag{4.3.12}$$

The density of the gas bubbles at the bottom of the tubing can be approximated by

$$\bar{\rho}_{G,tb} \approx \frac{(P_{res} - \rho_L g L_{bh}) M_G}{RT_t} \tag{4.3.13}$$

where P_{res} is the pressure in the reservoir. The average superficial velocity of the gas phase in the tubing now becomes

$$\bar{U}_{sg,t} = \frac{(\alpha^m_{G,tb}\bar{w}_{res} + w_{G_a,in})}{\bar{\rho}_{G,tb}\pi r^2} \tag{4.3.14}$$

The average mixture velocity in the tubing is defined as the sum of the average phase velocities in the tubing and is therefore given as

$$\bar{U}_{m,t} = \bar{U}_{sl,t} + \bar{U}_{sg,t} \tag{4.3.15}$$

We can now use the average mixture velocity to express the Reynolds number in the tubing as defined for multiphase flow:

$$Re_t = \frac{2r\bar{\rho}_{mix}\bar{U}_{m,t}}{\mu} \tag{4.3.16}$$

where μ is the constant viscosity.
The average liquid volume fraction inside the tubing is

$$\bar{\alpha}_{L,t} = \frac{x_3 - \rho_L S_{bh} L_{bh}}{V_t \rho_L} \tag{4.3.17}$$

The new friction factor that is used in the tubing can now be calculated. It is an explicit approximation of the implicit Colebrook-White equation which was proposed by Haaland in [19].

$$\frac{1}{\sqrt{\lambda_t}} = -1.8 log_{10}\left[\left(\frac{\epsilon/(2r)}{3.7}\right)^{1.11} + \frac{6.9}{Re_t}\right] \tag{4.3.18}$$

where ϵ is the wall roughness constant.
Pressure loss due to friction from the top of the tubing down to the gas injection point, now becomes:

$$F_t = \frac{\bar{\alpha}_{L,t}\lambda_t\bar{\rho}_{mix}\bar{U}^2_{m,t}L_t}{4r} \tag{4.3.19}$$

4.3.4 Inflow of Lift-Gas to Tubing

We can now insert the pressure drop due to friction (4.3.19) into the equation for the pressure in the tubing at the injection point (4.3.10), which results in:

$$P_{tb} = P_{tt} + \bar{\rho}_{mix} g L_t + \frac{\bar{\alpha}_{L,t}\lambda_t\bar{\rho}_{mix}\bar{U}^2_{m,t}L_t}{4r} \tag{4.3.20}$$

And by using the same equation for describing flow through a valve as in (4.3.5) we get the expression for the mass flow rate of gas injected into the tubing from the annulus:

$$w_{G_a,out} = K_a\sqrt{\rho_{G,ab} \cdot max\{P_{ab} - P_{tb}, 0\}} \tag{4.3.21}$$

4.3.5 Mass Flow Rate from the Reservoir to Riser

With the assumption of only fluid in liquid phase below the gas injection point in the tubing, the average liquid velocity at the bottom-hole is:

$$\bar{U}_{L,bh} = \frac{\bar{w}_{res}}{\rho_L S_{bh}} \tag{4.3.22}$$

and the Reynolds number at the bottom hole is:

$$Re_{bh} = \frac{2r_b \rho_L \bar{U}_{L,bh}}{\mu} \tag{4.3.23}$$

where r_b is the radius of the tubing below the gas injection point. Friction factor using the same correlation as in (4.3.18) becomes:

$$\frac{1}{\sqrt{\lambda_b}} = -1.8 log_{10}\left[\left(\frac{\epsilon_b/(2r_b)}{3.7}\right)^{1.11} + \frac{6.9}{Re_t}\right] \tag{4.3.24}$$

The pressure loss due to friction in the tubing below the gas injection point can now be calculated in the same way as in (4.3.19) and is expressed as:

$$F_b = \frac{\lambda_{bh} \rho_L \bar{U}^2_{L,bh} L_{bh}}{4r} \tag{4.3.25}$$

The pressure at the bottom-hole can now be calculated as:

$$P_{bh} = P_{tb} + F_b + \rho_L g L_{bh} \tag{4.3.26}$$

And the mass flow rate from the reservoir to the riser is expressed as:

$$w_{res} = PI \cdot max\{P_{res} - P_{bh}, 0\} \tag{4.3.27}$$

where PI is the productivity index. The productivity index expresses the ability of the reservoir to deliver fluids to the tubing, it is a constant in this model. Using the the gas mass fraction at the bottom of the tubing, $(\alpha^m_{G,tb})$, calculated in equation (4.3.12), and the mass flow rate from the reservoir just calculated, the mass flow rate of liquid and gas from the reservoir to the tubing can be calculated as:

$$w_{L_r,out} = (1 - \alpha^m_{G,tb}) w_{res} \tag{4.3.28}$$

$$w_{G_r,out} = \alpha^m_{G,tb} w_{res} \tag{4.3.29}$$

respectively.

4.3.6 Liquid and Gas Volume Fractions

With the expression for the pressure at the gas injection point in the tubing, calculated in (4.3.10), we can write a more accurate expression for the gas density at the same point:

$$\rho_{G,tb} = \frac{P_{tb} M_G}{R T_t} \tag{4.3.30}$$

The liquid volume fraction at the gas injection point in the tubing then becomes:

$$\alpha_{L,tb} = \frac{w_{L_r,out} \rho_{G,tb}}{w_{L_r,out} \rho_{G,tb} + (w_{G_a,out} + w_{G_r,out}) \rho_L} \tag{4.3.31}$$

Now the assumption used by Jahanshahi and Skogestad in [13] is applied. The assumption is that in an vertical gravity dominant two-phase flow pipe, there is approximately a linear relationship between the pressure and the liquid volume fraction. So it is assumed that

the gradient of the pressure along the tubing is constant in the desired smooth flow regimes. With the assumption of this linear relationship, the liquid volume fraction also maintains approximately a constant gradient along the tubing for the stable flow regimes. Jahanshahi and Skogestad further argues that this assumption suggests that the liquid volume fraction at the middle of the tubing is the average of the liquid volume fraction at the two ends of the tubing. However, the liquid volume fraction at the middle of the tubing is approximately equal to the average liquid volume fraction in the tubing. Jahanshahi and Skogestad therefore conclude that we can express the liquid volume fraction at top of the tubing as:

$$\alpha_{L,tt} = 2\bar{\alpha}_{L,t} - \alpha_{L,tb} \tag{4.3.32}$$

where the average liquid volume fraction in the tubing is calculated in (4.3.17). The mixture density at top of the tubing can now be written as:

$$\rho_{mix,t} = \alpha_{L,tt}\rho_L + (1 - \alpha_{L,tt})\rho_{G,tt} \tag{4.3.33}$$

4.3.7 Mass and Volumetric flow out the Production Choke

With the expression for the mixture density at the top of the tubing in equation (4.3.33), we can now write the expression for the mixture mass flow rate out the production choke on the top of the tubing as:

$$w_{out} = K_{pt} z_1 \sqrt{\rho_{mix,t} \cdot max\{P_{tt} - P_0, 0\}} \tag{4.3.34}$$

where K_{pt} is the constant valve parameter, and P_0 is the pressure at the receiving facility. The volumetric flow rate out the production choke is then:

$$Q_{out} = \frac{w_{out}}{\rho_{mix,t}} \tag{4.3.35}$$

The gas mass fraction at the top of the tubing is now:

$$\alpha^m_{G,tt} = \frac{(1 - \alpha_{L,tt})\rho_{G,tt}}{\alpha_{L,tt}\rho_L + (1 - \alpha_{L,tt})\rho_{G,tt}} \tag{4.3.36}$$

The resulting mass gas and liquid flow rates out from the tubing to the receiving facility is then expressed as:

$$w_{G_t,out} = \alpha^m_{G,tt} w_{out} \tag{4.3.37}$$

$$w_{L_t,out} = (1 - \alpha^m_{G,tt}) w_{out} \tag{4.3.38}$$

respectively. The model is complete.

4.4 The Constants used in Model

The constant used in this model are taken from the OLGA flow simulator case study provided by Gisle Otto Eikrem at Statoil. It is assumed to use somewhat realistic parameter values. All the constants and parameters that are used are listed in appendix (A.0.1).

4.4.1 Stability Map of Model

In the same way as was done for the OLGA model, as stability map of the low order model was created. Note that the low order model behaves as desired. Increasing the gas injection rate, or decreasing the production choke opening, moves the system towards the stable region in the plot. The stability map of each of the models are compared in chapter (5).

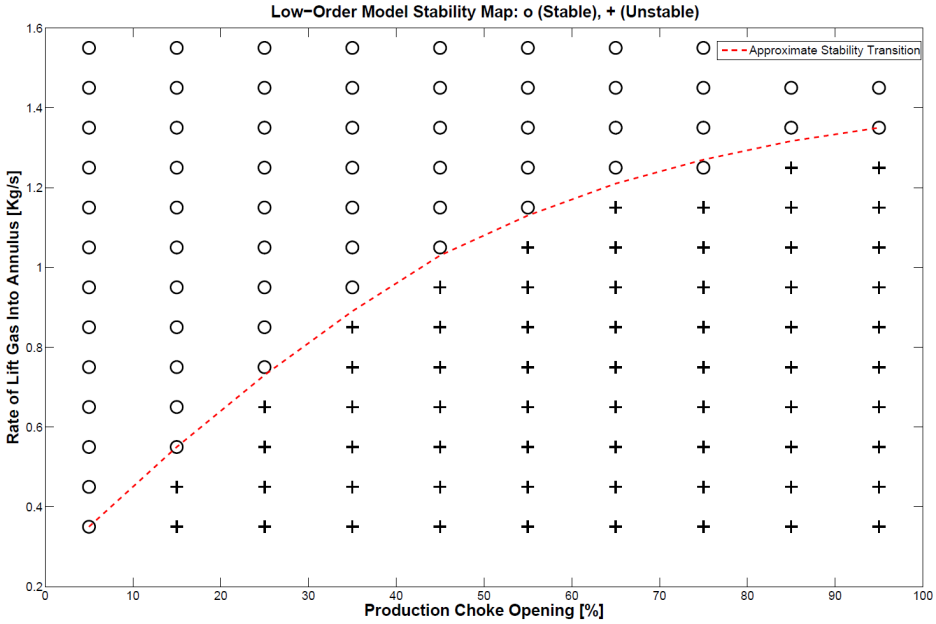

Figure 4.4.1: Low-Order Model Stability Map

Chapter 5

Compering and Fitting the Models

In this chapter the new low order model, which was derived in chapter (4), is fitted and compared to the OLGA flow simulator. As previously mentioned, OLGA is regarded as the real flow process in this thesis. The objective is therefore to make the response of the low order model as similar as possible to the gas lift case set up in OLGA. Thus, if the low order model is abel to sufficiently accurate reproduce the response of the advanced flow simulator, it is concluded as a valid model. This justifies it to be used in a simulation study to test out different control structures, for model based control, as well as to use it as a basis to perform a controllability analysis.

The low order model has 4 tuning parameters, i.e., constants, that can be altered to change the response. These parameters, which are used in equations (4.3.5), (4.3.11), (4.3.21) and (4.3.34), in the chapter (4), are adjusted to fit the outputs of the low order model to the OLGA simulator. The outputs are the measurements which are considered the most important candidates to be used in automatic control of the system. When the low order model is used in this thesis, the injection rate of gas into the annulus is set to a constant value, equal to the value set in the OLGA flow simulator case study. This was done to be able to easier fit the response of the two models.

5.1 Bifurcation Map

To compare the output response of the two models, and see how the adjustment of the fitting parameters affects the response of the low order model, it was decided to make a bifurcation diagram of both the low order model response, and the OLGA simulator response. A bifurcation diagram is a plot which shows how a model reacts when keeping all parameters constant except one designated bifurcation parameter. The bifurcation parameter, which in this case is the production valve opening, is incrementally changed, with an *5 percent* increment, from an almost fully closed to fully open valve. The other constant values used in the model are listed in table (A.1) in appendix (A.0.1). At each point, the system is simulated over a longer time period. From the outputs of the simulation series, the steady state, maximum and minimum value of the response over the whole simulation time is noted. Naturally, at the operating points where the system is stable, i.e., with low production valve openings, the steady state is equal to the maximum

and the minimum value. The result of the study is shown in figure (5.1.1):

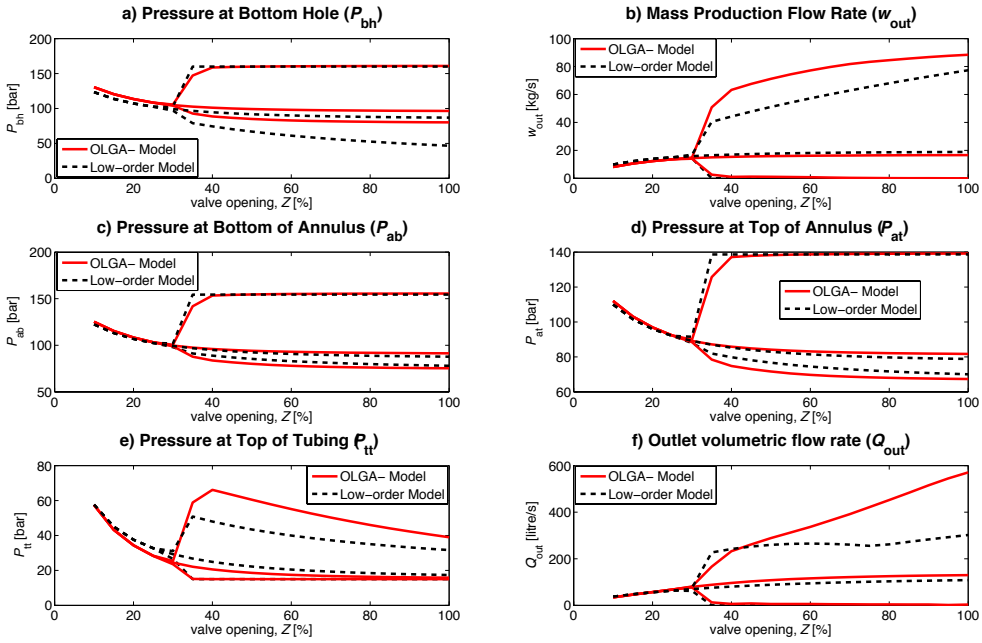

Figure 5.1.1: Bifurcation Diagram

It can be seen in the figure that the critical point, i.e., the point where the system turns unstable, is when the production valve reaches an opening of about *30* percent. The figure may be somewhat hard to interpret so here follows an explanation. For each of the subplots in the figure, there is actually plotted six different lines. Three red lines, corresponding to the OLGA flow simulator response, and three dotted black lines, corresponding to the low order model response. The three lines in the same color represent the steady state, minimum and maximum values of the response obtained over a longer simulation time at the specific operating point. As previously mentioned, as long as the system is stable, all the lines in the same color will be identical. However, when the system turns unstable, at the critical point, two of the three lines in the same color will diverge. That is, the maximum peak of the oscillations from the simulation at the respective point is the upper line in each figure, the minimum peak of the oscillations is the lower line, and the steady state value, which can only be maintained with feedback control, is the middle line. The objective is to fit the maximum, minimum and steady state lines of the two colors to each other. Of course, a perfect match is difficult, if not impossible to achieve, as the OLGA model has far more advanced dynamics than the low order model. The most important part to fit accurately in this case is considered to be the critical point, since we want the models to be stable or unstable at the same operating points. Far to much time was spent in this thesis to try fit the low order model to the OLGA model by chancing the value of the fitting parameters in the low order model. As can be seen, the accuracy of the fitting is not perfect. However, the coinciding of the responses is hopefully good enough to use the low order model as a basis to design controllers that can successfully be applied also to the advanced flow simulator.

5.2 Stability Map Comparison

The bifurcation diagram is a great tool for comparing and fitting the response. Unfortunately, the models are only compared when one parameter, is changed. Even though that parameter was one of the most important parameters, namely the production valve openings, there is one other parameter which has a huge influence on the system. To also fit the system to be stable and unstable with different combinations of gas injection rates and production vale openings, the low order stability map was fitted to the OLGA stability map. The final fitting and tuning can be seen in figure (5.2.1). In the figures it can be seen that the stability map of the two models are closely fitted. The final value of the fitting parameters in the low order model can be found in table (A.1) in appendix (A.0.1).

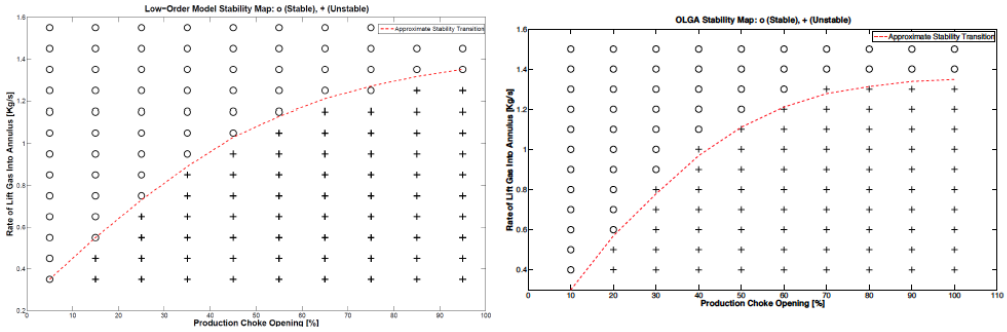

Figure 5.2.1: Stability Map Comparison

Chapter 6

Controllability Analysis of The Low-Order Model

The low-order model presented in this theses is a modification from the one that was derived in my project assignment,[1]. In the project assignment there was also conducted a controllability analysis. However, since the model has been changed in this thesis, and the tuning parameters are altered to fit the response to the OLGA flow simulator, the controllability bounds calculated in the project assignment are no longer valid. Therefore a new analysis is performed in this thesis. Naturally, most of what is presented in this chapter, which is necessary to be able to perform and evaluate the analysis, is more or less identical to the way it is presented in the project assignment. The results however, are different.

A controllability analysis is a mathematical tool which can be used to examine to what extent different control structures are suitable for stabilizing a specific system. A control structure is a specific combination of inputs, i.e., manipulated variables (MV), and outputs, i.e., controlled variables (CV), that may be used to control a system. The analysis give out specific numbers which may be compared to decide on the theoretically optimal measurements to be used for different objectives in control. Different objectives may be disturbance rejection, tracking a set point, or attenuate the effect of noise entering the system. However, the controllability analysis is a linear tool, which means that it can only be applied on a linear model. Therefore the non-linear low order model was linearized around a specific operating point, to be able to perform the analysis. The consequence of this is of course that the results are only truly valid for the linear model. With the assumption that the linear model gives a sufficient description of the dynamical behavior of the non-linear model, in a close neighborhood of the operating point, the results may also be valid for the non-linear model at the specific point. It should be kept in mind that the casing heading phenomenon is highly nonlinear, and because of this the results of the analysis should only be used as an indication of what the actual conditions may be. The control structures which seems most promising in the analysis is further tested in simulations of the non-linear model in chapter (9).

The analysis was performed with eight different measurement candidates. The candidates were evaluated both as how they would perform as single measurements for use in *SISO*

systems, and how they would perform when combined with other measurements, for use in both $SIMO$ and $MIMO$ systems. The measurements candidates were; the pressure deep in the tubing near the well, which we call the the bottom hole pressure (P_{bh}), the mixture mass flow rate out the production choke (w_{out}), the mixture density in top of the tubing ($\rho_{mix,t}$), the mass gas flow rate into the annulus ($w_{G_a,in}$), the pressure in the top of the tubing (P_{tt}), the pressure in the top of the annulus (P_{at}) , the pressure in the bottom of the annulus (P_{ab}) and the liquid volume fraction in the top of the tubing ($\alpha_{L,tt}$). How realistic it is that these measurements are available in the real facilities are discussed in section (7.1). In reality, some of the measurements may be very poor, inaccessible because of their location in a harsh environment, consisting of noise or suffer from a big time delay.

The theoretical background that is used to perform the analysis and interpret the controllability results is mainly based on the theory presented in chapter 5 and 6 in the book "*Multivariable Feedback Control - Analysis and Design*" written by Skogestad and Postlethwaite [20]. Note that it is not the more widely known conventional *state controllability* that is analyzed in this thesis, on the contrary we are exploring the concept of input-output controllability. This concept is defined in chapter 5 in [20], :

(Input-Output) controllability *is the ability to achieve acceptable control performance; that is, to keep the outputs (y) within specified bounds or displacements from their references (r), in spite of unknown but bounded variations, such as disturbances (d) and plant changes (including uncertainty), using available inputs (u) and available measurements (y_m and d_m).*

6.1 Linearization

The low order nonlinear model derived in chapter (4), was linearized around an equilibrium point. This was done to be able to perform the controllability analysis in the frequency domain. An equilibrium point is a system state which does not change when all inputs to the model are constant, including disturbances. With a specific production valve opening (z_1^*), and gas lift choke opening (z_2^*), the equilibrium point can be calculated by simultaneously solving the state equations (4.2.1, 4.2.2, 4.2.3) set equal to zero. The result is a steady state solution with a corresponding steady state oil production flow rate. However, this equilibrium point may be unstable, in which case the flow rate will not be sustained when various disturbances are present. The non-linear system may have several equilibrium points for each combination of valve openings. Each point results in a different linearized systems. It was shown in chapter (2.6.1) that the optimal operating points are located in the unstable region of the system. With that in mind, the unstable operating point corresponding to $z_1^* = 60\%$ *and* $z_2^* = 40\%$ was chosen to linearize around. The opening of $z_2^* = 40\%$ is the value that corresponded to a gas injection rate of *0.86 [kg/s]*. It can be seen in the stability map of the low-order model, in figure (4.4.1), that this operating point is far from the stable region.

Linearization of the nonlinear model was carried out in Matlab, in three different ways. The reason for using different methods was simply to confirm that the resulting linear system was correct. Both the *forward difference method* and the *central difference method*, which are numerical differentiation methods were implemented based on the theory presented in chapter 8 in [21]. The implementation code of the central difference method

is given in appendix (D.0.3). Also an analytical differentiation was performed by using the model equations directly with the symbolic differentiation function, which is part of the symbolic toolbox, in Matlab. The analytical procedure was however very slow, it was also very cumbersome since it had to be changed each time the model was changed. Nevertheless, the use of the three different differentiation methods resulted in very similar linear systems. It was therefore concluded that the linearization was correctly performed. The central difference method was chosen as default in the continuation of the work, as it was faster than the analytical, and it is supposed to be slightly more accurate then the forward difference method, [21].

The disturbance variables in the system was decided to be the reservoir pressure and the pressure in the source of the lift gas. At the linearization point they were set to the constant values of 160 bara and 140 bara, respectively. The rest of the constants in the model were set to the values given in table (A.1). The resulting linear state space model with $\triangle u = [\triangle z1, \triangle z2]^T$, $\triangle d = [d_1, d_2]^T = [\triangle P_{res}, \triangle P_{gs}]^T$, $\triangle x = [x_1, x_2, x_3]^T$, $\triangle y = [w_{G_a,in}, P_{at}, P_{tt}, P_{ab}, P_{bh}, w_{out}, \rho_{mix,t}, \alpha_{L,tt}]^T$ is given as:

$$\triangle \dot{x} = A\triangle x + B\triangle u + B_d\triangle d \tag{6.1.1}$$

$$\triangle y = C\triangle x + D\triangle u + D_d\triangle d \tag{6.1.2}$$

where $\triangle$ is used to indicate that this is deviation variables from the values at the equilibrium point. The matrices has the following values:

$$A = \begin{bmatrix} -0.0023 & 0.0027 & 0.0006 \\ 0.0038 & -0.0174 & -0.0011 \\ -0.0232 & -0.1444 & -0.0019 \end{bmatrix} \tag{6.1.3}$$

$$B = \begin{bmatrix} 0 & 4.1233 \\ -1.4343 & -3.5407 \\ -29.4095 & 13.5285 \end{bmatrix} \quad B_d = \begin{bmatrix} 0 & 0.0199 \\ -0.0099 & -0.0001 \\ 0.3853 & 0.0653 \end{bmatrix} \tag{6.1.4}$$

$$C = \begin{bmatrix} -0.0002 & 0 & 0 \\ 0.0275 & 0 & 0 \\ 0 & 0.1104 & 0.0016 \\ 0.0307 & 0 & 0 \\ -0.0032 & 0.0474 & 0.0110 \\ 0.0223 & 0.1474 & -0.0004 \\ 0.4510 & -0.5255 & -0.0605 \\ 0.0006 & -0.0008 & -0.0001 \end{bmatrix} \tag{6.1.5}$$

$$D = \begin{bmatrix} 0 & 2.1515 \\ 0 & 0 \\ 0 & 0 \\ 0 & 0 \\ 0 & 34.2327 \\ 30.8439 & -20.4151 \\ 0 & -412.4968 \\ 0 & -0.5509 \end{bmatrix} \quad D_d = \begin{bmatrix} 0 & 0.0104 \\ 0 & 0 \\ 0 & 0 \\ 0 & 0 \\ 0 & 0.1653 \\ -0.1284 & -0.0986 \\ -2.5950 & -1.9913 \\ -0.0035 & -0.0027 \end{bmatrix} \tag{6.1.6}$$

6.2 Scaling the Model

To be able to do a sensible controllability analysis, and to compare the different transfer functions in the system, the linear model was scaled in the way outlined in chapter 1.4 in [20]. The scaling was done so that all signals in the system were less than one in magnitude. The scaling factors are based on allowed magnitudes of the inputs signals, and expected magnitudes of the reference change and disturbances. The following three diagonal scaling matrices are introduced: the control error scaling ($\tilde{D_e}$), the input scaling ($\tilde{D_u}$) and the disturbance scaling ($\tilde{D_d}$). Given the unscaled control error ($\hat{e}$), the unscaled output ($\hat{y}$), the unscaled input ($\hat{u}$) and the unscaled disturbance ($\hat{d}$), the corresponding scaled variables are: $e = \tilde{D_e^{-1}}\hat{e}$, $y = \tilde{D_e^{-1}}\hat{y}$, $u = \tilde{D_u^{-1}}\hat{u}$ and $d = \tilde{D_d^{-1}}\hat{d}$, respectively. The resulting scaled transfer functions describing the linear system are given as:

$$G = \tilde{D_e^{-1}}\hat{G}\tilde{D_u} \tag{6.2.1}$$

$$G_d = \tilde{D_e^{-1}}\hat{G_d}\tilde{D_d} \tag{6.2.2}$$

where $\hat{G}$, and $\hat{G_d}$, are the unscaled transfer functions of the system. The scaling values used in this analysis were:

$$\tilde{D_u} = \begin{bmatrix} 0.4 & 0 \\ 0 & 0.4 \end{bmatrix} \tag{6.2.3}$$

$$\tilde{D_d} = \begin{bmatrix} 3 & 0 \\ 0 & 3 \end{bmatrix} \tag{6.2.4}$$

$$\tilde{D_e} = \begin{bmatrix} 0.05 & 0 & 0 & 0 & 0 & 0 & 0 & 0 \\ 0 & 1 & 0 & 0 & 0 & 0 & 0 & 0 \\ 0 & 0 & 1 & 0 & 0 & 0 & 0 & 0 \\ 0 & 0 & 0 & 1 & 0 & 0 & 0 & 0 \\ 0 & 0 & 0 & 0 & 1 & 0 & 0 & 0 \\ 0 & 0 & 0 & 0 & 0 & 2 & 0 & 0 \\ 0 & 0 & 0 & 0 & 0 & 0 & 20 & 0 \\ 0 & 0 & 0 & 0 & 0 & 0 & 0 & 0.23 \end{bmatrix} \tag{6.2.5}$$

where is it seen that both disturbance variables are expected a maximum variation of 3 *bar* around their nominal values.

6.3 Theory for Input-Output Controllability Analysis

The evaluation of the input-output controllability of the system is conducted by calculating the lower bounds on different closed-loop transfer functions in the system. This section therefore presents the different transfer functions, and how to calculate their minimum bounds. The resulting bounds that are calculated is further evaluated in section (6.4) where it is concluded on which measurements in the system that should be used for stabilizing control of the model.

6.3.1 Closed-Loop Transfer Functions in Model

Assume a linear plant transfer function model on the form $y = G(s)u + G_d(s)d$, where y is the output, d is the disturbance and u is the output of a feedback controller on the

form $u = K(s)(r - y - n)$, where $K(s)$ is the transfer function of the controller, r is the desired reference value and n is the measurement noise. The objective of the controller is to manipulate the input (u) such that the control error ($e = y - r$) remains as small as possible, in spite of disturbances (d). As shown in chapter 2.2.2 in [20], substituting the controller expression into the plant model yields the closed loop transfer function:

$$y = \underbrace{(I + GK)^{-1}GK}_{T} r + \underbrace{(I + GK)^{-1}}_{S} G_d d - \underbrace{(I + GK)^{-1}GK}_{T} n \tag{6.3.1}$$

where S and T is know as the sensitivity and the complementary sensitivity function respectively. In equation (6.3.1), S is the closed loop transfer function from the output disturbance to the outputs, and T is the closed loop transfer function from the reference signal to the output. The control error can now be expressed as:

$$e = y - r = -Sr + SG_d d - Tn \tag{6.3.2}$$

and the input as:

$$u = KSr - KSG_d d - KSn \tag{6.3.3}$$

It follows that in a controllability analysis the information about achievable performance and possible robustness problems can be evaluated by obtaining the lower bounds on the closed-loop transfer functions S, T, KS, SG, KSG_d and SG_d, see [20] for a more thorough explanation. Introducing the loop transfer function $L = GK$, we can express the sensitivity and the complementary sensitivity function as

$$S = (I + GK)^{-1} = (I + L)^{-1} \tag{6.3.4}$$

$$T = (I + GK)^{-1}GK = (I + L)^{-1}L \tag{6.3.5}$$

from where it is seen that $S + T = I$. To achieve perfect control we want $e = y - r = 0$. Consider again equation (6.3.2). As explained in section 2.6 in [20], the requirement to achieve perfect control in terms of disturbance rejection and command tracking we need $S \approx 0$, or equivalently, $T \approx I$, which again implies that L must be large in magnitude. But to eliminate the effect of the measurement noise we need $T \approx 0$, or equivalently, $S \approx I$, which implies that L must be small in magnitude. This shows that in feedback design there is a trade-off between good disturbance rejecting and tracking versus a small effect of the noise.

6.3.2 Pole and Zero Vectors and Directions

Central to the controllability analysis is the theory of pole vectors. Pole vectors are also used to calculate some of the bounds on the closed loop transfer functions. As explained in chapter 4 in [20], in multivariable systems, poles and zeros has directions associated with them. To quantify them we use the input and output pole and zero vectors of the system. Only output pole vectors are used in this project, and its direction is used for calculating the bound on sensitivity and complementary sensitivity function in equation (6.3.10). For the state space realization of the linear system, we have found an measurement matrix (C), in equation (6.1.5). The output pole vector ($\hat{y}_{pi}$) is now defined as:

$$\hat{y}_{pi} = Ct_i \tag{6.3.6}$$

where t_i is the right eigenvector of the state matrix (A) found in equation (6.1.3). The pole vectors give an indication of how much the $i'th$ mode is observed in the output. Now

pole directions (y_{pi}) are defined to be pole vectors with unit length, that is:

$$y_{pi} = \frac{\hat{y}_{pi}}{\| \hat{y}_{pi} \|_2} \tag{6.3.7}$$

It is shown in [22] that for a system with only one unstable pole, there is a relationship between the magnitude of the input and the magnitude of the pole vector elements. The measurement with the largest element in the output pole vector should be used for stabilizing control, as this corresponds to the minimum input usage for stabilization.

6.3.3 Minimum Peaks on Closed-Loop Transfer Functions

Skogestad and Postletwaite [20], derives some algebraic and analytic constraints for different closed-loop transfer functions. Bounds on peaks of the different transfer functions described in section (6.3.1) are considered using the H_∞ - norm, defined as

$$\|M(s)\|_\infty \triangleq \max_\omega \mid M(j\omega) \mid \tag{6.3.8}$$

which is the peak, i.e., the maximum value, of the frequency response of M.

6.3.4 Minimum Peaks on S and T

The lowest achievable peak on S and T is influenced by the RHP-zeros and RHP-poles of the system. Theorem 5.2 in chapter 5 in [20] states that a RHP-zero implies that a peak in $\mid S \mid$ is inevitable. It also tells us that the peak will increase if we reduce $\mid S \mid$ in other frequencies, which is refereed to as "*the second waterbed formula*". Denoting the minimum peak in S *as* $M_{S,min}$, the bound on $M_{s,min}$ for closed loop stability for a $SISO$ system is given in theorem 5.3 in [20] as :

$$M_{S,min} \geq \prod_{i=1}^{N_p} \frac{|z + p_i|}{|z - p_i|} \tag{6.3.9}$$

which must be satisfied for each RHP-zero z, where N_p denotes the number of RHP-poles, p_i , of the plant transfer function $G(s)$. The bound holds with equality for a system with a single unstable zero and no time-delays. The equation shows that the lowest achievable peak in S is closely related to the distance between the unstable poles and zeros, and it is noted that the bound approaches infinity as the distance $|z - p_i|$ approaches zero. Denoting the minimum peak for T as $M_{T,min}$, it is proved in Chen in [23], that the bound in equation (6.3.9) also apply for $M_{T,min}$. Chen further generalize the bound for $MIMO$ systems, with any number of unstable poles and zeros:

$$M_{S,min} = M_{T,min} = \sqrt{1 + \bar{\sigma}^2(Q_p^{-\frac{1}{2}} Q_{zp} Q_z^{-\frac{1}{2}})} \tag{6.3.10}$$

where $\bar{\sigma}$ is the maximum singular value[1]. The elements in Q_z, Q_p, Q_{zp}, are given as follows:

$$[Q_z]_{ij} = \frac{y_{z,i}^H y_{z,j}}{z_i + \bar{z}_j}, [Q_p]_{ij} = \frac{y_{p,i}^H y_{p,j}}{\bar{p}_i + p_j}, [Q_{zp}]_{ij} = \frac{y_{z,i}^H y_{p,j}}{z_i - p_j} \tag{6.3.11}$$

where $\bar{z}$, and $\bar{p}$, denotes the complex-conjugate of the zero and pole, respectively. And $y_{z,i}$ and $y_{p,i}$ are the direction vectors previously defined in equation (6.3.7), associated with the zero z_i and the pole p_i. And y^H is the conjugate transpose, also refereed to as the *Hermitian* transpose. Time delays will add additional limitations, but are not considered in the calculations done is this assignment.

[1] $\sigma_i(G) = \sqrt{\lambda_i(G^H G)}$

6.3.5 Lower Bound on KS

As seen in equation (6.3.3), the transfer function KS describes the effect the measurement noise n and the reference r has on the control input. It also contributes to the effect the disturbance has on the input. We desire that the peak of KS is small, particularly for unstable systems, as this will avoid a large change in the input signal in response to noise and disturbances. A large peak value in KS indicates that the input may easily saturate, which is highly unwanted as a saturated input will have a problem with stabilizing the system. For multiple and complex unstable poles , Glover shows in [24] that the following bound applies:

$$\|KS\|_\infty \geq \frac{1}{\sigma_H(\Omega(G)^*)} \tag{6.3.12}$$

where $\sigma_H(\Omega(G)^*)$ is the smallest *Hankel* singular value of the mirror image of the anti-stable part of G. The mirror image of the anti-stable part of G is the resulting system when mirroring all unstable parts of G into the LHP. The Hankel singular values are the square root of the eigenvalues of the product of the controllability and the observability gramians of the system, see pages 160-161 in [20].

An alternative bound that holds with equality for a single real RHP-pole (p) is given in [25] as:

$$\|KS\|_\infty \geq \mid G_s(p)^{-1} \mid \tag{6.3.13}$$

where $G_s$is the the stable version of an plant G found by mirroring all RHP poles into the LHP.

6.3.6 Lower Bound on SG_d and SG

In equation (6.3.2) it is seen that the transfer function SG_d describes how the disturbance d effects the control error. This bound should be kept small to suppress the influence of the disturbance to the system. In [23] the following bound for any unstable zero (z) is derived:

$$\parallel SG_d \parallel_\infty \geq \mid G_{d,ms}(z) \mid \prod_{i=1}^{N_p} \frac{|z+\bar{p}_i|}{|z-\bar{p}_i|} \tag{6.3.14}$$

the bound is tight for systems with one unstable zero. $G_{d,ms}$ is the stable minimum phase version of G_d, and can be calculated as defined in equation 5.27 in [20]:

$$G_{d,ms} = \prod_i \frac{s-p_i}{s+p_i} G_d \prod_j \frac{s+z_j}{s-z_j} \tag{6.3.15}$$

Consider again equation (6.3.2). With only disturbances (d_u) on the input variables (u) to the system, then G_d becomes G, and SG now becomes the transfer function from the input-disturbance to the error. We desire that the bound on SG is small so that the effect of input disturbances on the error is small. Since G_d now is G, the bound on SG can be calculated with the same equation (6.3.15) if $G_{d,ms}$ is replaced with G_{ms}.

6.3.7 Lower Bound on KSG_d

As seen in equation (6.3.3), the transfer function KSG_d is the transfer function from the disturbance d to the input u. For the disturbance to have a little effect in the input to

the plant, this bound should be small. For a system with multiple and complex unstable poles, [20] derive the following bound:

$$\| KSG_d \|_\infty \geq \frac{1}{\sigma_H(\Omega(G_{d,ms}^{-1}G))} \tag{6.3.16}$$

where $G_{d,ms}^{-1}$ is the inverse of the stable minimum phase version of G_d. An alternative bound which is tight for systems with a single real unstable pole is given in [20] as:

$$\| KSG_d \|_\infty = \mid G_s^{-1}(p) \mid \cdot \mid G_{d,ms}(p) \mid \tag{6.3.17}$$

6.4 Discussion of the Calculated Bounds

The minimum peaks on each of the different bounds presented in section, (6.3.4)-(6.3.7), were calculated in a Matlab script by Esmaeil Jahanshahi. The results of the calculations are presented in tables (C.1), (C.2), (C.3), in appendix (C). Based on the results several conclusions can be made about how suitable each of the measurement candidates are to be used for stabilizing control in combination with the respective manipulated variables.

6.4.1 Single Control Structures

We start by evaluating the bounds presented in table, (C.1), for single input single output control systems, with the production choke as the manipulated variable. The best measurement candidate can easily be seen to be the pressure in the bottom hole (P_{bh}), as it has the lowest peaks on all of the calculated bounds. Furthermore, this measurement has the greatest steady state gain, and the largest pole vectors. This means that a little change in the bottom hole pressure variable causes a larger change in the system dynamics when compared to using any of the other measurement candidates. The result is that when this measurement is used as the controlled variable, there is a lower chance that the manipulated variable, i.e., the production choke, will saturate when the controller is trying to stabilize the system or reject disturbances, than if any of the other measurements are used. Unfortunately, the pressure in the bottom hole is know not to be directly measurable, but this is discussed later in the thesis.

The second best measurement candidate can be seen in the table to be the pressure in the bottom of the annulus. This is justified by the same arguments, that all the peaks on the calculated bounds are lower than most of the other measurements. Surprisingly, the pressure in the top of the annulus has almost as low peak on the bounds as the annulus bottom pressure. However the peak on KS is larger, which means that measurement noise will have a larger effect on the manipulated variable, as explained in section (6.3.5). The result will be that the valve is more likely to saturate when using the top pressure in the annulus as the controlled variable, as opposed to using the bottom pressure in the annulus. This is also validated by the fact that the steady state gain for the top pressure is lower than for the bottom pressure.

The single worst measurement candidate to be used as the controlled variables can be seen in the table to be the liquid volume fraction in the top of the tubing. This is because it has high minimum peaks on all of the bounds, which in turns means that it is both very sensitive to measurement noise, responds poorly when exposed to disturbances, and it is very likely to saturate the manipulated variable when it tries to stabilize the system.

The second worst candidate is either the density mixture in the top of the tubing, or the pressure in the top of the tubing. While the density can be seen to have a higher peak on the KS bound, meaning that is will respond poorly to measurement noise, the tubing top pressure has the definitely largest peak on the SG bound, meaning that an input disturbance will have a large effect on the control error, as explained in section (6.3.6). Judging by the result of the analysis, these measurements are not recommend to be used as controlled variables in single measurement control structures.

6.4.2 Combined Control Structures

Next we evaluate the minimum peaks on the calculated bounds for control structures that uses two measurements and one single manipulated variable. These control structures are called Single Input Multiple Outputs (SIMO) in this thesis, and the bounds are presented in table (C.2), in appendix (C). The manipulated variable is still the production choke on the top of the tubing.

It can be seen in the table that all measurement pairs in which the pressure in the bottom hole is combined with any other measurement show to be some of the best control structures, with low peaks on all of the bounds. This is not surprising, as the analysis for single control structures showed the bottom hole pressure to be the single best measurement candidate. However, by combing it with other measurements, is shows slight improvements, as can be seen by small reductions in the minimum peaks for some of the bounds. It is interesting to see that when combining the bottom hole pressure in the tubing with one of the worst measurement candidates from the SISO analysis, namely the mixture density it the top of the tubing, the control structures obtains a lower peak in the KSG_{d1} bound, while the rest of the bounds remain identical. This means that when combing the two measurements, the control structure will improve its performance in rejecting disturbances in the reservoir pressure, compared to when only using the bottom hole pressure alone. The improvement however, is small.

The single best combined control structure, which has the lowest peaks on all of the bounds are the combination of the bottom hole pressure measurement with the tubing top pressure measurement. This control structure is only slightly better then when combining the bottom hole pressure with the mass production flow rate. Interestingly enough, a combination of the measurement in the top of the annulus and top of the tubing proves to be almost as good as the best combination structures with the bottom hole pressure. The only difference is that the top pressure combination has a higher peak in the KS bound, which unfortunately means that the input, i.e., the valve, is more likely to saturate when the system is exposed to measurement noise. However, as will be further discussed in section (7.1), a control structure which only uses top side measurements are favorable to any one using bottom pressure measurements, as the measurements near the surface are both more reliable and accessible.

6.4.3 Multivariable Control Structures

Finally it is tested if any control structures with two inputs and two outputs, a so called Multiple Input Multiple Output (MIMO) system, will show any improvements in control. In this case, both the production choke on the top of the tubing and the gas injection

choke on the top of the annulus, are the manipulated variables. The calculated minimum peaks on the bounds are presented in table (C.3), in appendix (C).

When comparing the MIMO results to the SIMO results, it is clear that improvement in adding the gas injection gas as an extra manipulated variable is poor. Of course there are some improvements by lower peaks in some of the bounds, however not so much that it seems to be worth the added complexity of the control structure. There are however other benefits of adding an extra input to the system. By having two manipulated variables, one may in theory control two controlled variables to their respective setpoint. Furthermore, if one controller breaks down, the other may be able to keep the system stable.

6.4.4 The Effect of The Disturbances

It is interesting to see that all of the control structures are more affected by a disturbance in the reservoir pressure, compared to a disturbance in the gas source pressure, containing the extra lift gas. This can be seen in tables (C.1), (C.2), and (C.3), as the minimum peaks in KSG_{d1} and SG_{d1} is much higher than the minimum peaks for the KSG_{d2} and SG_{d2} bounds. It is therefore decided that to restrict the number of different simulations scenarios, when testing the most promising control structures further, only a disturbance in the reservoir pressure is applied.

6.5 Selecting the Control Structures

Based on the above discussion of the controllability results, it was decided to test and compare some of the most promising control structures further in simulations. Since the pressure in the bottom hole showed great results, at least one control structure using it as the controlled variable, and the production choke as the manipulated variable should be tested. Furthermore the other promising control structure in which a combination of the top pressure measurement in the tubing with the top pressure measurement in the annulus will be tested. Also it is decided to test a state feedback control structure to see how it compares to the output feedback controllers.

The controllability results showed some improvements by adding the gas injection choke as an extra manipulated variable in the control structures. However, in the fall project assignment it was performed another analysis which considered the gas injection choke as a single manipulated variable in combination with the different measurements. The results proved this input to be inadequate to stabilize the system when any realistically disturbances entered the system. With that in mind, and to limit how many control structures to compare further in simulations, it was decided not to test any control structures involving the gas injection choke as a manipulated variable.

Chapter 7

Estimator for Gas-Lift System

7.1 Availability of Measurements and States

In section (6.4), the results of the controllability analysis proved that the single best measurement to use for both stabilizing control and disturbance rejection is the bottom hole pressure, which in some literature is referred to as the downhole pressure. See figure (1.2.1), for its location. Another good measurement candidate to use for control, was shown to be the pressure in the bottom of the annulus. These results are of course only based on a linearized model around one operating point of the low order model. However the low order model was fitted to the OLGA flow simulator which is believed to be of high accuracy, so it is assumed that the result of the analysis should be somewhat realistic and applicable for the real flow facilities as well. Even though the analysis proved the bottom pressures in both the annulus and tubing to be a good measurement candidates, it is not yet discussed to what degree these measurements are really available in the real facilities.

When considering the location of the bottom hole pressure, deep under the surface in the bottom of the tubing, near the reservoir, it is not surprising that this single measurement has shown in practice not the be very accessible. In [26], by Aamoe et al, it is stated that based on a Statoil report [27], the downhole pressure measurement is generally not available. Neither is the bottom pressure in the annulus. Further it is noted that in the case that they are available, the measurements must be considered unreliable, i.e., noisy or with a high rate of failure. This is due to the fact that the pressure senors are are located in harsh environment with high pressure and temperature. In addition, if the sensors are broken, they are inaccessible for maintenance due to their location. Nevertheless, engineers are continuously working on improving the down hole pressure measurements. In an article posted in *World Oil,* based on a case study performed by Schlumberger, [28], it is shown that they were able to achieve a sufficient pressure measurement, from the harsh environment, by using a signature quartz gauge in a gauge carrier. The duration of the study however, was only 15 days.

Based on the actual availability of the measurements, it is decided that an estimator should be introduced to the gas lift system when testing a control structure that uses the bottom hole pressure as the measurement. In this thesis the estimator is tested in different scenarios. The first scenario is to estimate the bottom hole pressure by only using the available top side pressure measurements, in the tubing and annulus. In this case the

estimator is tested when these measurements are available with or without noise. When noise is applied, it is white noise. In practice, these measurement would of course always be affected by noise to some extent. However, by assuming that this noise is small, it can be neglected. In the second scenario, the bottom hole pressure is considered available, but noisy. In this case, white noise is added to the measurement. It is also investigated if the estimator is able to sufficiently estimate the states in the low order model, so that the state estimates can be used in a state feedback controller.

7.2 Choice of Estimator

The Extended Kalman Filter (EKF) is one of the most widely applied estimators for non-linear systems, [29]. However one of the filter shortcomings is that it arrives at its estimate through linearization of the non-linear model. Years of research and use of the EKF has unfortunately proven that the filter has the disadvantage that it only provides sufficient estimates for system that are almost linear on the time scale of the updates, [30]. It has also been shown that it is hard to implement and difficult to tune. See chapter 14 in [29] for detailed examples on how the use of first-order linearization in the EKF, to update the mean of the state, results in erroneously estimates when applied to nonlinear systems.

A literature search, of former applied estimators in gas-lift systems, reveals that the standard EKF has already been tested in a similar study, performed by Eikrem et al. in [16]. Even though the state estimate results were adequate, they were to a large extent based on the availability of the down-hole pressure measurement. In the article it is also claimed, that from an industrial point of view, it is realistic that this measurement is available but unreliable, because of its location in a harsh environment. In another article covering estimation in gas-lift systems, by Aamoe et al. , [26], a non-linear state observer is designed using top measurements only. However it is assumed that one of the states, the mass of gas in the annulus, is measured. Promising results are achieved, but since the observer is designed using parts of the specific model equations directly, it may be difficult to apply the estimator, without modification, on other models.

Based on the type of estimators applied on gas-lift models in other similar work, there seems to be an absence in the use of the Unscented Kalman Filter (UKF). It was therefore decided to test this filter, which has shown promising results for other non-linear models, unrelated to gas-lift, [31]. The UKF also posses the desired property that it avoids local linearization when calculating the estimates, which, as explained above, is a source of error in the EKF. Instead the filter uses the non-linear model directly to propagate estimates forward in time, [32]. This seems promising for the model at hand.

7.3 The Unscented Kalman Filter

7.3.1 The Principle of The UKF

The unscented Kalman filter is based on the assumption that it is easier to approximate a probability distribution than it is to approximate an arbitrary nonlinear function or transformation [33]. The idea is to generate a set of perturbed points around the current state estimate. These perturbed points, which in the literature is commonly referred to

as sigma-points, are then further transformed by propagating them through the nonlinear system equations. The weighted average of the transformed points is further used in the calculation of the new state- and measurement -estimate, as explained in more detail in section (7.3.2.4). The sigma-points are selected so that the ensemble mean and covariance of the points are equal to the state estimate and state covariance matrix, respectively, at the previous time-step. How this is done in practice is shown in section *(7.3.2.3).* The idea is that the ensemble mean and covariance of the transformed vectors should give a good estimate of the true mean and covariance of the measurement, [29].

7.3.2 UKF Algorithm

There exist different versions of the filter with minor variations, but they are all based on the same principle previously explained in section (7.3.1). The version of the filter that is chosen to implement in this thesis is the one presented in [31], in which a modification from the original filter is made by introducing one extra sigma-point into the calculations of the state estimate. As a result of introducing this additional point, the original points in the set must be scaled to maintain the given covariance. The steps in UKF algorithm is presented below and the Matlab implementation is included in appendix (D.0.4).

7.3.2.1 The Filter Model

The nonlinear low-order model derived in section (4) can be presented on the following form:

$$x_{k+1} = f(x_k, u_k) + \phi_k \tag{7.3.1}$$

where, x_k , is the state vector at time-step k, u_k , is the control input at time-step k, f is the non-linear state equation, and ϕ_k is the state excitation noise. The measurements in the the model can similarly be written as:

$$y_k = h(x_k, u_{k-1}) + \psi_k \tag{7.3.2}$$

where, y_k, is the measurement vector at time-step k, h is the non-linear measurement equation, and ψ_k is the measurement noise.

The noise entering the state and measurement equations are both assumed to be zero mean, normally distributed and with know covariances, Φ and Ψ, respectively, [32]. Note that for simplicity it is assumed that both the noise on the states (ϕ_k) and measurements (ψ_k) enter the system equations linearly. The filter can easily be modified to handle noise which enters the system equations non-linearly, by augmenting the state vectors with the noise as shown in [29]. That was not emphasized in this simulation study.

7.3.2.2 Initializing The Filter

Prior to starting the estimation algorithm, the filter must be initialized with a start value for the mean of the state, $\hat{x}_0$. This can be the actual value, or a guess which seems reasonable. In this simulation study the actual value will of course be available from the model, but in the real facilities one can only assume the initial value, as it is not available to measure. Initial values for the state covariance P_x, is also necessary. The initial value of the covariance will only affect the transient of the estimate response, and its effect will fade out as time progresses when it is updated through the filter equations .

7.3.2.3 Calculating The Sigma-Points

At each iteration this version of the UKF filter calculates $2N+1$ sigma points, where N is the number of states in the model, i.e., 3, in the gas-lift model. The sigma-points, (x_S), at the current time step, are calculated through the use of the latest estimate of the state covariance, (P_x), from the previous iteration, in the following way:

$$\begin{cases} x_S^{(i)} = \hat{x}_{k-1} & , i = 1 \\ x_S^{(i)} = \hat{x}_{k-1} + \Gamma p^{(i)} & , i = 2, ..., N+1 \\ x_S^{(i)} = \hat{x}_{k-1} - \Gamma p^{(i)} & , i = N+2, ..., 2N+1 \end{cases} \tag{7.3.3}$$

where $p^{(i)}$ is the transposed i'th row in the matrix square root of the state covariance matrix, that is:

$$p^{(i)} = \left(\sqrt{P_x}\right)_i^T \tag{7.3.4}$$

defined so that $\left(\sqrt{P_x}\right)^T \left(\sqrt{P_x}\right) = P_x$, [32]. Γ is a constant scaling parameter defined to be:

$$\Gamma = \alpha\sqrt{(N+\kappa)} \tag{7.3.5}$$

which is tuned through the constants α, and κ. N is the previously defined state dimension. The α- parameter should ideally be a small number [34], however no smaller than zero and no greater than one, i.e. , $0 \leq \alpha \leq 1$. It controls the size of the sigma-point distribution [31], and according to [35] its value will only affect the higher order of the nonlinear system. The κ - parameter must be chosen $\kappa \geq 0$, to guarantee the semi-positive definiteness of the state covariance matrix [31]. Note that each of the sigma-points are vectors with the same dimension as the state vector, and that the, *i,* in $x_S^{(i)}$, indexes the sigma-point vector number, not the individual elements in the vector.

7.3.2.4 Transformation and The a-priori State Estimate

Each of the $2N+1$ sigma-points calculated in section (7.3.2.3) are transformed $(x_S \rightarrow x_T)$ by individually propagating them through the nonlinear system state equation, as follows:

$$x_T^{(i)} = f(x_S^{(i)}, u_{k-1}), i = 1, ..., 2N+1 \tag{7.3.6}$$

The transformed points are further combined to obtain the a-priori state estimate:

$$\hat{x}_k^- = \sum_{i=1}^{2N+1} (w_m^{(i)} x_T^{(i)}) \tag{7.3.7}$$

where $w_m^{(i)}$ is a weight defined as:

$$\begin{cases} w_m^{(i)} = \dfrac{\Gamma^2 - N}{\Gamma^2} & , i = 1 \\ w_m^{(i)} = \dfrac{1}{2\Gamma^2} & , i = 2, ..., 2N+1 \end{cases} \tag{7.3.8}$$

Now that the a-priori state estimate $(\hat{x}_k^-)$ is derived, the a-priori state covariance is calculated as the weighted average quadratic difference from the transformed points, in the following way:

$$P_x^- = \sum_{i=1}^{2N+1} w_c^{(i)} (x_T^{(i)} - \hat{x}_k^-)(x_T^{(i)} - \hat{x}_k^-)^T + \Phi \tag{7.3.9}$$

where $w_c^{(i)}$ is a weight defined as:

$$\begin{cases} w_c^{(i)} = \dfrac{\Gamma^2 - N}{\Gamma^2} + (1 - \alpha^2 + \beta) & , i = 1 \\ w_c^{(i)} = \dfrac{1}{2\Gamma^2} & , i = 2, ..., 2N + 1 \end{cases} \tag{7.3.10}$$

where β is a non-negative weighting parameter. According to [31], it is introduced to affect the weighting of the first sigma-point, so that the covariance of the ensemble remains identical to what it would be for the original filter algorithm that uses one less sigma-point. It is further stated that knowledge of the higher order moments of the probability distribution can be incorporated in the βparameter, and that the choice, $\beta = 2$, is optimal for a Gaussian prior probability distribution.

7.3.2.5 Transformation and The a-priori Measurement Estimate

The same principle is used to estimate the measurement. Each of the sigma-points derived in equation (7.3.3), are transformed ($x_S \rightarrow y_T$) by individually propagating them through the nonlinear system measurement equation, as follows:

$$y_T^{(i)} = h(x_S^{(i)}, u_{k-1}), i = 1, ..., 2N + 1 \tag{7.3.11}$$

The weighted mean of the transformed outputs, i.e., the a-priori measurement estimate, is calculated in a similar way to what is done in equation (7.3.7), that is:

$$\hat{y}_k^- = \sum_{i=1}^{2N+1} (w_m^{(i)} y_T^{(i)}) \tag{7.3.12}$$

Using the a-priori measurement estimate, the measurement covariance (P_y^-) is found in the following way:

$$P_y^- = \sum_{i=1}^{2N+1} w_c^{(i)} (y_T^{(i)} - \hat{y}_k^-)(y_T^{(i)} - \hat{y}_k^-)^T + \Psi \tag{7.3.13}$$

note that the weights (w_m and w_c) are the same as defined in equation (7.3.8) and (7.3.10) respectively.

7.3.2.6 Cross-Covariance, Kalman Gain and UKF-Estimate

Now that we have the a-priori estimates, the transformed states and the transformed measurements, the cross covariance is given as:

$$P_{xy} = \sum_{i=1}^{2N+1} w_c^{(i)} (x_T^{(i)} - \hat{x}_k^-)(y_T^{(i)} - \hat{y}_k^-)^T \tag{7.3.14}$$

Using this, we can now calculate the Kalman gain:

$$K_k = P_{xy} P_y^{-1} \tag{7.3.15}$$

Finally the UKF estimates and state covariance is updated according to the standard Kalman update equations:

$$\hat{x}_k = \hat{x}_k^- + K_k(y_k - \hat{y}_k^-) \tag{7.3.16}$$

$$P_x = P_x^- - K_k P_y^- K_k^T \tag{7.3.17}$$

where y_k is the actual measurement entering the filter at time-step k. The estimation algorithm is complete, and repeats itself at the next time-step when a more recent measurement becomes available.

7.4 Estimation with model uncertainty

The Unscented Kalman filter is tested on two different models in this report, the low-order model and the OLGA-model. As previously stated, the OLGA-model is regarded to be the real flow process in this work. The estimator however, uses the system equations from the low-order model, as described in section (7.3.2.1). When the estimator is used in this thesis, the objective is to estimate the states and measurements that are considered unmeasurable. The estimates are based on the outputs that are considered available. Consequently, when the estimator is applied on the OLGA-model, the optimal estimate will to a large degree depend on how accurately the low-order model is able to replicate the OLGA-model. The resulting estimates of the OLGA-models unmeasurable states and outputs, can only be as good as the compliance, i.e., the match of the models. This is now elaborated in greater detail.

Consider the case in which the objective is to obtain an estimate of the bottom-hole pressure in the OLGA-model, when the available measurement is the pressure in the top of the tubing. The UKF will use the difference between the latest estimation and measurement, of the top-pressure, to update the state-estimate. This is shown in equation (7.3.16). Note that the estimated top-pressure is based on the filter-model (which is the low-order model), but the measured top-pressure is the output from the OLGA-model. The resulting estimated state is used as input to the measurement-equation in the filter-model, to retrieve the bottom-hole pressure estimate. However, because of the model uncertainty, the state-estimate that corresponds to an exact estimate of the OLGA-model top-pressure, may not necessarily produce an exact estimate of the OLGA states or OLGA bottom hole pressure. This is a result of the model-mismatch, i.e., the low-order model does not replicate real process (the OLGA-model) in a perfect manner. Consequently the error in the estimate of the states, and outputs, that can not be measured, will depend on the difference between the models at that point. It is previously shown in the bifurcation diagrams in figure (5.1.1) that the low-order model fails to reproduce the exact same outputs as the OLGA-model. An estimation error is therefore expected when the UKF is applied on the OLGA model. A possible solution could be to include parameter estimation into the estimation algorithm. However, as the bottom hole pressure is just one of several control structures that are tested in this thesis, it was decided not too spend any more time on further enhancing the filter.

7.5 Open Loop Estimation

In this section, the derived estimator is tested in open loop simulations of both the low order model and the OLGA flow simulator in different scenarios.

7.5.1 Low-Order Model Estimation

First the estimator is applied to the low order model.

7.5.1.1 Estimation Results Using Top Pressure Measurements

In this first scenario, the estimator is tested when the available measurements are the top pressure in the annulus and the top pressure in the tubing. White noise is added to the two measurements. The objective is to estimate the real value of the top measurements, that is, to filter out the noise. Furthermore the states and bottom hole pressure in the tubing are estimated. The initial states of the estimator is set to different values than the actual real values, even though it is difficult to see it in the plotted results. This is because an accurate estimate is reached fast, and the simulations is over a longer time period. The tuning parameters in the filter, which was explained above, is set to the following values:

UKF Tuning Parameters				
Ψ		$\begin{bmatrix} 0.968 & 0 \\ 0 & 0.968 \end{bmatrix}$		
Φ	1e-04*	$\begin{bmatrix} 1 & -0.1 & 0.1 \\ -0.1 & 1 & -0.1 \\ 0.1 & -0.1 & 1 \end{bmatrix}$		
α	0.001			
β	2			
κ	0			

The estimation results of the bottom hole pressure in given in figure (7.5.1) below.

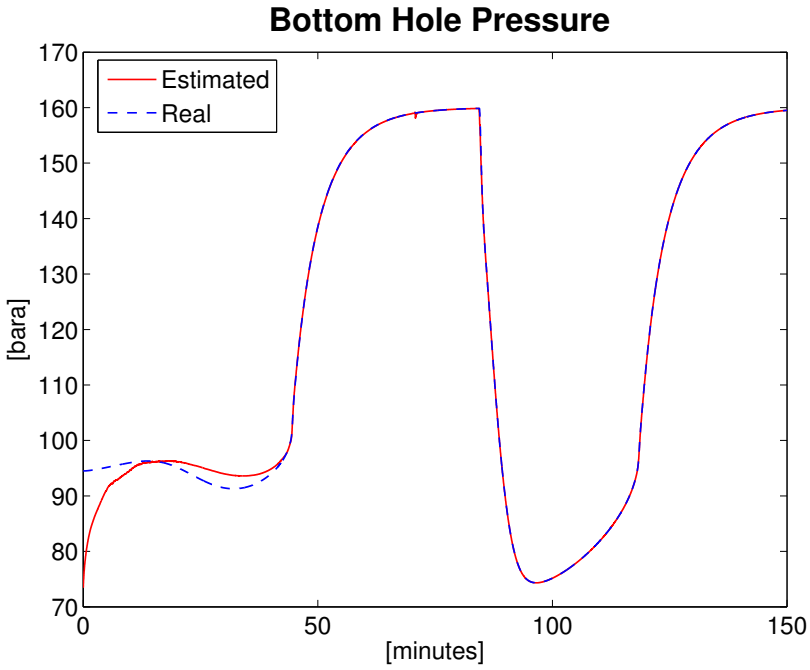

Figure 7.5.1: Open Loop Bottom Hole Pressure Estimation

It seems like the UKF is successful in achieving an accurate estimate of the bottom hole

pressure by only using two noisy top pressure measurements. This proves promising for further using the estimator in combination with a controller.

The estimation of the states are shown in figure (7.5.2).

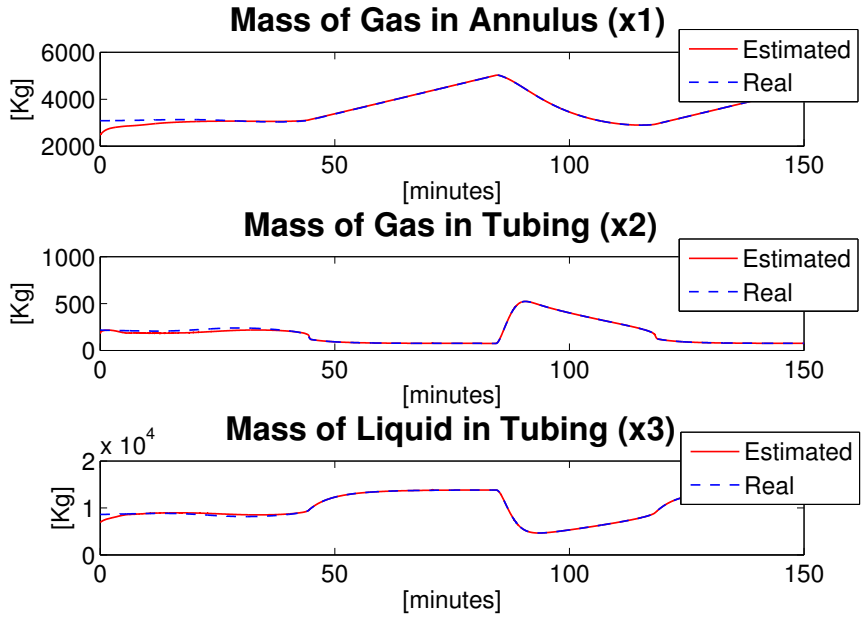

Figure 7.5.2: Open Loop State Estimation

It can bee seen that an accurate estimate of the states are also reached rapidly, which enables for the use of a state feedback estimator where the actual states are replaced with the estimated states. Figure (7.5.3) shows the noisy measurements which is feed to the estimator, the real value of the pressures, and the estimated value by the UKF.

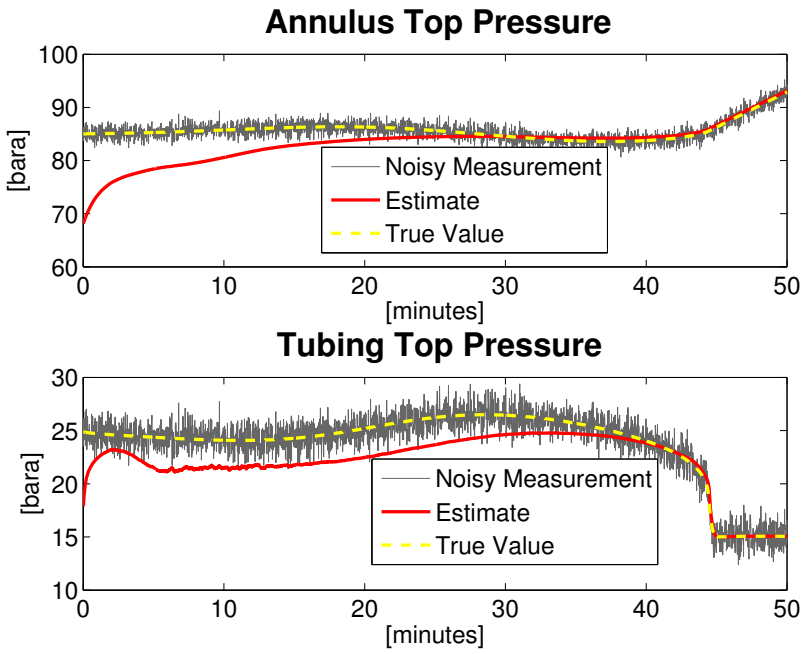

Figure 7.5.3: Open Loop Top Pressures Estimate

It can be seen that the estimator filters out the noise and rapidly reaches the correct values of the pressures. To conclude, the estimator shows very promising result when applied to the low order model. Of course, since the estimator is based on the same model equations as the low order model, and it is only added white noise to the measurements, the results are not that impressing. It will be more interesting to see how the estimator works on the OLGA simulator with different dynamics.

7.5.2 OLGA Model Estimation

Next the estimator is applied to the advanced OLGA flow simulator. This is a greater challenge, as the estimator is based on the low order model equations.

7.5.2.1 Estimation Results Using Top Pressure Measurements

In the first scenario, it is tested if the estimator is able to produce an accurate estimate of the bottom hole pressure in the tubing when two perfect top pressure measurements are available. The two available measurements are once again the top pressure in the annulus and the top pressure in the tubing. The tuning parameters in the UKF are set to the following values:

UKF Tuning Parameters	
Ψ	$1e-4 * \begin{bmatrix} 1 & 0 \\ 0 & 1 \end{bmatrix}$
Φ	$\begin{bmatrix} 5 & -0.1 & 0.1 \\ -0.1 & 1 & -1 \\ 0.1 & -1 & 100 \end{bmatrix}$
α	0.001
β	2
κ	0

Figure (7.5.4) shows the response of the estimation of the bottom hole pressure in the tubing.

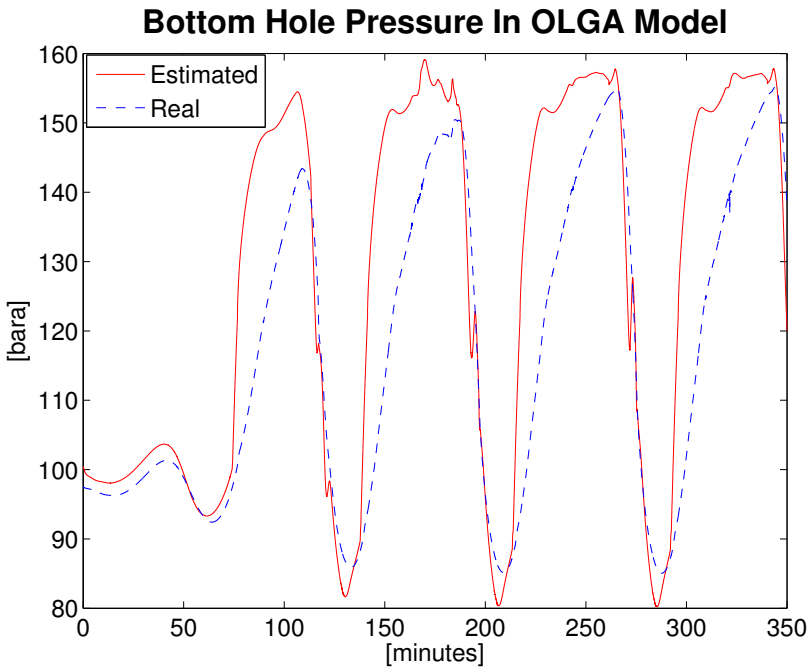

Figure 7.5.4: OLGA Open Loop Bottom Hole Pressure Estimate

The estimate is far from perfect. It may seem like the estimate is sufficient at some points through the simulation, but by a closer inspection it is noted that the difference between the estimate and the actual value is at most about 15 bars. This estimate is probably not adequate to be used for control. Further in figure (7.5.5), the estimate of the states are shown.

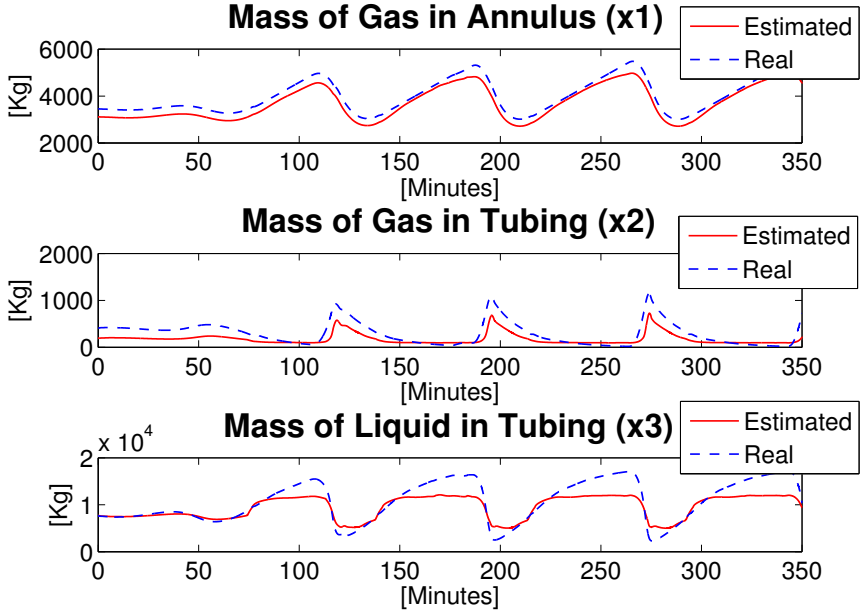

Figure 7.5.5: OLGA Open Loop State Estimation

Also the estimate of the states shows a big discrepancy from the actual values. Especially the third state (x_3) , i.e., the liquid mass in the tubing, is poorly estimated. It is concluded that any control structure that uses these estimates will probably not perform in a sufficient manner.

7.5.2.2 Estimation Results Using Top Pressures and Noisy Bottom Hole Pressure Measurements

In this scenario, the two top pressure, i.e., the pressure in the top of the annulus, and the pressure in the top of the tubing, are consider available without noise. Furthermore, a noisy measurement of the bottom hole pressure in the tubing is also available. White noise is added to the bottom hole pressure measurement. How realistic this scenario is can be discussed, but it is probably not very likely. The tuning parameters for the UKF is now set to:

UKF Tuning Parameters	
Ψ	$1e-4 * \begin{bmatrix} 1 & 0 & 0 \\ 0 & 1 & 0 \\ 0 & 0 & 1 \end{bmatrix}$
Φ	$\begin{bmatrix} 5 & -0.1 & 0.1 \\ -0.1 & 1 & -1 \\ 0.1 & -1 & 100 \end{bmatrix}$
α	0.001
β	2
κ	0

The noisy bottom hole pressure measurement, as well as the actual value of the bottom hole pressure, and the estimated value is shown in figure (7.5.6).

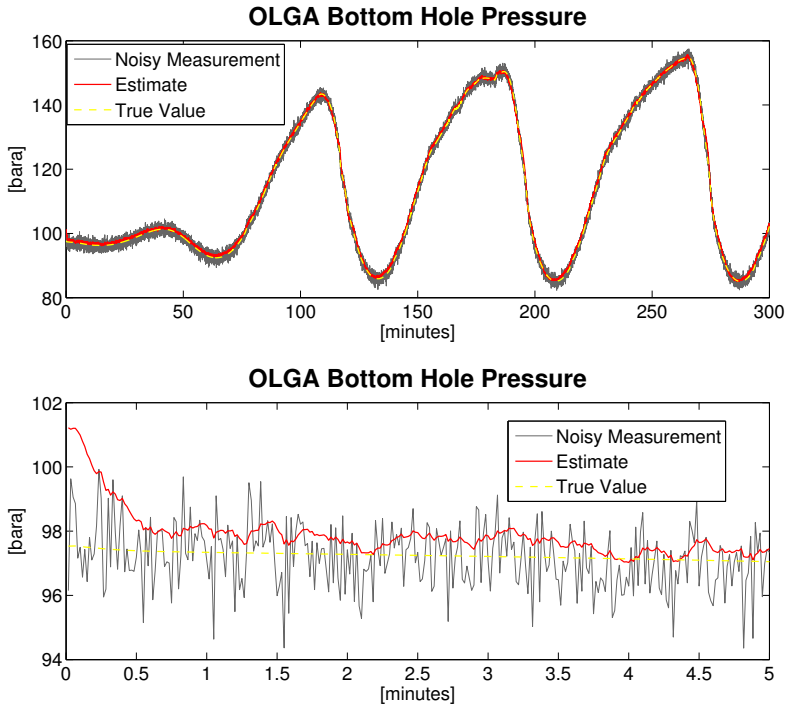

Figure 7.5.6: OLGA Open Loop Noisy Bottom Hole Pressure Estimate

It can be seen in the figure that an adequate estimate of the real bottom hole pressure value is reached. It is therefore concluded that this scenario could be tested further in simulations when combined with a controller. Figure (7.5.7) shows the response of the state estimations.

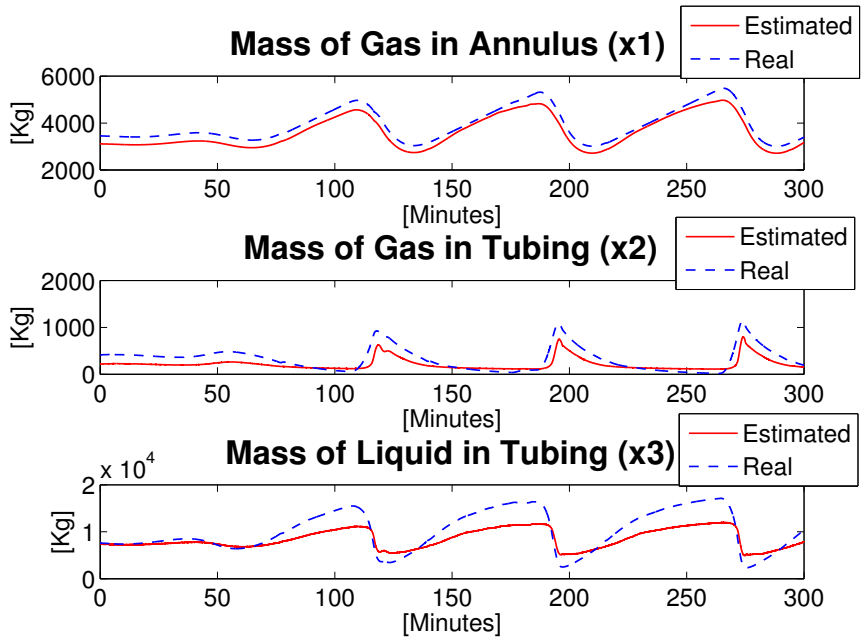

Figure 7.5.7: OLGA Open Loop State Estimation

The figure shows that there is still a big discrepancy in the estimation of the states. To improve the estimation results, the filter tuning parameters could be further altered to hopefully achieve better results. However, far too much time was spent on tuning, and this was the best result that could be achieved. This goes to show that maybe more time should be spent on fitting the response of the low order model to the OLGA simulator. But when so much time have to be spent on implementing and tuning the filter, it is possibly better to first try control figurations which uses available measurements to stabilize the gas lift system.

7.5.3 Choosing Control Structures With Estimation

Based on the open loop estimation results, the following conclusion is reached on which control structures, combined with an estimator, that should be further tested in simulations. First of all, for the low order model, all estimation results proved more than accurate by only using noisy top pressure estimates. Therefore any of the control structures could be tested in combination with the estimator. However, estimation results on the OLGA simulator was not great. It is therefore decided only to test configurations where both the top side pressures are available without noise, and the tubing bottom hole pressure is available with noise.

Chapter 8

Controllers for The Casing Heading Instability

8.1 Proportional Integral Controller

The proportional integral (PI) controller is one of the most widely applied controllers in the process industry, mainly due to its simplicity in implementation and tuning. The transfer function from its input, the control error e, to its output, the control signal u, can be described as:

$$K(s) = \frac{u}{e}(s) = K_p(1 + \frac{1}{\tau_I s}) \tag{8.1.1}$$

where K_p is the proportional gain, τ_I is the integral time and s is the Laplace variable. The gain K_p and the integral time τ_I are the tuning parameters in the controller. The gain is the stabilizing part, and the integral time is adjusted to remove steady state error. Derivate action can also be included to the controller to achieve the more know Proportional Integral Derivative (PID) controller. This is however discarded in this work, as it is uncommon to use in process control applications. This is because the improvement in performance as result of the added derivative action is usually too small to justify the added complexity and the increased sensitivity to measurement noise, [20]. The PI-controller is applied in most of the control structures in this thesis.

Unfortunately, the PI controller may suffer from a problem which is called integrator-windup. In such a case, the integral part of the controller builds up when the input is saturated. This happens because the controller is not aware of that the signal it is sending into the process is saturated. Because of saturation in the input signal, there is a discrepancy between the control signal the controller thinks is being applied , and the actual control signal at is saturation limit. The result is that when the controller does not achieve the response it wishes, it will further try to increase or decrease the control signal, depending on if the valve is fully open or closed respectively. This is because the integral of the error is continuously increasing when the input is saturated. Therefore, a simple anti-windup scheme is implemented in the PI-controllers used in this thesis. The change in the controller algorithm is that as long as the control signal is saturated, i.e., the valve is fully closed or fully open, the integral of the error is kept constant. That is, the integration of the error is stopped when the input is saturated.

8.2 Linear Quadratic Regulator

The Linear Quadric Regulator (LQR) is a state feedback controller which is optimal in the sense that it computes the control signal by minimizing a defined quadratic cost function subject to a linear system. Basically it is just another way to calculate the constant proportional gain, K, in a state feedback controller on the form:

$$u = -Kx \tag{8.2.1}$$

Consider a linear system on state space form, the optimization problem may then be defined as:

$$\min_{u,x} J(u,x) = \int_{t=0}^{t=\infty} [x^T Q x + u^T R u] d\tau \tag{8.2.2}$$

subject to the linear system dynamics

$$\dot{x} = Ax + Bu \tag{8.2.3}$$

The objective is to minimize the cost function over en infinite time horizon, subject to the system dynamics. The A and B matrices are part of the linear system description. They are obtained through linearization of the nonlinear low order model, as describes in section (6.1). The Q and R are weighting matrices for the states and the inputs, respectively. They are assumed to be symmetric, and its is required that R is positive definite, which means that all eigenvalues of the matrix is greater than zero, while Q is required to be at least positive semidefinite, meaning that all eigenvalues of the matrix must be greater or equal to zero. The weighting matrices are the tuning parameters in the controller. Further it is required that all uncontrollable states in the model have stable dynamics, i.e., the pair *(A,B)* have to be stabilizable, [36].

To solve the optimization problem, the *lqr-function* in Matlab is used. This function calculates the optimal feedback controller by solving the associated Riccati equation:

$$A^T S + SA - (SB)R^{-1}(BS^T) + Q = 0 \tag{8.2.4}$$

The state feedback gain is further derived from S through the following equation

$$K = R^{-1}(B^T S) \tag{8.2.5}$$

as explained in the Matlab reference guide, [37].

The standard version of the LQR controller does not include integral action, which is necessary to remove stationary deviation. To include integral action in the controller, the linear system equations can be augmented with an integral state (x_i), i.e., $x = \begin{bmatrix} x_1 & x_2 & x_3 \end{bmatrix}^T \rightarrow \tilde{x} = \begin{bmatrix} x_1 & x_2 & x_3 & x_i \end{bmatrix}^T$. The integral state is decided to be the integral of the error in the annulus top pressure measurement, that is: $x_i = \int e \, d\tau = \int (P^*_{at} - P_{at}) \, d\tau$, where P^*_{at} is the setpoint reference for the annulus top pressure. Figure (8.2.1), taken from the Matlab documentation [37], shows the resulting control setup:

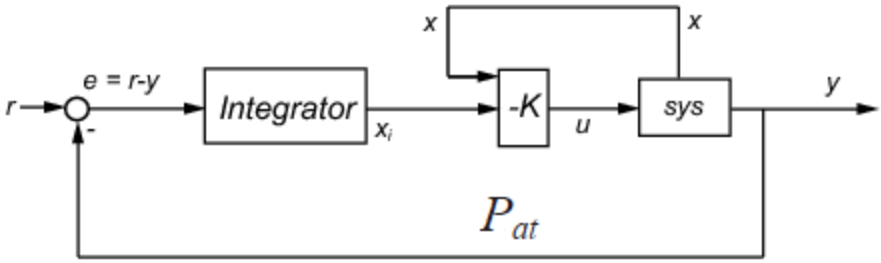

Figure 8.2.1: LQR Controller Setup

The system matrices are augmented as follows:

$$\tilde{A} = \begin{bmatrix} A & 0 \\ -C & 0 \end{bmatrix}, \tilde{B} = \begin{bmatrix} B \\ -D \end{bmatrix} \tag{8.2.6}$$

where the C and D matrices in the measurement equation in the linear model. Only the parts of the C and D matrices that describe the pressure in the top of the annulus are used in (8.2.6). The optimization problem is now solved as explained in equations, (8.2.4)-(8.2.5), with the augmented matrices. The resulting optimal gain matrix K can now be expressed as, $K = \begin{bmatrix} K_x & K_i \end{bmatrix}^T$, where K_x is the normal part of the gain dedicated to the normal states, and K_i is the gain designed for the integral state. Anti-windup is implemented in the same way as described for the PI-controller. That is, if the control signal is saturated, the integral of the error is kept constant.

It is important to note that the controller only uses a linear system model. The consequence of this is of course that when it is applied on the nonlinear model, the controller is only valid in a close neighborhood of the point it was linearized about. A possible solution to this may be to adapt the gain by relinearize the system when the operating point is changing. This is however not done in this work. Furthermore, when the controller is applied on the OLGA model, the performance is of course dependent of how accurate the low order model is able to reproduce the response of the advanced flow simulator. That is, if the low order model is a poor description of how OLGA will behave at a certain point, the low order model based LQR controller is likely to produce an invalid controller gain.

Due to the fact that the LQR is a linear controller, a final modification has to be done to apply it on the nonlinear system. Assuming that the nonlinear model $\dot{x} = f(x, u)$ is linearized about an operating point $(\bar{x}, \bar{u})$, the final LQR control law, with integral action, for the nonlinear system is:

$$u = -K_x(x - \bar{x}) - K_i x_i + \bar{u} \tag{8.2.7}$$

8.3 Linear Quadratic Gaussian Control

One of the LQR controllers biggest drawbacks, is that it is a state feedback controller, i.e., it needs the full state to be able to compute the control signal. The states of the

gas lift model are the respective masses of gas and liquid in the tubing and annulus volume. It is not realistic to assume that these states are measurable. Instead of feeding the controller with the true states, one may achieve a suboptimal solution by applying feedback from the estimated states. The UKF filter that was presented in chapter (7) is used to estimate the states based on two different scenarios. The first scenario considers that only the top pressures measurements, in the annulus and in the tubing, are available. This is tested both with and without noise on the measurements. Further in the second scenario we assume that in addition to the top pressures, there is also a noisy bottom hole pressure measurement available. For simplicity it is assumed that the noise entering the measurement is white. When using a LQR in combination with an Kalman filter, it is in the literature named the Linear Quadratic Gaussian (LQG) controller. Note that the best possible result that this controller can achieve, is when a perfect state estimate is feed into it, which makes it identical to the LQR controller. Thus, if the LQR controller shows poor performance, the LQG controller will most likely be even worse, as it is a suboptimal solution.

The final LQG control law for the nonlinear system, with integral action included in the same way as for the LQR controller, is:

$$u = -K_x(\hat{x} - \bar{x}) - K_i x_i + \bar{u} \tag{8.3.1}$$

where $\hat{x}$ is the estimated states, i.e., the output from the unscented Kalman filter. The controller structure is shown in figure (8.3.1).

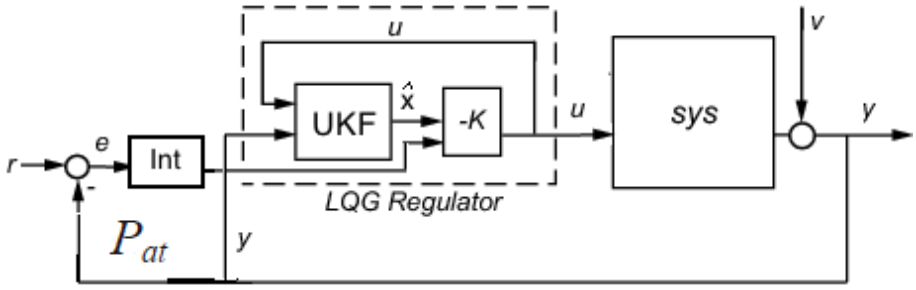

Figure 8.3.1: LQG Controller Setup

8.4 Cascade Control

A cascade control structure is also tested in the thesis. This is a simple setup with a PI-controller in series with a P-controller. The inner loop consist of a P-controller which gets it setpoint from the outer loop consisting of a PI-controller. The main reason for using a cascade controller is that by adding an controller in the inner loop, it changes the system dynamics that the outer loop sees. Hopefully this will provide the outer loop with a system which is easier to control. The inner loop should be faster than the outer loop for this control structure to make sense. When tuning the controllers, the inner loop is tuned first. The cascaded setup can be seen in figure (8.4.1).

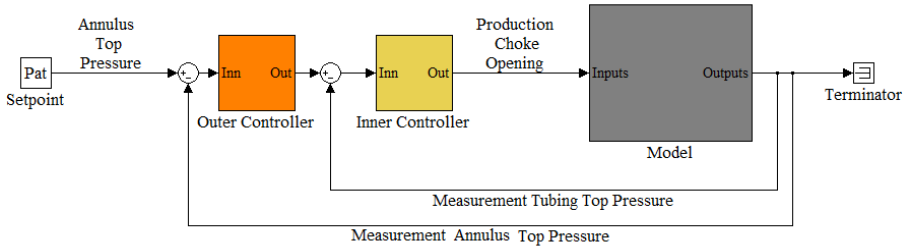

Figure 8.4.1: Cascade Control Configuration

Chapter 9

Simulation Study : The Low-Order Model

This chapter investigates how the most promising results from the controllability analysis behaves in simulations on the nonlinear low order model. The interesting part is to see how valid the results from the analysis, which is based on a linear version of the model, actually are to the nonlinear model.

9.1 Bottom Hole Pressure Control

The bottom hole pressure proved to be the best measurement candidate to use for both stabilization and disturbance rejection, based on the results of the analyses. It is therefore further tested in simulations in two different scenarios. In the first scenario we consider that the measurement is available without noise. As previously discussed, this is an unrealistic assumption. However, simulations are first conducted with the perfect measurement available to verify the result of the analysis. Also, by using the perfect measurement we avoid the use of the estimator and thereby exclude it as an potential source of error.

9.1.1 Measured Bottom Hole Pressure PI Control

A simple PI-controller is applied. The tuning parameters are found by trial and error in simulations, and the final constants are listed below.

Tuning Parameters	
K_p	-1/10
τ_I	100

First a simulation without any disturbances is performed. The system is started with a small perturbation from the chosen unstable equilibrium point. The open loop system is simulated in 120 minutes, before the controller is started. The red *(X)* in the plot marks the time when the controller is started. The result can be seen in figure (9.1.1).

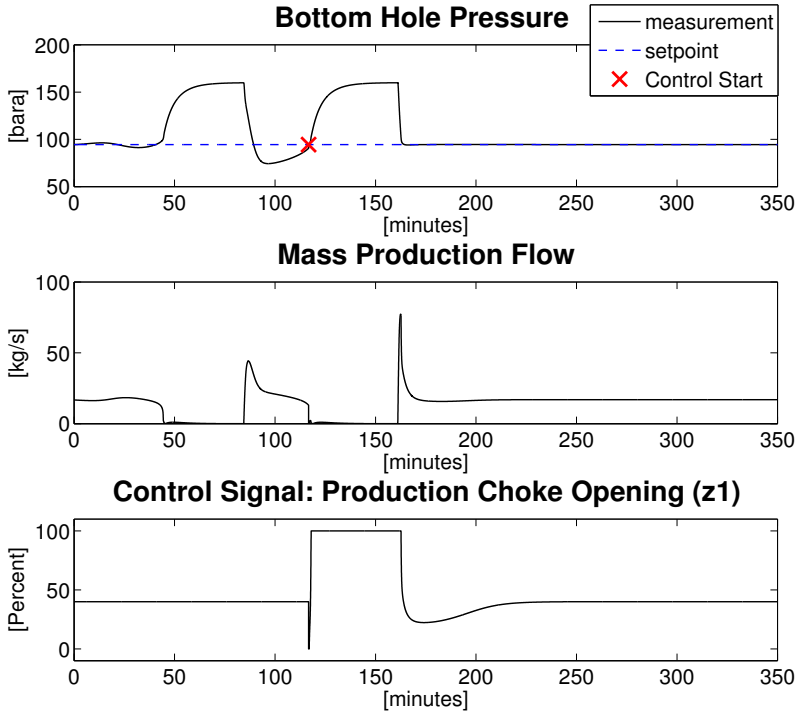

Figure 9.1.1: Bottom Hole Pressure Control

A second simulation sequence is conducted with a disturbance in form of a sine wave in the reservoir pressure. Again the open loop system, without disturbances, is simulated in 120 minutes, before the controller is started. When the simulation time reaches 225 minutes, the disturbance in the reservoir is applied. This is marked by the black *(+)* in the plot. The result can be seen in figure (9.1.2).

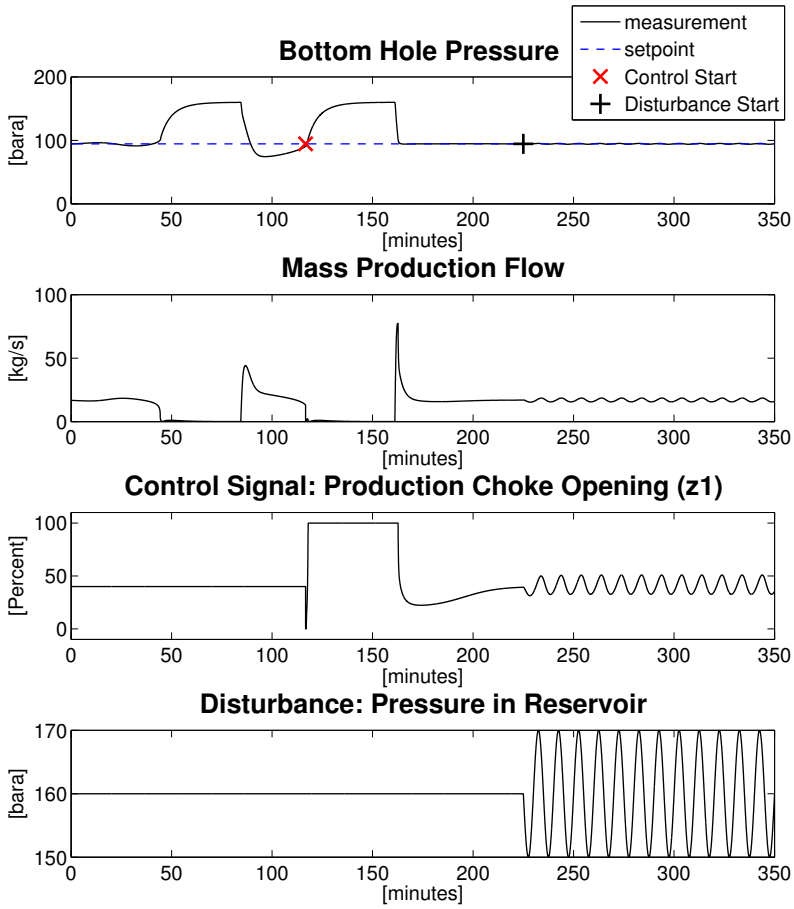

Figure 9.1.2: Bottom Hole Pressure Control With Disturbance

9.1.2 Estimated Bottom Hole Pressure PI Control

As previously discussed, the more realistic scenario is that the bottom hole pressure has to be estimated when it is to be used in a control structure. In the following scenario, the only measurements which are considered available are the pressure in the top of the annulus and the pressure in the top of the tubing. Furthermore, these measurements are in this scenario affected by white noise. The objective is therefore to use the Unscented Kalman Filter, presented in section (7), to estimate the tubing bottom hole pressure based on the two available noisy measurements. In the simulations, the system is once again started in a point which is a small perturbation from the chosen unstable equilibrium point. The system is simulated in open loop 120 minutes before the controller is applied. However, the estimator is activated from simulation start with an initial estimate which differs from the real state. The tuning parameters of the estimator, is set to the same constant as was applied in section (7.5.1.1). Figure (9.1.3) shows the control results and the estimated bottom hole pressure.

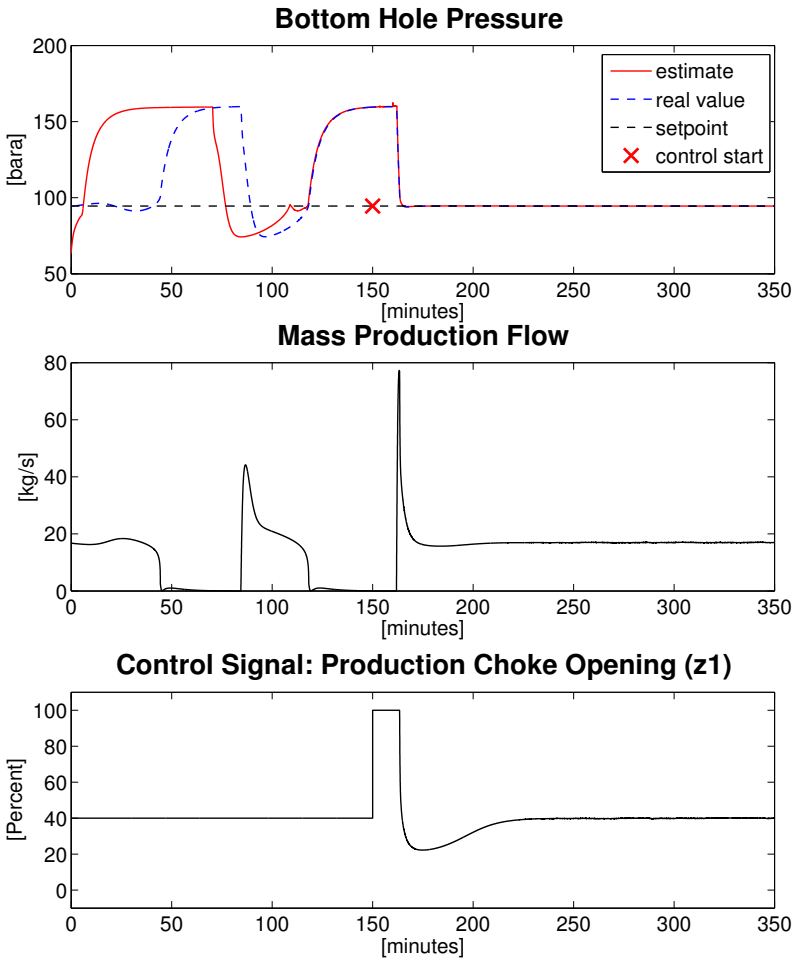

Figure 9.1.3: Estimated Bottom Hole Pressure Control

In figure (9.1.4) the estimated top pressures and the noisy measurements are plotted.

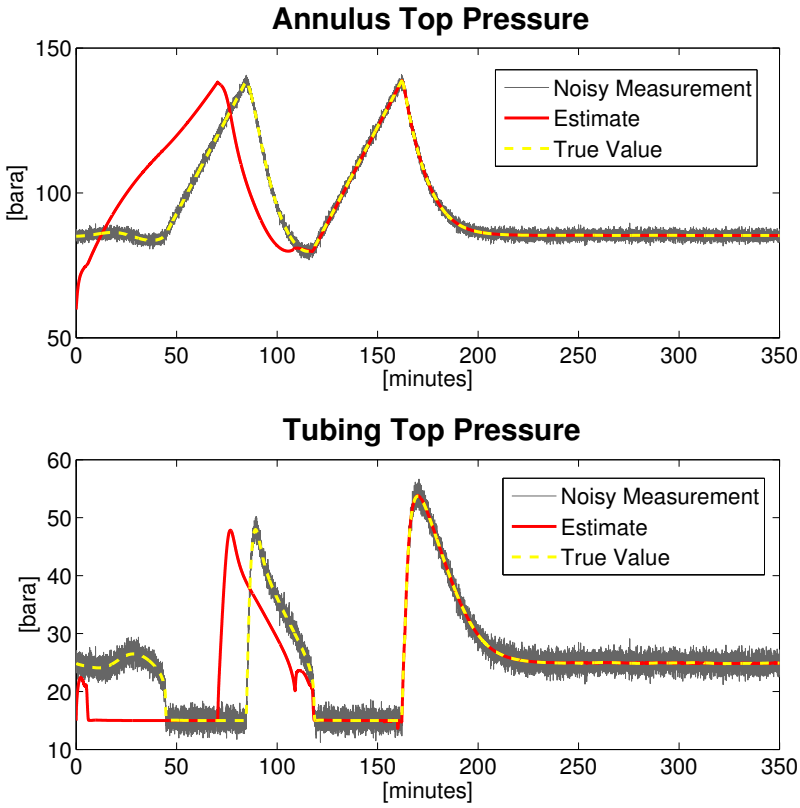

Figure 9.1.4: Estimated Top Pressures

9.2 Cascaded Top Pressures Control

One other control structure which proved promising in the analysis was when combining the two top pressure measurements. This was decided to test in a cascade control structure in the setup presented in section (8.4), with the tubing top pressure as the inner loop, and the annulus top pressure as the outer loop. It is favorable to use only top pressure measurements in a control structure, since these measurements are considered more reliable and accurate. In this scenario, these two measurements are considered available without noise. Noise could be added, but it was shown in section (7.5.3) that the UKF is able to accurately estimate the low order model top pressures anyway. Thus it was decided not to simulate this control structure with noise, as it will only increase the complexity of the control structure.

The inner pressure loop, i.e., the tubing top pressure controller is set to be a P-controller. That is, the inner loop does not have integral action, therefore a stationary error in this variable is expected. The reference signal for the inner loop is provided by the outer loop, as was shown in section (8.4). The outer loop, i.e., the annulus top pressure, is a PI-controller. The tuning parameters for the two controller are found by trial and error in simulations, and is listed in the following table:

Tuning Parameters	Inner Loop (P-controller)	Outer Loop (PI-controller)
K_p	0.02	-2
τ_I	–	450

The simulation study is conducted similar to how is was done for the bottom hole pressure. First the system is started with a small perturbation from the chosen unstable equilibrium point. The system is simulated for 150 minutes before the controller is started, which is depicted with the red *(X)* in the plot. First the setup is tested without disturbances. The response can be seen in figure (9.2.1).

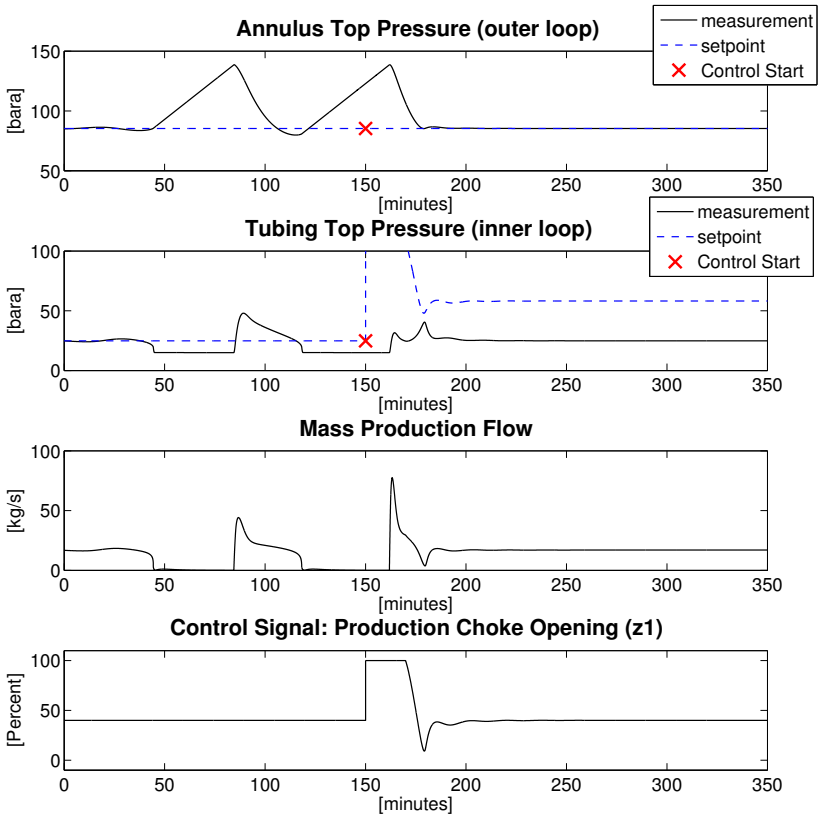

Figure 9.2.1: Cascade Control without Disturbance

Secondly the same control structure is tested with a small disturbance in the reservoir pressure. The control setup is exposed to a smaller disturbance than the one applied in the bottom hole pressure control configuration simulations. The reason for this is that the controllability analysis proved that the top pressures are more sensitive to disturbances, more specifically this control structure is more likely to saturate when disturbances grow big. The response can be seen in figure (9.2.2).

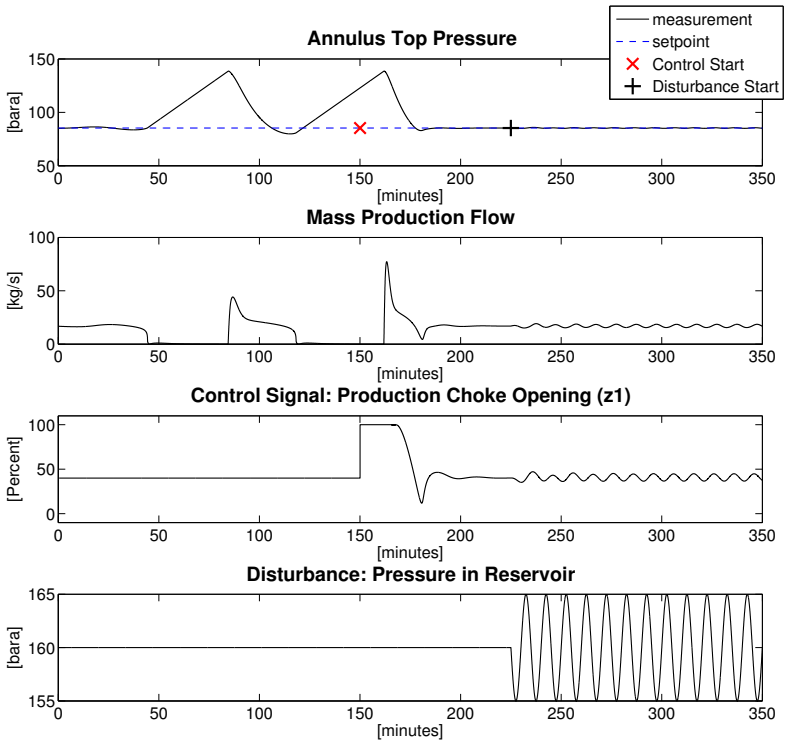

Figure 9.2.2: Cascade Control with small Disturbance

Finally, the top pressure control structure is tested with a big disturbance in the reservoir pressure. The disturbance is at the same size as the one applied to the bottom hole pressure control configuration. Once again, the simulations are started in open loop from a perturbation from the unstable operating point. The controller is activated 150 minutes into the simulations, and the disturbances are applied from 225 minutes. The response can be seen in figure (9.2.3).

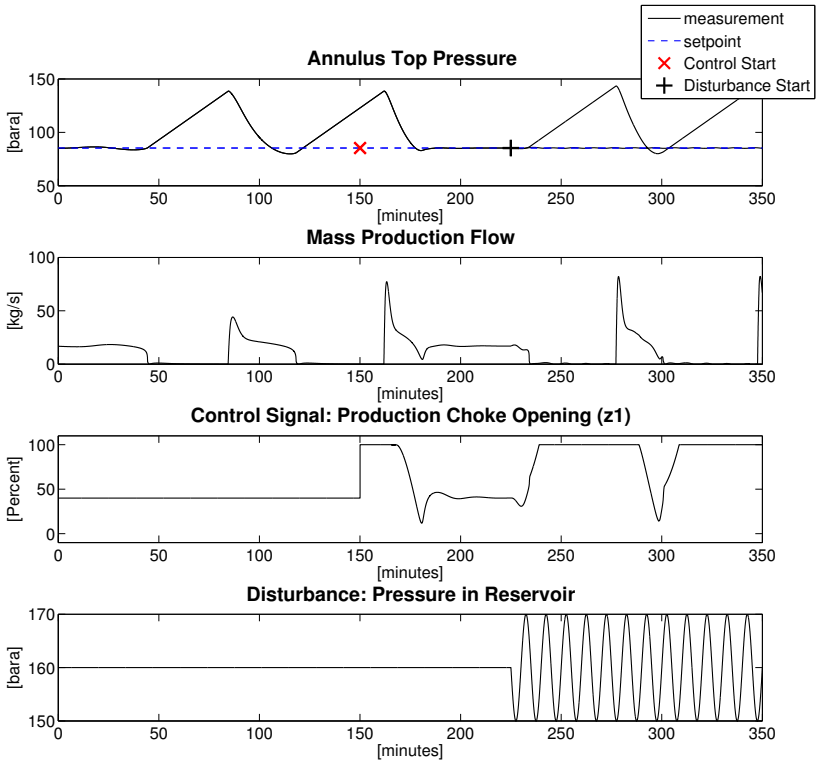

Figure 9.2.3: Cascade Control with big Disturbance

9.3 LQR-controller with Integral Action

The final control structure to be tested in simulations is a state feedback configuration. It was previously mentioned that it is unrealistic that these states are available as measurements. However, the control structure is tested first without the extra complexity of adding an estimator. The LQR controller was derived in section (8.2), and achieves integral action by measuring the top pressure in the annulus. The tuning parameters, i.e. the weighting matrices where found by trial and error in simulations, with the requirements for the parameters, that was as listen in section (8.2) in mind. The used values are listen in the following table.

Tuning Parameters	
Q	$\begin{bmatrix} 1 & 0 & 0 & 0 \\ 0 & 1 & 0 & 0 \\ 0 & 0 & 1 & 0 \\ 0 & 0 & 0 & 1 \end{bmatrix}$
R	10^4

Notice the heigh weight on R, which punishes the control signal. The reason for the high value is to try to keep the valve opening from saturating. The last element in Q is the weight on the augmented state, i.e., the integral state.

First a simulation is performed without disturbances. Again, the system is started with an perturbation from the unstable operating point and is run for 120 minutes before the controller is activated. The resulting response can be seen in figure (9.3.1).

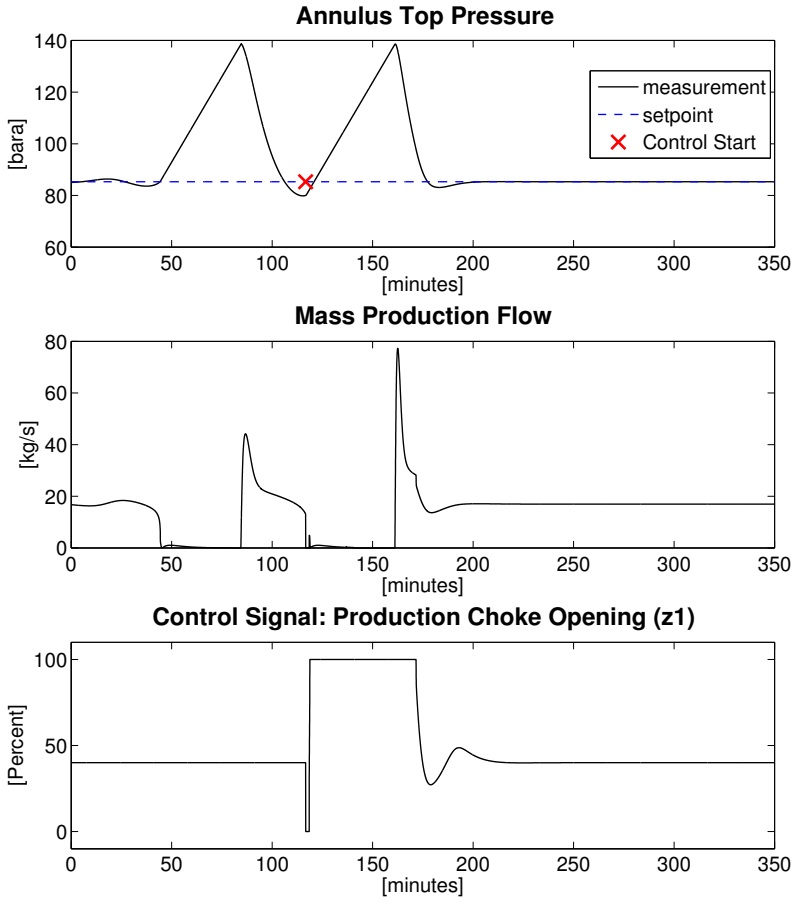

Figure 9.3.1: LQR Control

Secondly a simulation is performed with disturbances. The disturbances is activated 225 minutes into the simulations, and have the same magnitude as was used for the bottom hole pressure control configuration. The response of the annulus top pressure, the mass production flow, the control signal and the disturbance is shown in figure (9.3.2).

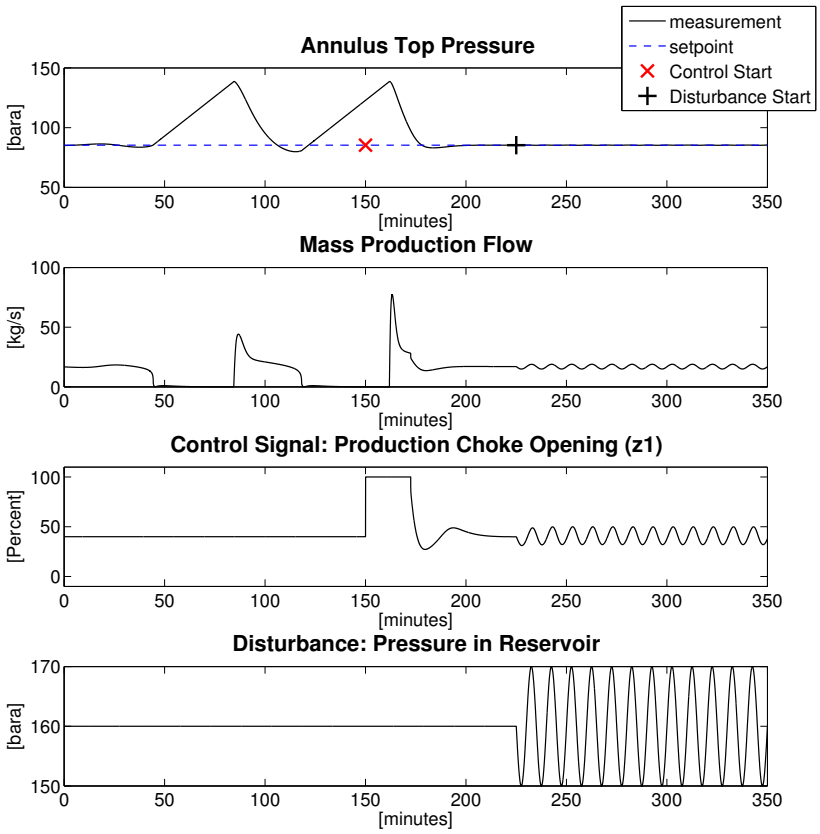

Figure 9.3.2: LQR Control with disturbances

The response of the states are shown in figure (9.3.3).

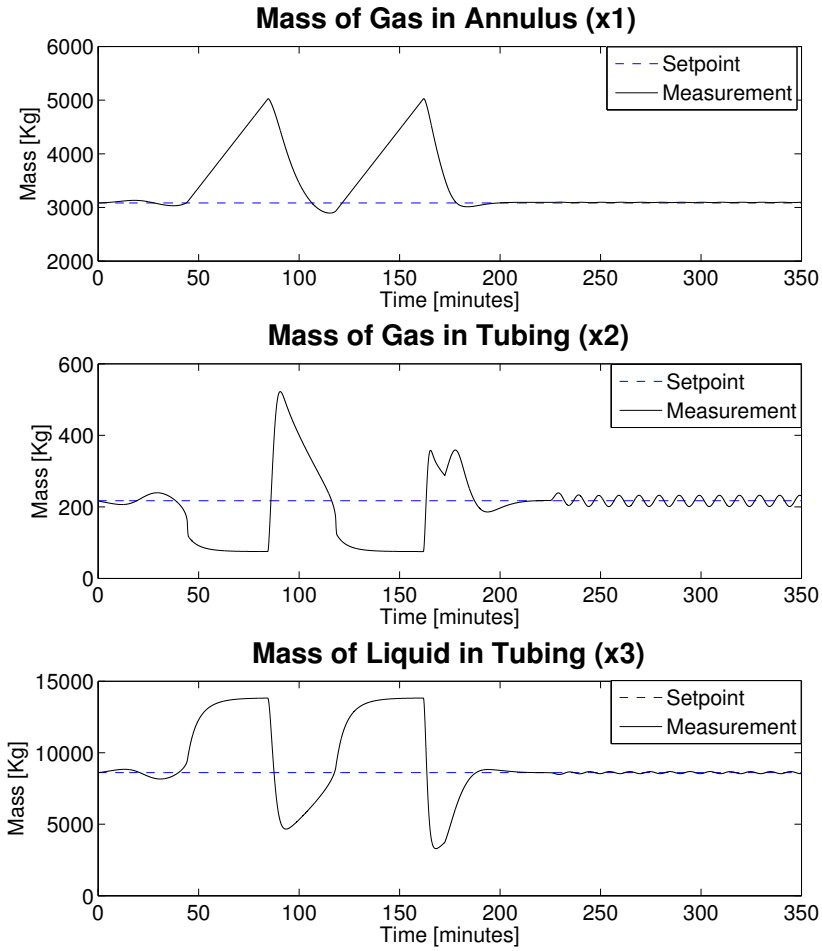

Figure 9.3.3: LQR Control - response of states

9.4 LQG-controller with Integral Action

Since the states cannot be considered available to be used directly in the real facilities, we also test the LQG controller to perform a more realistic simulation study. In which case, the estimated states from the UKF are feed back to the LQR controller, as was explained in section (8.3). The states are estimated from two noisy measurements, the top pressure in the annulus and the top pressure in the tubing. The initial estimated states are different from the true values of the states. In the simulations, the system is once again started in a point which is a small perturbation from the chosen unstable equilibrium point. The system is simulated in open loop 120 minutes before the controller is started. However, the estimator is activated from simulation start with an initial estimate which differs from the real state. The response of the annulus top pressure, which is used for integral action, as well as the production mass flow and the control signal, can be seen in figure (9.4.1).

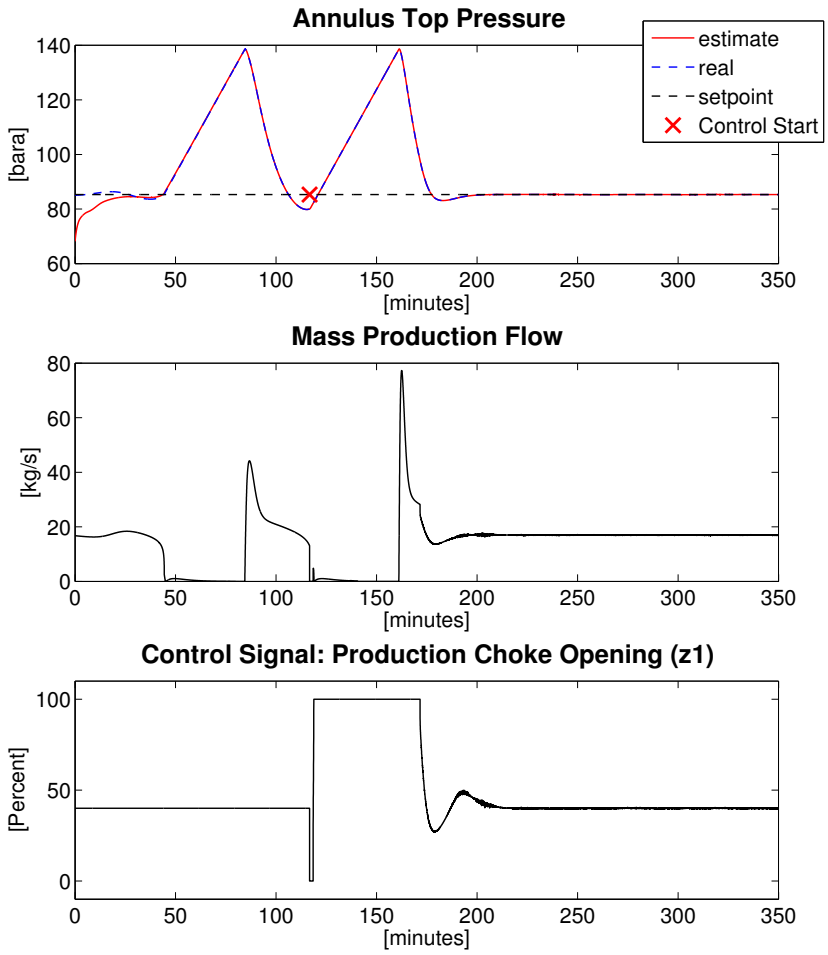

Figure 9.4.1: LQG control results

The estimate and response of the states are shown in figure (9.4.2).

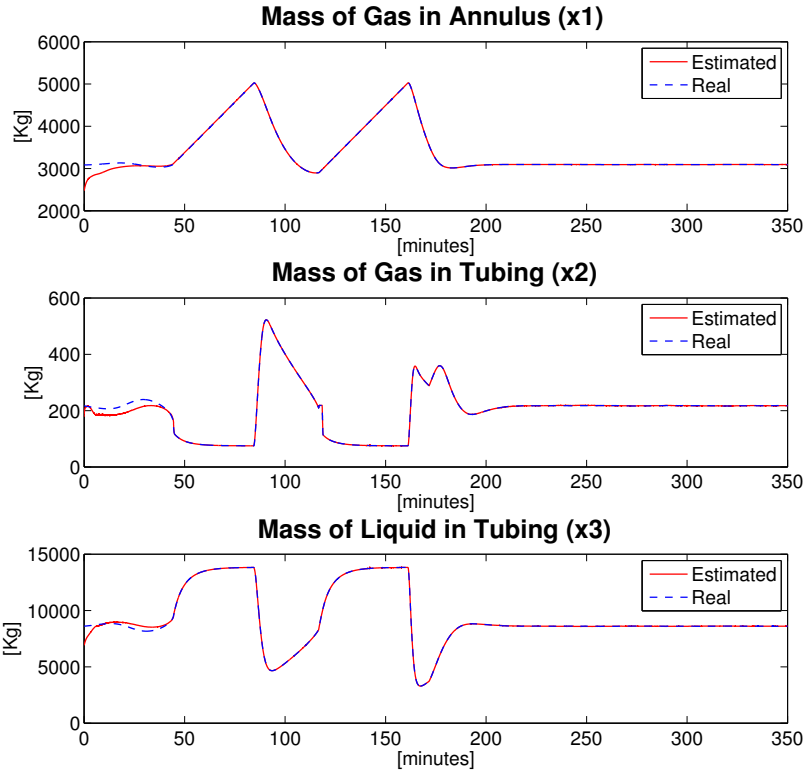

Figure 9.4.2: Estimated and Controlled States

The noisy measurement and estimate of the top pressure are shown in figure (9.4.3).

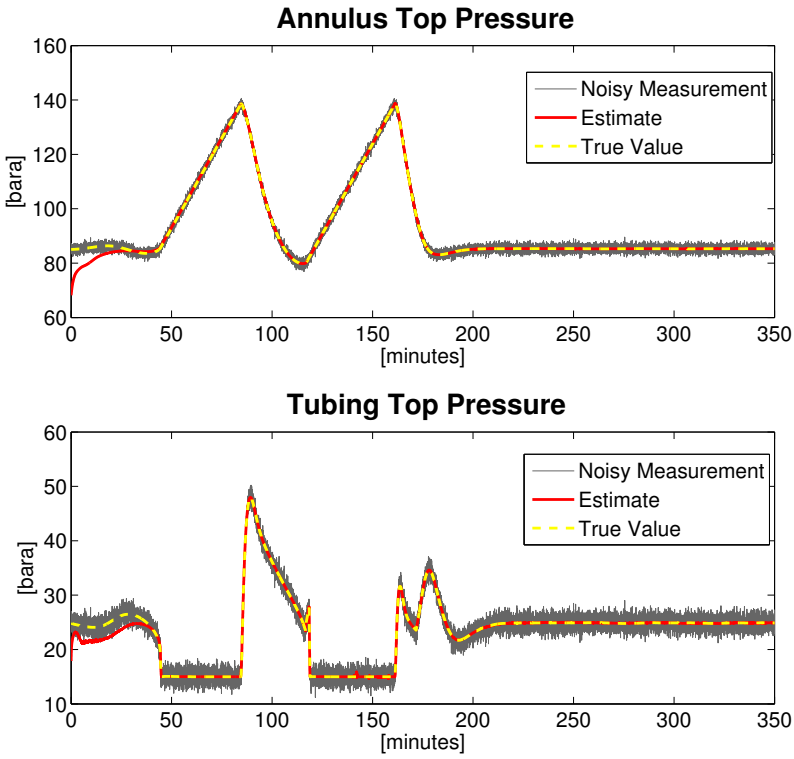

Figure 9.4.3: Estimated Top Pressures

9.5 Discussion Of Low Order Model Simulation Results

The results obtained in the controllability analysis were further confirmed in the simulations. The bottom hole pressure proved to be the single best measurement candidate to use for control, if available. The control configuration with the bottom hole pressure as the controlled variable, and the production choke as the manipulated variable, was able to stabilize the system without stationary deviation, and proved effective in rejecting disturbances in the reservoir pressure. However, as discussed in section (7.1), one may not assume that the the bottom hole pressure is a reliable measurement. Fortunately, the simulations result of the control structure which uses the estimated bottom hole pressure also provides a sufficiently good performance, due to the fact that the estimator is able to accurately estimate the real value which is needed for control.

The analysis further showed that a control structure which uses a combination of the top pressures, in this case the cascaded control configuration, should perform almost as good as the control structure which uses the pressure in the bottom hole as the controlled variable. When considering that these measurements are in fact available and reliable, this control configuration should be the preferred alternative of the two configurations. Simulations proves that the cascaded control structure it is able to both stabilize the system and effectively reject the disturbances. The main drawback of this control structure compared to the configuration using the pressure in the bottom hole, can be seen when

comparing figure (9.1.2) and (9.2.3). The bottom hole pressure control structure is shown superior in stabilizing the system when the disturbances grow to a certain size. One reason for why the cascaded control structure is not able to stabilize the system when the system is affected by big disturbances may be because the input, i.e., the control signal, seems to more easily saturate with this setup. However, interesting work in applying feedforward from the disturbances that affect the system, to reduce the magnitude of the plant input moves, has been researched in an paper by Hovd and Bitmead, [38]. Supplementing such a structure into the proposed cascaded control structure could maybe improve the disturbance rejection properties of the controller. This is not investigated further in this thesis.

Even though a state feedback controller structure was not considered in the analysis, it was tested in simulations with the LQR controller. The controller was able to stabilize the system, and reject disturbances at the same magnitude as the bottom hole pressure control structure was able to suppress. However the states can not be considered available in the real facilities. The LQG controller which instead used the estimated states proved just as sufficient performance because the estimator was able to accurately estimate both the states and the annulus top pressure, which was needed for control.

One thing is noted when performing the simulations. It could be an idea to introduce a constraint on the rate of change on the opening of the valve. In these simulations, it is possible for the valve to move from fully closed to fully open instantaneously. This is unphysical and may be a potential source of error in the results. However, the dynamics of the system is very slow, with a period time of several hours, so how much this constraint would in fact change the control results is questionable.

To summarize and conclude on the result of the simulation study on the low order model, the bottom hole pressure control structure is proven as the best setup to use for control. That is if the measurement is available, or if it can be accurately estimated. The LQR controller showed equal good performance, if the states are available for feedback, or if an accurate estimate of them are obtained. However, the bottom hole pressure control structure is still preferred because of its simplicity in implementation. If estimation results are poor, the cascaded top pressure configuration is recommended, as it relies on only measurements which are considered available. The structure is able to stabilize the system and reject disturbances of certain magnitudes. How the cascaded control structures compares to the bottom hole pressure control structure on the OLGA model is investigated in the next chapter.

Chapter 10

Simulation Study : The OLGA Model

In this chapter the same control structures that where tested on the low order model is applied on the OLGA simulator. This provides a view of how robust the controllers are when tested on different models, and will hopefully provide a deeper insight of how the different controller will respond to a more real life situation. The result of the simulations are discussed in the end of the chapter.

10.1 The Matlab OLGA Connection

To be able to use controllers developed in Matlab directly on the OLGA flow simulator, a communication channel had to be set up between the programs. New to he latest version of the flow simulator, OLGA 7, is that there is no longer a built in Matlab-OLGA connection toolbox, which was included in earlier versions of the software. Instead other client programs are now intended to interact with OLGA through the use of an OPC server. The server is set up by the OLGA simulator, and a framework to connect and interact with this server was implemented in Matlab. The framework uses the Matlab OPC Toolbox to create a data access object which is used to read and write values from and to the OLGA simulator. The simulator mode is set to external, in the server settings in OLGA. This options lets the client program manually decide on how and when to run simulations by adjusting certain time variables that the simulator is depending on. A more detailed description on how to enable an OPC server in OLGA, and different ways to manage the server interaction, can be found in the OPC-server guide documentation which is included in the OLGA software package.

10.2 Bottom Hole Pressure Control

10.2.1 Measured Bottom Hole Pressure PI Control

The same tuning parameters which was applied for the bottom hole pressure control configuration for the low order model was applied to the OLGA flow simulator. The simulator is started at the chosen unstable operating point, and the controller is activated

280 minutes into the simulations. No disturbances are applied. The result can be seen in figure (10.2.1).

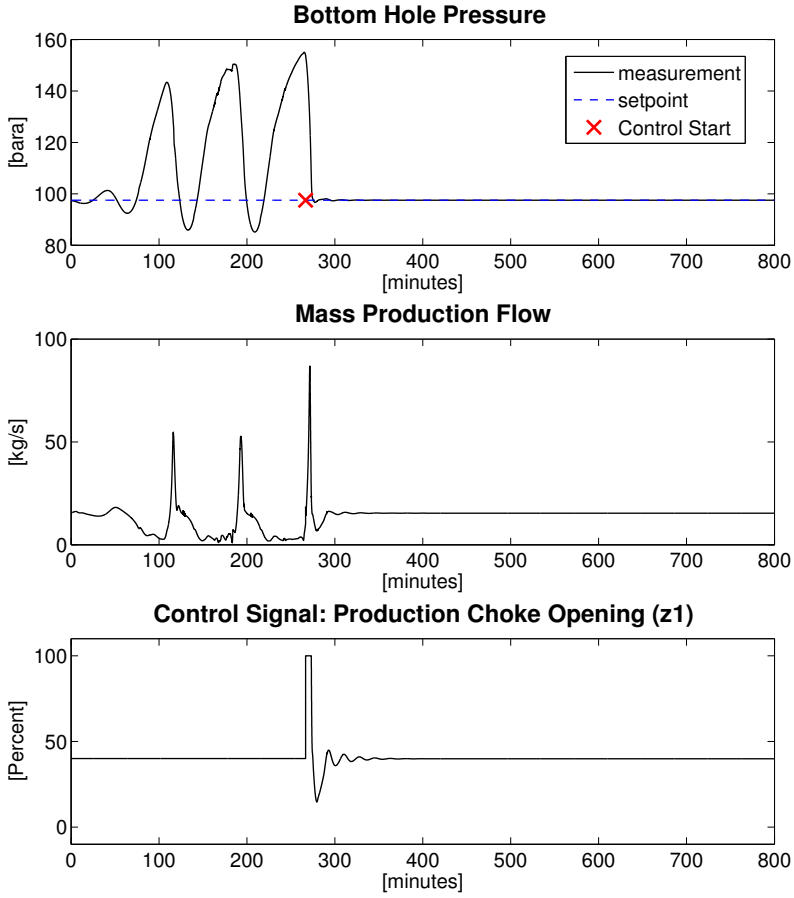

Figure 10.2.1: OLGA Bottom Hole Pressure Control

10.2.2 Estimated Bottom Hole Pressure PI Control

The next control structure tested on the OLGA flow simulator is to use the estimated bottom hole pressure as the controlled variable. The bottom hole pressure is estimated with the use of the UKF which is based on the low order model equations. Perfect measurements of the top pressure in the tubing and the annulus are used, as well as a noisy measurement of the bottom hole pressure. The initial states used in the estimator is very close to the actual initial states. The tuning of the UKF constants are are set to the same constants as in section (7.5.2.2). The control results are shown in figure (10.2.2).

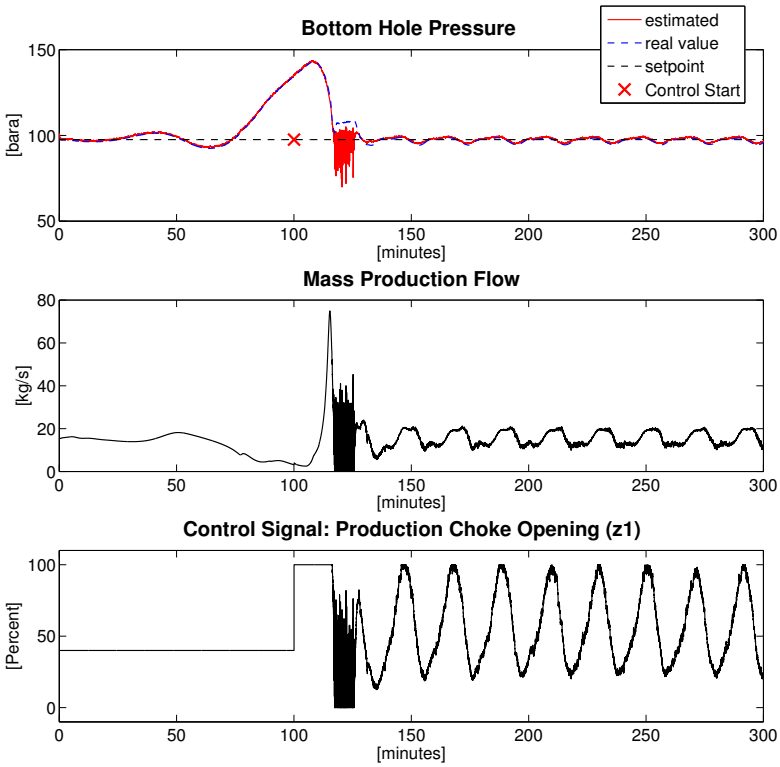

Figure 10.2.2: Estimated Bottom Hole Pressure Control

The estimation result of the bottom hole pressure, as well as the noisy measurement is shown in figure (10.2.3).

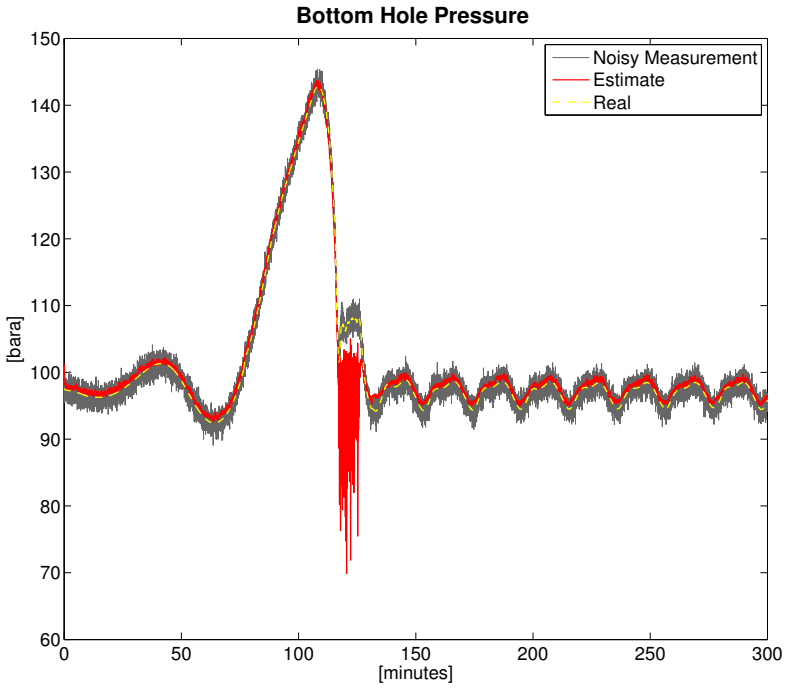

Figure 10.2.3: Estimated Bottom Hole Pressure

10.3 Cascaded Top Pressure Control

The next control configuration to be tested on the OLGA flow simulator is the cascaded top pressure control configuration. In these simulations, both measurements are assumed to be available without noise. Unfortunately, the same tuning as was used for the low order model did not respond good in the OLGA simulations. New tuning parameters where found by trial and error, and resulted in decreasing the proportional term for the outer controller loop. The new parameters are shown in the following table:

Tuning Parameters	Inner Loop (P-controller)	Outer Loop (PI-controller)
K_p	0.02	-3
τ_I	–	450

The system is simulated 100 minutes before the controller is started. No disturbances are applied to the system. The response is shown in figure (10.3.1).

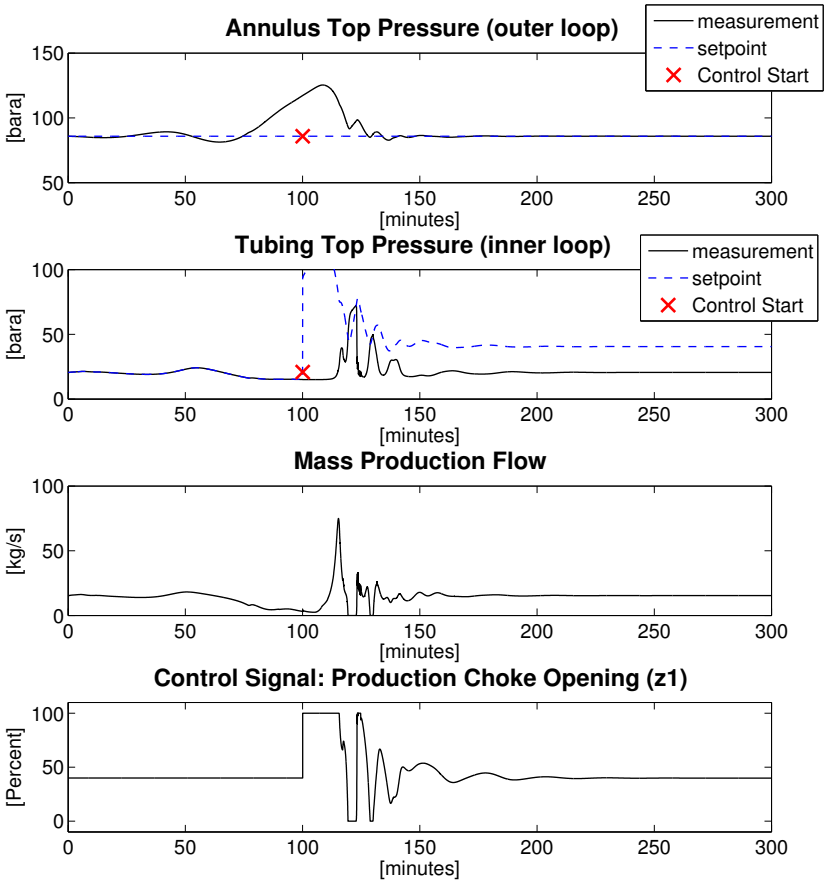

Figure 10.3.1: OLGA Cascade Control

10.4 LQR-controller with Integral Action

The state feedback controller is also tested on the OLGA simulator. The same tuning parameters that was obtained for the low order model is applied. First the simulations is in open loop, then the controller is activated 100 minutes into the simulations. The response of the annulus top pressure which is used for integral action, as well as the response of the mass production flow and the control signal is given in figure (10.4.1).

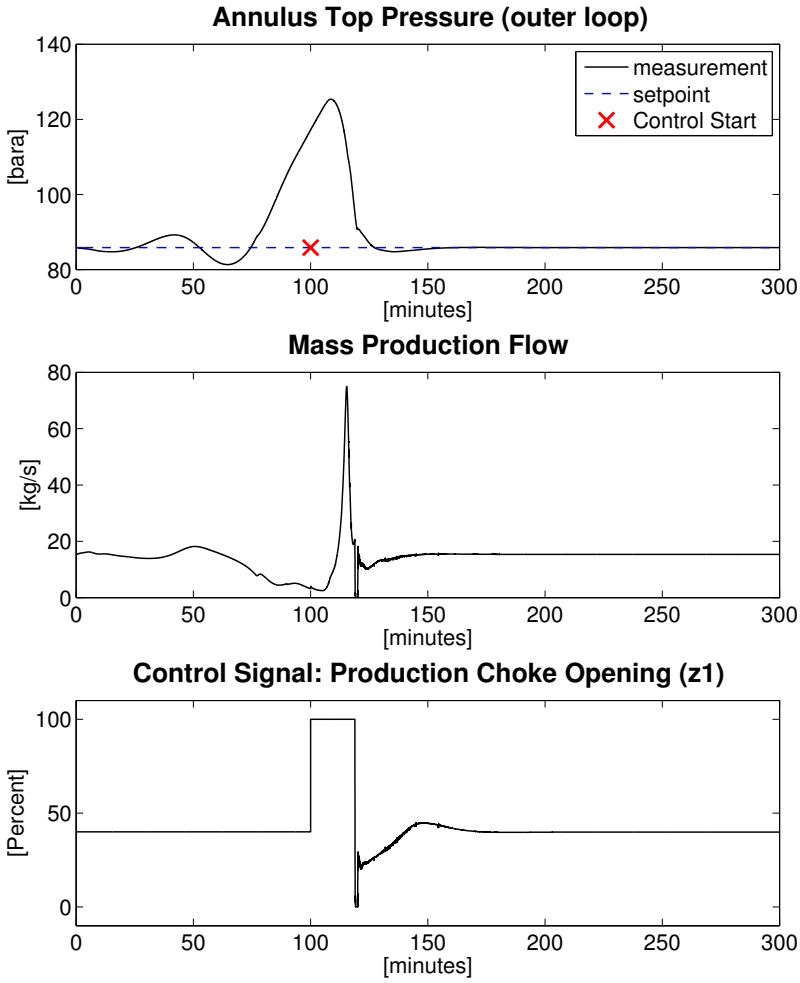

Figure 10.4.1: OLGA LQR Control

The response of the states are given in figure (10.4.2).

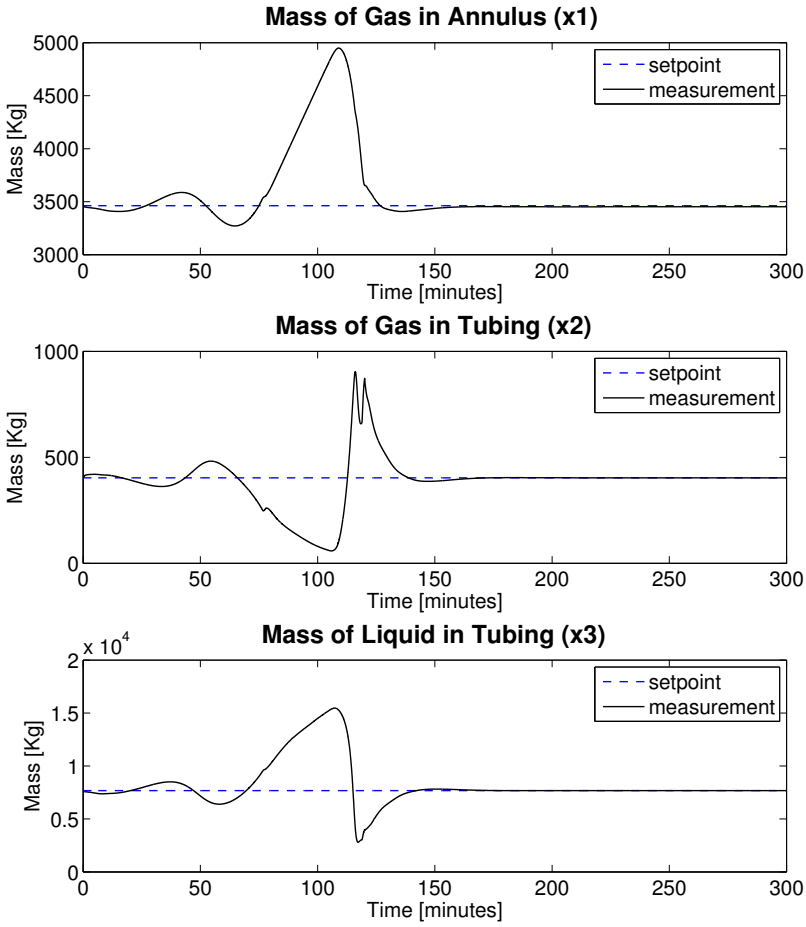

Figure 10.4.2: OLGA LQR Control - State Response

10.5 LQG-controller with Integral Action

Finally the LQG controller is tested on the OLGA flow simulator. The states are estimated through the UKF by using perfect measurement of the top pressure in the tubing and annulus, as well as a noisy measurement of the bottom hole pressure. The tuning of the weights are the same as applied for the LQR controller with real state feedback. The tuning parameters for the UKF filter are the same as applied in section (10.2.2). Figure (10.5.1) shows the response of the OLGA top pressure, the mass production flow and the control signal.

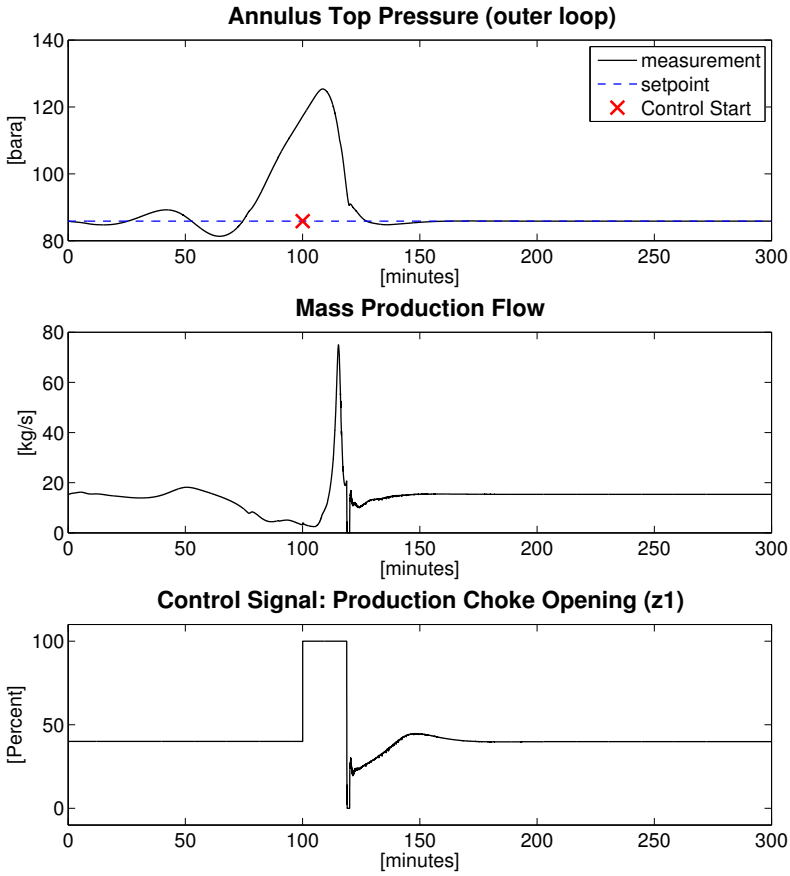

Figure 10.5.1: OLGA LQG Control

The estimate and response of the states are shown in figure (10.5.2).

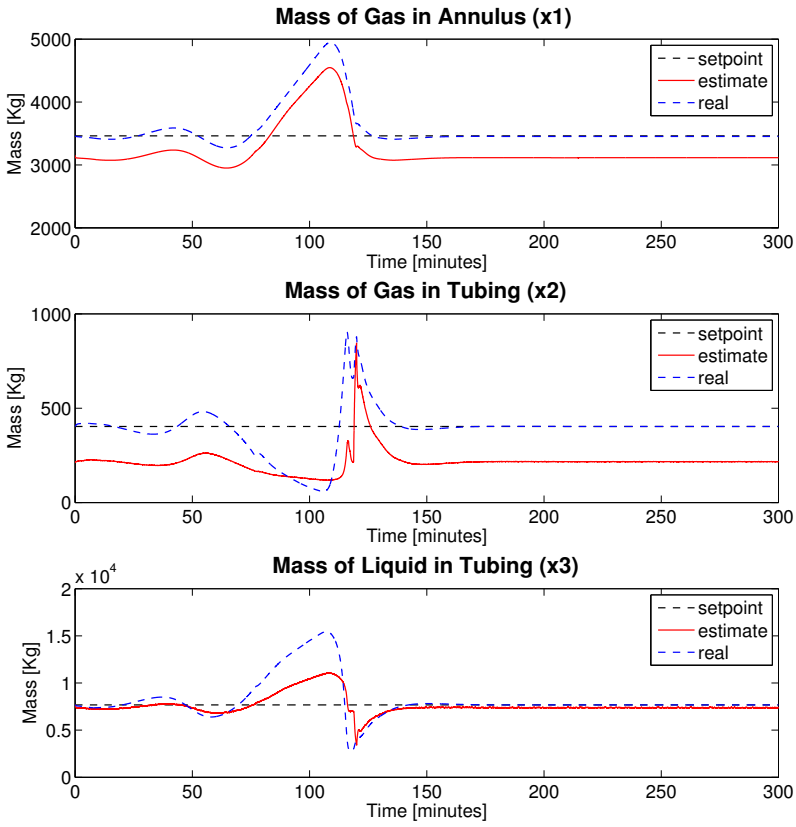

Figure 10.5.2: OLGA LQG Control State Estimate

The estimate and response of the bottom hole pressure in the tubing, as well as the noisy measurement can be seen in figure (10.5.3).

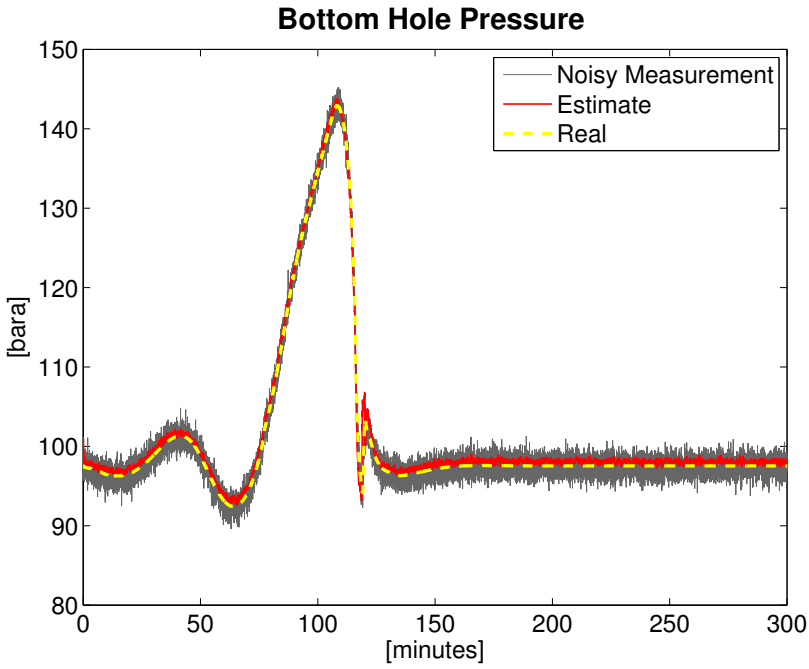

Figure 10.5.3: OLGA LQG Control Bottom Hole Pressure Estimate

10.6 Discussion of OLGA Simulation Results

The first thing to notice after having tested the different control configurations on the OLGA flow simulator, is that all of the control structures which requires estimation show worse response than when applied to the low order model. This is of course due to the fact that the estimator is not able to accurately enough estimate either the states or the outputs which are needed for control. However, if estimation results are put a side, all of the control structures which uses real measurements are able to stabilize the system. And if available, the bottom hole pressure is still one of the best measurement candidates to be used for control.

When the control configuration that uses the estimated bottom hole pressure is applied, it shows the worst response of all the simulations performed on the OLGA model. It is able to reduce the oscillations, but not remove them entirely. One possible explanation for this may be that the estimator provides an insufficient estimate of the the bottom hole pressure. The result is that the controller is feed with the wrong error between the setpoint and the actual value of the bottom hole pressure. When the controller tries to remove this stationary deviation, it actually increases the real error. So the problem is really the interaction between the estimator and the controller. This control structure is therefore not recommended if a better estimator is not applied. The estimation results could improve by further fitting the low order model better to the response of the OLGA simulator.

The LQR controller with measured states seems to be able to stabilize the system without stationary deviation. And surprisingly the LQG controller also shows sufficient performance even though the estimate of the states is poor. This is probably because it uses the

annulus top pressure for integral action, and this measurement is feed to the controller without noise.

With a more realistic view on the results, it seems that either a better estimator is needed, or one should use the cascaded top pressure control structure. This control structure is abel to stabilize both the low order model and the OLGA flow simulator and has the favorable property that is only uses measurement which are considered available. Even though the LQG controller was able to match the response of the cascaded control structure, the LQG controller is far more complex to implement, and the estimator may of coursed have to be tuned for each different flow facility. The recommendation is therefore to use the cascaded top pressure control configuration which is simple to set up and easy to tune.

Chapter 11

Conclusion and Further Work

To conclude, this thesis has shown several things. First of all, the final version of a new nonlinear low order gas lift model is derived. The new model includes a friction term for the pressure drop in the tubing. Also, instead of using the average of the phases in the whole volume to calculate respective phase fractions in the top of the tubing, a new more accurate way is proposed. The model is compared to the more advanced OLGA flow simulator, and the it is seen that the model is capable of successfully reproduce the casing heading instability to a certain accuracy, which aims to show that using an overly complicated model of a gas lift system is not necessary for the applications of controller design for the casing heading instability.

Secondly it is shown that automatic control should be applied to gas lift system to optimize production with respect to maximizing the production rate flow and minimize the use of lift gas. This is justified through a thorough simulation study which shows that the optimal operating conditions lies in an unstable region, where the desired production flow can not be maintained without automatic control.

Thirdly it has been shown, through both a controllability analysis and in simulations, that the bottom hole pressure in the tubing is the single best candidate to be used as the controlled variable, when the production choke is used as the manipulated variable, to prevent the casing heading instability. However, since it is not realistic that this measurement is available in the real facilities, one either needs to provide a good estimator, or find a new way to measure it. As long as there does exists adequate technology to obtain a sufficient accurate measurement, this control structure is not recommend. The state feedback LQR controller was proven to be a good control strategy for both stabilization and rejection of unknown disturbances, however, this control structure suffers from the same flaw as the bottom hole pressure control configuration, which is that it is based on measurements which can not be considered available. In this case, it is the states of the model, i.e., the masses of gas and liquid in the system. The final recommended control strategy in this thesis is to use a cascade controller which only relies on what is considered available top pressures in the system and is easy to implement. The cascaded control structures uses a proportional controller on the tubing top pressure in the inner loop, and a proportional integral controller on the annulus top pressure in the outer loop. This control structures shows good result in the controllability analysis, and is successfully able to stabilize the system in simulations of both the new low order model and the newest version of the advanced OLGA flow simulator. However, it is sensitive to disturbances,

and was not able to stabilize the system when the disturbance in the reservoir pressure was too big.

Finally, the controllability analysis also shows many other different control configurations which are possible control structures, even though they were not tested further in simulation in this thesis.

There are many different subjects to be dealt with for any further work on gas lift systems. For example, the controllability analysis revealed many other promising control structures that could be tested on gas lift systems, but they where not tested in simulations in this thesis. Also the control structures that were tested in simulations were not exposed to any disturbances when applied to the OLGA flow simulator, only when tested on the low order model. This would be interesting to test further in the OLGA model, and might reveal more information of their performances. Another subject which might be interesting to investigate in further work is to performed a nonlinear analysis of the new low order model, as the controllability analysis performed in this thesis is based on linear theory. Furthermore it would be interesting to see if the recommended cascaded control structure would improve its ability to reject disturbances if feedforward from the disturbance is included in the control setup. Another possibility is to include feedforward from an estimation of the disturbances, if they can not be measured. The most interesting thing to test in further work is however to apply the most promising control structure on a real gas lift facility.

Bibliography

[1] H. Hjelseth Hansen, "Control strategies on new low order gas lift model," 2011.

[2] M. B. Jadid, A. L. M. Opsa, and A. Vasperl, "The pressure's on: Innovations in gas lift," *Oilfield Review*, vol. 18, no. 4, 2006.

[3] A. P. I. Exploration and P. Dept, *API Gas Lift Manual*. Vocational training series, American Petroleum Institute, 1994.

[4] O. Bratland, *Multi-phase Flow Assurance*. Unpublished, 2010.

[5] "Schlumberger oilfield glossary," 2012.

[6] A. Satter, G. Iqbal, and J. Buchwalter, *Practical enhanced reservoir engineering: assisted with simulation software*. PennWell Corp., 2008.

[7] G. Eikrem, O. Aamo, and F. B., "On instability in gas lift wells and schemes for stabilization by automatic control," *SPE Production & Operations*, vol. 23, no. 2, pp. 268–279, 2008.

[8] J. W. A.F. Bertuzzi and F. Poettmann, "Description and analysis of an efficient continuous-flow gas-lift installation," *Journal of Petroleum Technology*, vol. 5, no. 11, 1953.

[9] Z. Xu and M. Golan, "Criteria for operation stability of gas-lift wells," 1989.

[10] J. Barker and R. Gomez, "Formation of hydrates during deepwater drilling operations," *Journal of Petroleum Technology*, vol. 41, no. 3, pp. 297–301, 1989.

[11] G. Eikrem, *Stabilization of gas-lift wells by feedback control*. PhD thesis, NTNU, 2006.

[12] A. Torre, Z. Schmidt, R. Blais, D. Doty, and J. Brill, "Casing heading in flowing oil wells," *SPE Production Engineering*, vol. 2, no. 4, pp. 297–304, 1987.

[13] E. Jahanshahi and S. Skogestad, "Simplified dynamical models for control of severe slugging in multiphase risers," in *World Congress*, vol. 18, pp. 1634–1639, 2011.

[14] S. Group, *OLGA OPC Server Guide Vesion 7.0*, 2011.

[15] S. Group, *OLGA User Manual 7.1*, 2011.

[16] G. Eikrem, L. Imsland, and B. Foss, "Stabilization of gas-lifted wells based on state estimation," in *International Symposium on Advanced Control of Chemical Processes*, 2004.

[17] O. Egeland and J. T. Gravdahl, *Modeling and simulation for automatic control.* Marine Cybernetics, 2002.

[18] T. Ahmed, *Reservoir engineering handbook, Third Edition.* Gulf Professional Publishing, 2006.

[19] S. Haaland, "Simple and explicit formulas for the friction factor in turbulent pipe flow," *J. Fluids Eng.;(United States)*, vol. 105, no. 1, 1983.

[20] S. Skogestad and I. Postletwaite, *Multivariable Feedback Control, Analysis and Design, Second Edition.* John Wiley and Sons, Ltd, 2005.

[21] J. Nocedal and S. J. Wright, *Numerical Optimization, Second Edition.* Springer, 2006.

[22] K. Havre and S. Skogestad, "Selection of variables for stabilizing control using pole vectors," *Automatic Control, IEEE Transactions on*, vol. 48, no. 8, pp. 1393–1398, 2003.

[23] J. Chen, "Logarithmic integrals, interpolation bounds, and performance limitations in mimo feedback systems," *Automatic Control, IEEE Transactions on*, vol. 45, no. 6, pp. 1098–1115, 2000.

[24] K. Glover, "Robust stabilization of linear multivariable systems: relations to approximation," *International journal of control*, vol. 43, no. 3, pp. 741–766, 1986.

[25] K. Havre and S. Skogestad, "Achievable performance of multivariable systems with unstable zeros and poles," *International Journal of Control*, vol. 74, no. 11, pp. 1131–1139, 2001.

[26] O. Aamo, G. Eikrem, H. Siahaan, and B. Foss, "Observer design for multiphase flow in vertical pipes with gas-lift—-theory and experiments," *Journal of process control*, vol. 15, no. 3, pp. 247–257, 2005.

[27] H. Berge and G. Halvorsen, "Downhole monitoring 'i&' acquisition," 2004.

[28] Z. A. Khan and B. K. Behera, "Solving the challenges of time, temperature and pressure," pp. 75–78, 2012.

[29] D. Simon, *Optimal state estimation: Kalman, H [infinity] and nonlinear approaches.* John Wiley and Sons, 2006.

[30] S. Julier and J. Uhlmann, "Unscented filtering and nonlinear estimation," *Proceedings of the IEEE*, vol. 92, no. 3, pp. 401–422, 2004.

[31] R. Kandepu, B. Foss, and L. Imsland, "Applying the unscented kalman filter for nonlinear state estimation," *Journal of Process Control*, vol. 18, no. 7-8, pp. 753–768, 2008.

[32] M. Hovd, *Lecture notes for the course advanced control of industrial processes.* Unpublished, Used in lecture at NTNU, TTK4210, November 2011., 2011.

[33] S. Julier, J. Uhlmann, and H. Durrant-Whyte, "A new method for the nonlinear transformation of means and covariances in filters and estimators," *Automatic Control, IEEE Transactions on*, vol. 45, no. 3, pp. 477–482, 2000.

[34] R. Van Der Merwe, *Sigma-point Kalman filters for probabilistic inference in dynamic state-space models*. PhD thesis, University of Stellenbosch, 2004.

[35] Q. Song and J. HAN, "An adaptive ukf algorithm for the state and parameter estimations of a mobile robot," *Acta Automatica Sinica*, vol. 34, no. 1, pp. 72–79, 2008.

[36] B. Foss, "Linear quadratic control, lecture notes for the course optimization and control ntnu 2010." 2010.

[37] MATLAB, *version 7.13.0.564 (R2011b)*. Natick, Massachusetts: The MathWorks Inc., 2011.

[38] M. Hovd and R. Bitmead, "Feedforward for stabilization," tech. rep., Technical report, Engineering Cybernetics Norwegian University of Science and Technology and Department of Mechanical and Aerospace Engineering of California San Diego, 2007.

Appendix A

Model Constants

A.0.1 Low-Order Model Constants

Table A.1: Constant Values in Model

Symbol	Description	Value	Unit
R	universal gas constant	8.314	[J/Kmol]
g	gravity	9.81	m/s^2
μ	viscosity	0.364e-03	Pa.s
ρ_L	liquid density	760	kg/m^3
M_G	gas molecular weight	0.0167	[kg/mol]
T_a	annulus temperature	348	K
V_a	annulus volume	64.34	m^3
L_a	annulus length	2048	m^3
P_{gs}	gas source pressure	140	bar
V_t	tubing volume	25.03	m^3
S_{bh}	cross-section below injection point	0.00314	m^2
L_{bh}	length below injection point	75	m
T_t	tubing temperature	369.4	K
GOR	mass gas oil ratio	0	fraction
P_{res}	reservoir pressure	160	bar
$\bar{w}_{res}$	average mass flow from reservoir	18	kg/s
r	tubing radius	0.067	m
r_b	bottom hole radius	0.0067	m
L_t	tubing length	2048	m
PI	productivity index	2.47e-6	kg/(s.Pa)
K_{gs}	gas-lift choke constant	9.98 × 10−5	-
K_a	injection valve constant	1.40 × 10−4	-
K_{pt}	production choke constant	2.90 × 10−3	-
ϵ	wall roughens tubing	3e-5	m
ϵ_b	wall roughens bottom hole	4.5e-5	m

Appendix B

OLGA Simulator Settings

The following setting are the output report generated by the OLGA flow simulator. It describes how the gas lift case is composed in detail. Everything from pipe and section lengths, to material used in the pipes and options for the simulator, as well as boundary conditions, is listed.

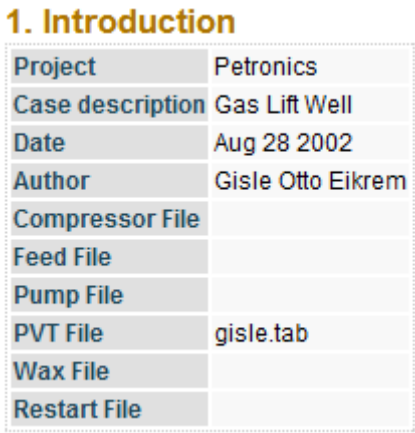

1. Introduction

Project	Petronics
Case description	Gas Lift Well
Date	Aug 28 2002
Author	Gisle Otto Eikrem
Compressor File	
Feed File	
Pump File	
PVT File	gisle.tab
Wax File	
Restart File	

Figure B.0.1: OLGA Setup Parameters Part 1

2. Simulation Options

Overall setting	Flow model	OLGA
	Mass eq scheme	1STORDER
	Compositional model	OFF
	Debug	OFF
	Drilling	OFF
	Phase	THREE
	Elastic walls	OFF
	Void in slug	SINTEF
	Steady state	ON
	User defined plug-in	OFF
	Temp. calc.	WALL
	Wax deposition	OFF
	Restart	OFF
Integration	Simulation starttime	0 h
	Simulation stoptime	10 h
	Minimum time step	0
	Maximum time step	1

Figure B.0.2: OLGA Setup Parameters Part 2

3. System Layout - Graphics

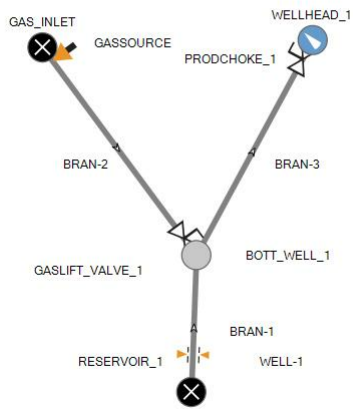

Figure B.0.3: OLGA Setup Parameters Part 3

4. System Layout - Table

4.1 Summary

4.1.1 Overall

No. of Branches	No. of Pipes	No. of Sections
3	9	130

4.1.2 Flows

Branches	No. of Pipes	No. of Sections	Min. Section Length	At	Max. Section Length	At
BRAN-1	1	2				
BRAN-2	5	28	5 M	PIPE_3	101.4 M	PIPE_2
BRAN-3	3	24	10 M	PIPE_1B	105.555555555556 M	PIPE_3

4.2 Layout

Pipe no.	Branch	Label	Diameter	Roughness	XEnd	YEND	Wall
1 - 1	BRAN-1	PIPE_1	0.2	4.5E-05	0	-2000	WELL
2 - 1	BRAN-2	PIPE_3	0.05 M	4.5E-05 M	50 M	48 M	STEEL-1
2 - 2	BRAN-2	PIPE_2	0.2 M	4.5E-05 M	50 M	-1980 M	STEEL-1
2 - 3	BRAN-2	PIPE_1B	0.2 M	4.5E-05 M	10 M	-1980 M	STEEL-1
2 - 4	BRAN-2	PIPE_1A	0.2 M	4.5E-05 M	10 M	-2000 M	STEEL-1
2 - 5	BRAN-2	PIPE_1	0.2 M	4.5E-05 M	0 M	-2000 M	STEEL-1
3 - 1	BRAN-3	PIPE_3	0.124 M	4.5E-05 M	0 M	-100 M	STEEL-1
3 - 2	BRAN-3	PIPE_2	0.124 M	4.5E-05 M	0 M	48 M	STEEL-1
3 - 3	BRAN-3	PIPE_1	0.124 M	3E-05 M	30 M	48 M	WELL

Figure B.0.4: OLGA Setup Parameters Part 4

5. Insulation and Walls

5. 1 Material

Label	Density	Conductivity	Heat Capacity	E-modulus
STEEL	7817	50 W/m-K	500	
SOIL_1	2500	2.3 W/m-K	1320	
SOIL_2	2500	0.2 W/m-K	1320	
NEOPRENE	1115	0.163 W/m-K	2009	
ASPHALT	2120	0.698 W/m-K	800	
L_CONCRETE	1900	1.2 W/m-K	880	
H_CONCRETE	3050	1.2 W/m-K	880	
INSULATION	200	0.04 W/m-K	670	
WATER	1000	0.592 W/m-K	4200	
CARCAS	3978	1000 W/m-K	460	
RILSAN	1040	0.33 W/m-K	2300	
ZETAWIRE	3978	0.93 W/m-K	460	
TAPE	780	1.16 W/m-K	1	
POLYETEN	940	0.41 W/m-K	2300	
COFOAM	540	0.07 W/m-K	1050	
TITAN	4540	20 W/m-K	520	
POLYCHLOROPRENE	1580	0.27 W/m-K	1070	
VIKOTHERM	1000	0.13 W/m-K	1500	

Figure B.0.5: OLGA Setup Parameters Part 5

5. 2 Walls

Label	Material	Wall thickness	Elastic
WELL	STEEL	0.0115	OFF
	WATER	0.02135	
	STEEL	0.012	
	H_CONCRETE	0.03332	
	SOIL_1	0.1	
	SOIL_1	0.2	
	SOIL_1	0.6	
	SOIL_2	1.5	
RISER_F6	CARCAS	0.0054	OFF
	RILSAN	0.0055	
	ZETAWIRE	0.014	
	RILSAN	0.003	
	POLYETEN	0.008	
	POLYETEN	0.006	
	COFOAM	0.0055	
	TAPE	0.00075	
	RILSAN	0.007	
TITAN-1	TITAN	0.021	OFF
	POLYCHLOROPRENE	0.008	
TITAN-2	TITAN	0.021	OFF
	POLYCHLOROPRENE	0.008	
	VIKOTHERM	0.016	
	POLYCHLOROPRENE	0.005	
STEEL-1	STEEL	0.021	OFF
	POLYCHLOROPRENE	0.008	
	VIKOTHERM	0.03	
	POLYCHLOROPRENE	0.005	

Figure B.0.6: OLGA Setup Parameters Part 6

6. Boundary Conditions

6. 1 Nodes

Label	Type	Pressure	Temperature	GMF
BOTT_WELL_1	INTERNAL			-1
GAS_INLET	CLOSED			-1
RESERVOIR_1	CLOSED			-1
WELLHEAD_1	PRESSURE	15 bara	50	-1

6. 2 Heattransfer

Branch	Pipe	Interpolation	Houteroption.	Hambient	Tambient
BRAN-1	PIPE_1	SECTIONWISE	HGIVEN	1000	108
BRAN-2	ALL	SECTIONWISE	HGIVEN	1000	108
BRAN-2	PIPE_2	SECTIONWISE	HGIVEN	1000	108
BRAN-2	PIPE_3	SECTIONWISE	HGIVEN	1000	5
BRAN-3	PIPE_3	SECTIONWISE	HGIVEN	1000	(108, 101, 94, 88, 81, 74, 67, 61, 54, 47, 40, 35, 30, 23, 17, 13, 9, 5)
BRAN-3	PIPE_2	SECTIONWISE	HGIVEN	1000	5
BRAN-3	PIPE_1	SECTIONWISE	HGIVEN	1000	5

6. 3 Sources

Label	Abs. Pos.	Branch	Pipe	Section	Massflow	Type	Time	Pressure	Temperature	GMF	Gas fraction eq	Oil fraction eq	water fraction eq
GASSOURCE		BRAN-2	PIPE_3	1	0.8	MASS	0	160 bara	60	1	1	1	1

6. 4 Wells

Label	Branch	Pipe	Section	GMF	Inj. option	Prod. option
WELL-1	BRAN-1	PIPE_1	1	-1	LINEAR	LINEAR

Figure B.0.7: OLGA Setup Parameters Part 7

7. Equipment

7. 1 Valves

Label	Branch	Pipe	Section	Diameter	Opening	CD
GASLIFT_VALVE_1	BRAN-2	PIPE_1B	4	0.025	1	0.84
PRODCHOKE_1	BRAN-3	PIPE_1	3	0.07	0.4	0.84

7. 2 Position

Label	Branch	Pipe	Section
WELL1	BRAN-1	PIPE_1	1
BRAN1	BRAN-1	PIPE_1	2
INJPOINT_TP	BRAN-1	PIPE_1	2
GASINJ1	BRAN-2	PIPE_2	1
BRAN2	BRAN-2	PIPE_2	11
GASINJ2	BRAN-2	PIPE_3	1
GC_UP	BRAN-2	PIPE_1B	4
GC_DOWN	BRAN-2	PIPE_1B	3
WELLHEAD1	BRAN-3	PIPE_1	3
BRAN3	BRAN-3	PIPE_3	11
PC_UP	BRAN-3	PIPE_1	3
PC_DOWN	BRAN-3	PIPE_1	2

Figure B.0.8: OLGA Setup Parameters Part 8

Appendix C

Calculated Controllability Bounds

SISO:

Resulting bounds for the single input single output (SISO) control schemes. The input, i.e., the manipulated variable, is the production valve at the top of the tubing.

Table C.1: Controllability Results SISO Systems

Measurement	Value	Dy	G(0)	Pole vector	|S|=|T|	|KS|	|SG|	|KSGd1|	|KSGd2|	|SGd1|	|SGd2|
$w_{G_a,in}$ [kg/s]	0.86	0.05	0.76	0.0004	1	3.04	0	0.23	1.987	0	0
P_{at} [bar]	81.16	1	5.22	0.0031	1	0.44	0	0.23	0.1	0	0
P_{tt} [bar]	20.89	1	5.72	0.0028	3.06	0.38	10.49	0.25	0.11	0.69	0.42
P_{ab} [bar]	90.35	1	5.81	0.0034	1	0.4	0	0.23	0.1	0	0
P_{bh} [bar]	88.56	1	6.95	0.0089	1	0.11	0	0.23	0.09	0	0
w_{out} [kg/s]	18.51	2	0.88	0.0024	1	0.49	0	0.3	0.11	0	0
$\rho_{mix,t}$ [kg/m^3]	186.96	20	1.61	0.0013	3.11	1.24	3.77	0.56	0.29	0.71	0.38
$\alpha_{L,tt}$ [frac]	0.23	0.23	0.17	0.0001	3.11	10.83	0.43	0.57	0.3	0.08	0.04

SIMO:

Resulting bounds for single input multiple output (SIMO) control schemes. The input, i.e., the manipulated variable, is the production valve at the top of the tubing.

Table C.2: Controllability Results SIMO systems

Measurement	Pole vector	|S|=|T|	|KS|	|SG|	|KSGd1|	|KSGd2|	|SGd1|	|SGd2|
P_{ab},w_{out}	0.0034	1	0.26	0	0.13	0.05	0	0
P_{ab}, $\rho_{mix,t}$	0.0034	1	0.36	0	0.2	0.08	0	0
P_{ab}, $w_{G_a,in}$	0.0034	1	0.4	0	0.12	0.1	0	0
P_{at}, P_{bh}	0.0089	1	0.11	0	0.12	0.05	0	0
P_{at}, P_{tt}	0.0031	1	0.26	0	0.12	0.05	0	0
P_{at}, $\rho_{mix,t}$	0.0031	1	0.39	0	0.2	0.08	0	0
P_{at}, $w_{G_a,in}$	0.0031	1	0.44	0	0.12	0.1	0	0
P_{at}, w_{out}	0.0031	1	0.27	0	0.13	0.05	0	0
P_{bh}, $\rho_{mix,t}$	0.0089	1	0.11	0	0.2	0.09	0	0
P_{bh}, $w_{G_a,in}$	0.0089	1	0.11	0	0.12	0.1	0	0
P_{bh}, w_{out}	0.0089	1	0.1	0	0.13	0.05	0	0
P_{tt}, P_{bh}	0.0089	1	0.1	0	0.12	0.05	0	0
P_{tt}, $\rho_{mix,t}$	0.0028	1	0.34	0	0.21	0.1	0	0
P_{tt}, $w_{G_a,in}$	0.0028	1	0.37	0	0.12	0.12	0	0
P_{tt}, w_{out}	0.0028	1	0.3	0	0.14	0.06	0	0
Q_{out}, $w_{G_a,in}$	0.0024	1	0.47	0	0.13	0.12	0	0

MIMO:

Resulting bounds for the Multiple Input Multiple Output (MIMO) control schemes The manipulated variables are the production valve at the top of the tubing and the gas choke at the top of the annulus.

Table C.3: Controllability Results MIMO systems

Measurement	Pole vector	|S|=|T|	|KS|	|SG|	|KSGd1|	|KSGd2|	|SGd1|	|SGd2|
P_{ab},w_{out}	0.0034	1.00	0.12	0.00	0.08	0.03	0.00	0.00
P_{ab}, $\rho_{mix,t}$	0.0034	1.50	0.14	2.00	0.11	0.05	0.34	0.12
P_{ab}, $w_{G_a,in}$	0.0034	1.00	0.16	0.00	0.09	0.07	0.00	0.00
P_{at}, P_{bh}	0.0089	1.00	0.07	0.00	0.08	0.03	0.00	0.00
P_{at}, P_{tt}	0.0031	1.59	0.13	11.00	0.08	0.03	0.96	0.62
P_{at}, $\rho_{mix,t}$	0.0031	1.00	0.13	0.00	0.08	0.03	0.00	0.00
P_{at}, $w_{G_a,in}$	0.0031	1.52	0.15	1.87	0.11	0.05	0.32	0.11
P_{at}, w_{out}	0.0031	1.00	0.18	0.00	0.09	0.07	0.00	0.00
P_{bh}, $\rho_{mix,t}$	0.0089	1.00	0.07	0.00	0.08	0.04	0.00	0.00
P_{bh}, $w_{G_a,in}$	0.0089	1.02	0.07	7.71	0.11	0.06	1.05	0.52
P_{bh}, w_{out}	0.0089	1.00	0.07	0.00	0.09	0.09	0.00	0.00
P_{tt}, P_{bh}	0.0089	1.20	0.07	16.73	0.08	0.04	1.04	1.04
P_{tt}, $\rho_{mix,t}$	0.0028	2.05	0.19	0.00	0.09	0.04	1.04	1.04
P_{tt}, $w_{G_a,in}$	0.0028	2.15	0.20	19.48	0.12	0.06	1.69	1.69
P_{tt}, w_{out}	0.0028	2.69	0.25	19.38	0.09	0.09	1.14	1.14
Q_{out}, $w_{G_a,in}$	0.0024	1.00	0.30	0.00	0.10	0.09	0.00	0.00

Appendix D

Matlab Implementation Codes

In this appendix some of the essential Matlab implementations codes used in this thesis are given.

D.0.2 The Low Order Gas Lift Model

```
function [x_dot,y] = v1_gaslift_model0(x,u,par)
%% **** States **********
x1=x(1);      %Gas mass in annulus
x2=x(2);      %Gas mass in riser
x3=x(3);      %Liquid mass in riser (whole system, tubing+BH)

%% ***** Inputs ******
u1=u(1);     %Valve opening top choke
u2=u(2);     %Valve opening of to injection choke
%% ****** Disturbances ******
GOR = u(3);        % Mass GOR from reservoir (d1) [-]
P_r = u(4)*1e5;    % Rservoir pressure (d2) [bar]
P_gs = u(5)*1e5;   % Gass source pressure (d3) [bar]
P0 = u(6)*1e5;     % Separator Pressure (d4) [bar]

%% Density of gas inside riser
%rho_G_r=x2/(par.V_r + par.L_bh*par.S_bh - x3/par.rho_L);
if (par.V_r - (x3-par.rho_L*par.L_bh*par.S_bh)/par.rho_L) >0
    rho_G_r=x2/(par.V_r - (x3-par.rho_L*par.L_bh*par.S_bh)/par.rho_L);
else
    rho_G_r=0;
end

%% ************* Average mixture density ***************
rho_mix=(x2+x3-par.rho_L*par.V_bh)/(par.L_r*pi*par.r_r^2);
rho_mix=max(rho_mix,0);
alpha_L_av = x3/(par.rho_L*(par.V_bh+par.V_r));
```

```
alpha_L_av=max(alpha_L_av,0);
%% Pressure riser top
P_r_t=rho_G_r*par.R*par.T_r/(par.M_G_r_t); P_r_t=max(P_r_t,0);
alpha_G_m_in = GOR/(GOR+1);
rho_G_r_in = (P_r - par.rho_L*par.g*par.L_bh)...
            *par.M_G_r_t/(par.R*par.T_r);
%% ********* Pressure at bottom of annulus *********************
P_a_t = (par.R*par.T_a*x1/(par.M_G_a*par.V_a));
P_a_b= P_a_t + (x1*par.g*par.L_a/par.V_a) ;

%% ********* Density of gas in the gas injection tank ************
rho_G_in= P_gs*par.M_G_a/(par.R*par.T_a);

%% ********** Injected gas into annulus *****************
%w_G_a_in = par.K_s*u2*sqrt(rho_G_in*max(P_gs-P_a_t,0));
w_G_a_in =u2;
%% ********** Density of gas in bottom of annulus **********
rho_G_a_b= P_a_b*par.M_G_a/(par.R*par.T_a);

%% ************  Calculating Friction of Riser **********
w_r_in_av = 14.6;
Usl_av=(1-alpha_G_m_in)*w_r_in_av/(par.rho_L*pi*(par.r_r^2));
Usl_av=max(Usl_av,0);
Usg_av= (alpha_G_m_in*w_r_in_av+w_G_a_in)/(rho_G_r*pi*(par.r_r^2));
Usg_av=max(Usg_av,0);
U_M_av=Usl_av+Usg_av;
Re=(2*rho_mix*U_M_av*par.r_r)/par.my; Re=max(Re,0);

%% Haaland Friction Factor
temp = -1.8*log10((par.ew/par.D_w/3.7)^1.11+6.9/Re);
lambda=(1/temp)^2;
F_riser=real(alpha_L_av*(lambda*rho_mix*(U_M_av^2)*...
                         (par.L_r+par.L_h))/(4*par.r_r));
F_riser=max(F_riser,0);

%% *********** Pressure at bottom of tubing *****************
P_r_b=P_r_t + (rho_mix*par.g*par.L_r) +F_riser;
if P_r_b<0 %Check for positive pressure in bottom of riser
   P_r_b=0;
end

%% *********  Injection gas flow rate from annulus to riser *********
if (P_a_b - P_r_b)>0 && rho_G_a_b>0
    w_G_a_out = par.K_a*sqrt(rho_G_a_b*(P_a_b - P_r_b));
else
    w_G_a_out = 0; %Gas mass flow out of annulus
end
```

```
%% Liquid velocity at bottom hole
Ul_b= w_r_in_av/(par.rho_L*pi*(par.r_r^2));
Ul_b=max(Ul_b,0);
%% Reynolds number at bottom-hole:
Re_b=(2*par.rho_L*Ul_b*par.r_r)/par.my;
Re_b=max(Re_b,0);
%% Friction factor at bottom-hole:
%lambda_b=0.0056+(0.5*(Re_b^(-0.32)));
%% Darcy Friction Factor
temp = -1.8*log10((par.ew/par.D_b/3.7)^1.11+6.9/Re_b);
lambda_b=(1/temp)^2;
%% Pressure loss due to friction from injection point to bottom-hole:
F_b=real((lambda_b*par.rho_L*(Ul_b^2)*(par.L_bh))/(4*par.r_r));
F_b=max(0,F_b);
%% Bottom-hole pressure
P_bh=P_r_b+par.rho_L*par.g*par.L_bh +F_b; P_bh=max(P_bh,0);

%% Liquid Inflow rate
if (P_r_b >= P_r)
    w_r_in=0;
else
    w_r_in=par.PI*(P_r-P_bh);
end
w_L_r_in = (1-alpha_G_m_in)*w_r_in; w_L_r_in=max(w_L_r_in,0);
w_G_r_in = alpha_G_m_in*w_r_in; w_G_r_in=max(w_G_r_in,0);
%% **********  Gas density in bottom of riser **************
rho_G_r_b=P_r_b*par.M_G_r_t/(par.R*par.T_r);
rho_G_r_b=max(rho_G_r_b,0);

%% Alpha liquid in
%alpha_G = x2/(x2+x3);

if ( ((w_G_a_out+w_G_r_in) >0)&&(w_L_r_in >0) )
    alpha_L_in= (w_L_r_in*rho_G_r_b)...
        /(w_L_r_in*rho_G_r_b+(w_G_a_out+w_G_r_in)*par.rho_L) ;
elseif (w_L_r_in >0)
    alpha_L_in=1;
else
    alpha_L_in=0;
end
alpha_L_in=max(alpha_L_in,0);
alpha_L_in=min(alpha_L_in,1);
%% ******** Liquid volume fraction top of riser **************
if ( (2*alpha_L_av - alpha_L_in )> 0 )
    alpha_L_t=2*alpha_L_av - alpha_L_in;
else
    alpha_L_t=0;
end
```

```
alpha_L_t=min(1,alpha_L_t);
alpha_L_t=max(0,alpha_L_t);
%% ***********  Density mixture top of riser *****************
rho_M_t= alpha_L_t*par.rho_L +(1-alpha_L_t)*rho_G_r;
rho_M_t=max(0,rho_M_t);
%% ********* Liquid mass fraction top of riser ***************
if ((alpha_L_t*par.rho_L +(1-alpha_L_t)*rho_G_r) > 0)
    alpha_L_m_t=(alpha_L_t*par.rho_L)...
        /(alpha_L_t*par.rho_L +(1-alpha_L_t)*rho_G_r);
else
    alpha_L_m_t=0;
end
alpha_L_m_t=min(1,alpha_L_m_t);
alpha_L_m_t=max(0,alpha_L_m_t);
alpha_G_m_t=1-alpha_L_m_t;

%% **********  Mixture flow out of riser ***************
if (P_r_t-P0)>0
    if(rho_M_t==0)
        w_mix_r_out=0;
    else
        w_mix_r_out=par.K_r*u1*sqrt(rho_M_t*(P_r_t-P0));
    end
else
    w_mix_r_out=0;
end
w_mix_r_out=max(0,w_mix_r_out);
%% Mass liquid flow rate out of riser
w_L_r_out=(1-alpha_G_m_t)*w_mix_r_out;
w_L_r_out=max(w_L_r_out,0);
w_L_r_out=min(w_L_r_out,w_mix_r_out);
%% Mass gas flow rate out of riser
w_G_r_out=alpha_G_m_t*w_mix_r_out;
w_G_r_out=max(0,w_G_r_out);

%% Derivatives
x1_dot = w_G_a_in - w_G_a_out;
x2_dot = (w_G_a_out+w_G_r_in) - w_G_r_out;
x3_dot = w_L_r_in - w_L_r_out;

%% Derivatives vector
x_dot=[x1_dot;x2_dot;x3_dot];

%% Measurements vector
y=[w_G_a_in;P_a_t;P_r_t;P_a_b;P_bh;w_mix_r_out;rho_M_t;alpha_L_t];

end
```

D.0.3 The Central Difference Method

```
function [A,B,C,D] = central_difference(x0,u0,par)
format long
dx_value = 1e-7;
du_value = 1e-7;

Ns=3; %Number of states
Nm=8; %Number of measurements
Nu=6; %Number of inputs

A = zeros(Ns,Ns);
B = zeros(Ns,Nu);
C = zeros(Nm,Ns);
D = zeros(Nm,Nu);

dx= zeros(Ns,1);
for i =1:Ns
    dx(i)=dx_value;
    x1 = x0 + dx;
    x2= x0 - dx;
    xdot1=v1_gaslift_model([],x1,u0,'derivatives',par);
    xdot2=v1_gaslift_model([],x2,u0,'derivatives',par);

    y1 = v1_gaslift_model([],x1,u0,'measurements',par);
    y2 = v1_gaslift_model([],x2,u0,'measurements',par);

    A(:,i) = (xdot1-xdot2)/(2*dx(i));
    C(:,i) = (y1-y2)/(2*dx(i));
    dx(i)=0;
end

du=zeros(Nu,1);
for i =1:Nu
    du(i)=du_value;
    u1 = u0 + du;
    u2= u0 - du;

    xdot1=v1_gaslift_model([],x0,u1,'derivatives',par);
    xdot2=v1_gaslift_model([],x0,u2,'derivatives',par);

    y1 = v1_gaslift_model([],x0,u1,'measurements',par);
    y2 = v1_gaslift_model([],x0,u2,'measurements',par);

    B(:,i) = (xdot1-xdot2)/(2*du(i));
    D(:,i) = (y1-y2)/(2*du(i));
    du(i)=0;
```

```
end
%Remove last column which is just transfer function from P0
%B(:,end)=[];
%D(:,end)=[];

end
```

D.0.4 The Unscented Kalman Filter

```
function [x_est y_est P] = augmented_UKF_weights(xh,ym,P,u,par)
% This version augments the sigmapoints with one extra point
% and uses different tunings parameters


%% Solver Options
M=eye(3);               % Mass Matrix for ODE-solver
dT=1;                   % Time for Inegration
T_span = [0 dT];        % Integrate from time=0 to dT
options=odeset('AbsTol',1e-10,'RelTol',1e-10,'MaxStep',100,'Mass',M);

%%
format('long')

%% Dimension Parameters
olga_sensors=[2 3];  % Availabe Measurements in OLGA model
matlab_sensors=[2 3]; % Available Measurements in Gaslift Model
%senors=[5];
Nx = length(xh);          % Number of States
Ns = (2*Nx) +1;              % Number of Sigma Points
Ny = length(olga_sensors);           % Number of Measured Measurements

%% Noise (uncertainty)
%V= 1e-4*eye(2);  % Measurement Noise tuning, no noise
V = 0.967798873798523*eye(2); %Tuning White Noise
a=1;
b=1;
c=1;
W=1e-5*[10 -a b; -a 10 -c; b -c 10];

%% Scaling Parameters
betta=2; % Tuning Parameter must be non-negavtive
alpha=1e-3;%1; % Tuning Parameter must be 0<=alpha<=1
kappa=0;%1; % Tuning Paramerer must be >=0
```

```
%%
lambda=(alpha^2)*(Nx+kappa) - Nx;
gamma=sqrt(Nx+lambda);

%% Weights
wm0 = lambda/(Nx+lambda);
wm = ones(2*Nx,1)*(1/(2*(Nx+lambda)));
wc = ones(2*Nx +1,1)*((lambda/(Nx+lambda)) + (1 -(alpha^2) +betta));
for i=2:1:length(wc)
    wc(i)=(1/(2*(Nx+lambda)));
end

%% Start UKF Algorithm

%% Calculate Sigma Points
[S0, valid] = chol(P);
if valid >0 % P is not positive definitt, can not use chol
    S=sqrt(abs(P));
else
    S=S0;
end


Xs=zeros(Nx,Ns);
for i=1:1:(Nx+1)
    if i==1
        Xs(:,i)= xh;
    else
        Xs(:,i)   = xh + gamma*S(i-1,:)';
        Xs(:,i+Nx) = xh - gamma*S(i-1,:)';
    end
end


%% Apply Constraints on sigma Points
%Xs=sigma_constrain(Xs);

%% Propegate Sigma Points through System
Xs_prop=zeros(Nx,Ns);
 for i=1:1:Ns
    [t,state]=ode15s(@v1_gaslift_model,T_span,...
                     Xs(:,i),options,u,'derivatives',par);
    state=state(end,:);
    Xs_prop(:,i) = state;
 end
%Xs_prop=sigma_constrain(Xs_prop);
```

```
%% Calculate apriori state estimate
 %X_ap=zeros(Nx,Ns);
 xh=zeros(Nx,1);
 for i=1:1:Ns
     if i==1
         xh = xh +wm0*Xs_prop(:,i);
     else
        xh = xh +wm(i-1)*Xs_prop(:,i);
     end
 end

%% Calculate the apriori covariance of states
P=zeros(Nx,Nx);
for i=1:1:Ns
    P= P + wc(i)*( (Xs_prop(:,i) -xh)*(Xs_prop(:,i) -xh)' );
end
P=P+W;
%% Get Measurements from Propegated sigmapoints

Ys=zeros(Ny,Ns);
for i=1:1:Ns
    y_full=v1_gaslift_model([],Xs_prop(:,i),u,'measurements',par);
    y=y_full(matlab_sensors);
    Ys(:,i)=y;
end

%% Calculate Means of Measurements
yh=zeros(Ny,1);
for i=1:1:Ns
    if i==1
        yh= yh +wm0*Ys(:,i);
    else
        yh= yh + wm(i-1)*Ys(:,i);
    end
end

%% Calculate the measurement Covariance

Py=zeros(Ny,Ny);
for i=1:1:Ns
    Py = Py + (wc(i)*( (Ys(:,i) -yh)*(Ys(:,i) -yh)' ));
end
Py=Py+V;
Py

%% Calculate the state measurement cross Covariance
Pxy=zeros(Nx,Ny);
for i=1:1:Ns
```

```
    Pxy= Pxy + wc(i)*((Xs_prop(:,i)-xh)*(Ys(:,i)-yh)');
end

%% Calculate Kalman Gain
K=Pxy/Py;

%% Update Covariance
P= P - K*Py*K';

%% Calculate Posteori Estmate
x_est= xh + K*(ym(olga_sensors) -yh);
y_est_full=v1_gaslift_model([],x_est,u,'measurements',par);
y_est=y_est_full;


end
```

Appendix E

Conference Paper

The following conference paper was submitted and accepted to the 2012 International Symposium on Advanced Control of Chemical Processes, (ADCHEM 2012), where it will be presented in Singapore in July 2012. The paper is based partly on results from my project assignment [1], partly from results in this master thesis, and finally on some independent work conducted by my co-supervisor Esmaeil Jahanshahi. The paper starts by introducing the new low-order model and compares it to the OLGA flow simulator. Following that, the controllability results of the low-order model are presented, and the results from the analysis are used to conclude on the controllable variables best suited for stabilizing control. The paper ends with a simulation study of some of the proposed control structures, where a robust H-infinity controller is applied for stabilizing the linearized version of the low-order model.

Control structure design for stabilizing unstable gas-lift oil wells

Esmaeil Jahanshahi, Sigurd Skogestad [1] and Henrik Hansen

Department of Chemical Engineering, Norwegian University of Science and technology, Trondheim, NO-7491 (e-mail: skoge@ntnu.no).

Abstract: Active control of the production choke valve is the recommended solution to prevent casing-heading instability in gas-lifted oil wells. Focus of this work is to find a simple yet robust control structure for stabilization of the system. In order to find suitable control variables, a controllability analysis of the system with different candidate control variables and two alternative manipulated variables was performed. Moreover, to include robustness and performance requirements at the same time, the controllability analysis was extended to a mixed sensitivity $\mathcal{H}_\infty$ optimization problem. A control structure using only the available top-side pressure measurements was found to be effective to stabilize this system.

Keywords: Oil production, two-phase flow, gas-lift, controllability, $\mathcal{H}_\infty$ control.

1. INTRODUCTION

Gas-lift is one of the processes which are used to artificially lift oil from wells where there is insufficient reservoir pressure to produce from the well. This method is also used for increasing the production rate of oil wells. In this process, gas is routed from the surface into the annulus and then injected deep into the tubing in order to be mixed with the fluid from the reservoir. This reduces the density of the column of fluid in the tubing and lightens it, Leads to a lower pressure at the bottom-hole. Hence the production rate from the low pressure reservoir is increased.

Gas-lifted oil wells often become unstable at their decline stages. The unstable operation is characterized by large oscillatory variations in the pressure and the production rate. There are several phenomena causing instability in gas-lifted oil wells; we focus on the "casing-heading" instability in this paper.

The oscillatory flow condition is undesirable and an effective solution is needed to prevent it. The conventional solutions include reducing the opening of the production choke valve and increasing the amount of the injected gas. However, closing the production choke increases the back pressure of the valve, and reduces the production rate from the oil well; also increasing the injected gas is costly.

Automatic control was first used by Jansen et al. (1999) to stabilize unstable gas-lifted oil wells. Measurements such as pressure, flow rate or fluid density are used as the control variables and the top-side choke valves are the manipulated variables. The bottom-hole pressure in well is the recommended control variable for anti-slug control of gas-lift wells, but this measurement is not available usually. Therefore, Eikrem et al. (2004) and Aamo et al. (2005) utilized model-based observers to estimate bottom-hole pressure from top-side measurements.

We look for other possibilities for anti-slug control of gas-lift oil wells. In this way, we examine all of possible measured variables of the system to find suitable control variables for stabilization. In addition, we consider the gas-lift choke valve as a secondary manipulated variable and we examine if using the second manipulated variable improves the control. Similar works on control structure design for stabilizing riser slugging has been done by Sivertsen et al. (2009), Storkaas and Skogestad (2007).

The controllability analysis is used as a tool to find control variables satisfying performance and robustness requirements. The controllability is evaluated by minimum achievable peaks of different closed-loop transfer functions. The control variables or combinations of them resulting in smaller peaks are preferred (Skogestad and Postlethwaite (2005)).

However, the controllability analysis is a mathematical tool for linear systems. Knowing that nature of the system and even the simplified model used in this work is highly nonlinear, the controllability analysis only gives insight into the necessary conditions and limitations.

For the controllability analysis and the model-based control design, a simple dynamical model of the system is preferred. First, a three-state model for casing-heading instability was developed in ABB AS, then Dvergsnes (1999) added two states for energy in annulus and tubing. Imsland (2002) ignored the two energy states, but he used more sophisticated pressure drop calculations. A simplified version of the Imsland model was used by Eikrem et al. (2004) which is the basis of the model presented in this paper. We add a pressure loss term due to friction, also we use a new approach by Jahanshahi and Skogestad (2011) for calculating phase fractions and density at top of the tubing.

This paper is organized as the following. A modified simplified model for the casing heading instability is introduced in Section 2. Afterwards, the theoretical background for the controllability analysis is given in Section 3, then controllability analysis results are presented in Section 4. In section 5, we choose suitable control structures, and finally the main conclusions and remarks will be summarized in Section 6.

[1] Corresponding author

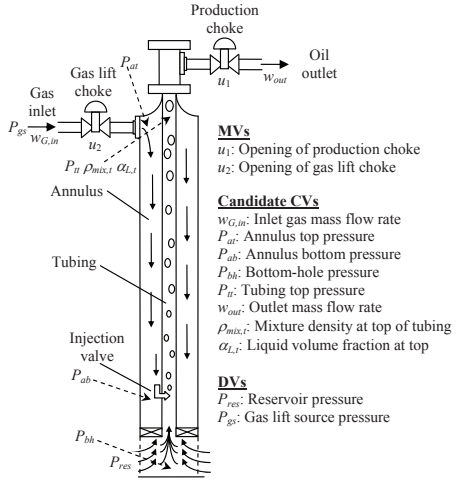

Fig. 1. Schematic presentation of candidate control variables and manipulated variables

2. SIMPLIFIED DYNAMICAL MODEL

A schematic illustration of gas-lift oil wells is shown in Fig. 1. Similar to the model introduced by Eikrem et al. (2004), state variables of our model are x_1 mass of gas in the annulus, x_2 mass of gas in the tubing and x_3 mass of liquid in the tubing. We consider also production of gas from the reservoir, therefore our state equations are in the following form:

$$\dot{x}_1 = w_{G,in} - w_{G,inj} \tag{1}$$

$$\dot{x}_2 = w_{G,inj} + w_{G,res} - w_{G,out} \tag{2}$$

$$\dot{x}_3 = w_{L,res} - w_{L,out} \tag{3}$$

In this model, $w_{G,in}$ is the mass flow rate of inlet gas to the annulus and $w_{G,inj}$ is the mass flow of injected gas from the annulus into the tubing. $w_{G,res}$ and $w_{L,res}$ are gas and liquid mass flow rates from the reservoir to the tubing. $w_{G,out}$ and $w_{L,out}$ are the mass flow rates of gas and oil outlet from the tubing, respectively.
There is only gas phase inside the annulus, and pressure at top of the annulus can be calculated by ideal gas law.

$$P_{at} = \frac{RT_a x_1}{M_G V_a} \tag{4}$$

Then, the pressure at bottom of the annulus is given by

$$P_{ab} = P_{at} + \frac{x_1 g L_a}{V_a}, \tag{5}$$

Thus, the density of the gas phase at this point is

$$\rho_{G,ab} = \frac{P_{ab} M_G}{RT_a}. \tag{6}$$

The inlet gas to the annulus comes from a source tank or a compressor with the pressure P_{gs}, and the density of gas through the gas-lift choke can be written as:

$$\rho_{G,in} = \frac{P_{gs} M_G}{RT_a} \tag{7}$$

Therefore, gas mass flow into the annulus is

$$w_{G,in} = K_{gs} u_2 \sqrt{\rho_{G,in} max(P_{gs} - P_{at}, 0)}. \tag{8}$$

Because of high pressure, the fluid from the reservoir is saturated (Ahmed (2006)). Hence, we assume that distance between the bottom-hole and the injection point, L_{bh}, is filled by liquid phase. This must be accounted for in calculating the volume of gas in the tubing. Consequently, the density of gas at top of the tubing follows as

$$\rho_{G,t} = \frac{x_2}{V_t + S_{bh} L_{bh} - x_3/\rho_L}. \tag{9}$$

Pressure at top of tubing using ideal gas law:

$$P_{tt} = \frac{\rho_{G,t} R T_t}{M_G} \tag{10}$$

Average mixture density inside tubing:

$$\overline{\rho}_{mix} = \frac{x_2 + x_3 - \rho_L S_{bh} L_{bh}}{V_t} \tag{11}$$

Average liquid volume fraction inside tubing:

$$\overline{\alpha}_L = \frac{x_3 - \rho_L S_{bh} L_{bh}}{V_t \rho_L} \tag{12}$$

GOR is the constant mass ratio of gas and liquid produced from the reservoir, and gas mass fraction at bottom of the tubing is

$$\alpha^m_{G,b} = GOR/(GOR + 1). \tag{13}$$

Before calculating the inlet mass flow rate from the reservoir by use of the bottom-hole pressure in equation (27), the pressure drop due to friction is needed to determine the bottom-hole pressure. However, we need to know the inlet flow rate to calculate the friction term. We evade this problem by using an average of the inlet flow rate, $\overline{w}_{res}$, in calculation of friction terms.
Average superficial velocity of liquid phase in tubing:

$$\overline{U}_{sl,t} = \frac{4(1 - \alpha^m_{G,b})\overline{w}_{res}}{\rho_L \pi D_t^2} \tag{14}$$

Average superficial velocity of gas phase:

$$\overline{U}_{sg,t} = \frac{4(w_{G,in} + \alpha^m_{G,b}\overline{w}_{res})}{\rho_{G,t} \pi D_t^2} \tag{15}$$

We have not calculated flow rate of the injected gas from the annulus into the tubing yet, instead we use $w_{G,in}$ in equation (15); we believe averages of these two variables are equal.
Average mixture velocity in tubing:

$$\overline{U}_{m,t} = \overline{U}_{sl,t} + \overline{U}_{sg,t} \tag{16}$$

Reynolds number of flow in tubing:

$$Re_t = \frac{\overline{\rho}_{mix} \overline{U}_{m,t} D_t}{\mu} \tag{17}$$

An explicit approximation of the implicit Colebrook-White equation proposed by Haaland (1983) is used as the friction factor in the tubing.

$$\frac{1}{\sqrt{\lambda_t}} = -1.8\log_{10}\left[\left(\frac{\epsilon/D_t}{3.7}\right)^{1.11} + \frac{6.9}{Re_t}\right] \tag{18}$$

Pressure loss due to friction in tubing:

$$F_t = \frac{\overline{\alpha}_L \lambda_t \overline{\rho}_{mix} \overline{U}_{m,t}^2 L_t}{2D_t} \tag{19}$$

Pressure at bottom of the tubing where gas being injected from annulus:

$$P_{tb} = P_{tt} + \overline{\rho}_{mix} g L_t + F_t \tag{20}$$

Mass flow rate of gas injected into tubing:

$$w_{G,inj} = K_{inj}\sqrt{\rho_{G,ab} max(P_{ab} - P_{tb}, 0)} \tag{21}$$

Liquid velocity at bottom-hole:

$$\overline{U}_{l,b} = \frac{\overline{w}_{res}}{\rho_L S_{bh}} \tag{22}$$

Reynolds number of flow at bottom-hole:

$$Re_b = \frac{\rho_L \overline{U}_{l,b} D_b}{\mu} \tag{23}$$

Friction factor at bottom-hole:

$$\frac{1}{\sqrt{\lambda_b}} = -1.8\log_{10}\left[\left(\frac{\epsilon/D_b}{3.7}\right)^{1.11} + \frac{6.9}{Re_b}\right] \tag{24}$$

Pressure loss due to friction from bottom-hole to injection point:

$$F_b = \frac{\lambda_b \rho_L \overline{U}_{l,b}^2 L_{bh}}{2D_b} \tag{25}$$

Pressure at bottom-hole:

$$P_{bh} = P_{tb} + F_b + \rho_L g L_{bh} \tag{26}$$

Mass flow rate from reservoir to tubing:

$$w_{res} = PI max(P_{res} - P_{bh}, 0) \tag{27}$$

Mass flow rate of liquid from reservoir to tubing:

$$w_{L,res} = (1 - \alpha_{G,b}^m) w_{res} \tag{28}$$

Mass flow rate of gas from reservoir to the well:

$$w_{G,res} = \alpha_{G,b}^m w_{res} \tag{29}$$

Density of gas at bottom of tubing:

$$\rho_{G,tb} = \frac{P_{tb} M_G}{R T_t} \tag{30}$$

Liquid volume fraction at bottom of tubing:

$$\alpha_{L,b} = \frac{w_{L,res}\rho_{G,tb}}{w_{L,res}\rho_{G,tb} + (w_{G,inj} + w_{G,res})\rho_L} \tag{31}$$

With the same assumptions used by Jahanshahi and Skogestad (2011), liquid volume fraction at top of the tubing can be written as

$$\alpha_{L,t} = 2\overline{\alpha}_L - \alpha_{L,b}, \tag{32}$$

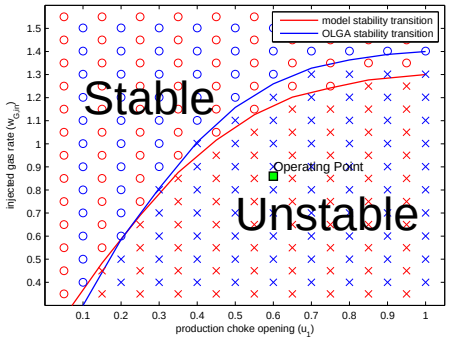

Fig. 2. Stability transition of system, blue markers for OLGA and red markers for simplified model

Then, the mixture density at top of the tubing will be

$$\rho_{mix,t} = \alpha_{L,t}\rho_L + (1 - \alpha_{L,t})\rho_{G,t}. \tag{33}$$

Mass flow rate of mixture from production choke:

$$w_{out} = K_{pr} u_1 \sqrt{\rho_{mix,t} max(P_{tt} - P_0, 0)} \tag{34}$$

Volumetric flow rate of production choke:

$$Q_{out} = w_{out}/\rho_{mix,t} \tag{35}$$

Gas mass fraction at top of tubing:

$$\alpha_{G,t}^m = \frac{(1 - \alpha_{L,t})\rho_{G,t}}{\alpha_{L,t}\rho_L + (1 - \alpha_{L,t})\rho_{G,t}} \tag{36}$$

Mass flow rate of outlet gas from tubing:

$$w_{G,out} = \alpha_{G,t}^m w_{out} \tag{37}$$

Mass flow rate of outlet liquid from tubing:

$$w_{L,out} = (1 - \alpha_{G,t}^m) w_{out} \tag{38}$$

The simplified model was fitted to a test case implemented in the OLGA simulator. Constants and parameters used in the model are given in Table 1. The stability map of the system is shown in Fig. 2 where stability transitions of the OLGA model and the simplified model are compared. The controllability analysis and all simulations are performed at the operating point $u_1 = 0.6$ and $w_{G,in} = 0.86$ $[kg/s]$ which is located in the unstable region of the stability map. It was not possible to add the gas-lift choke to the OLGA model, therefore we used a constant gas source equal to $w_{G,in} = 0.8$ $[kg/s]$ in the OLGA model and we fitted the model with the constant gas rate. Then, we added the gas-lift choke valve to the Matlab model so that the simplified model gives $w_{G,in} = 0.8$ $[kg/s]$ when the gas-lift choke opening is $u_2 = 0.4$ and the production choke opening is $u_1 = 0.3$. The system switches from stable to unstable at this operating point. Finally, we opened the production valve to $u_1 = 0.6$ in order to make the system unstable; the inlet gas rate becomes $w_{G,in} = 0.86$ $[kg/s]$ at this operating point.

3. CONTROLLABILITY ANALYSIS: THEORETICAL BACKGROUND

The state controllability is not considered in this work; instead the concept of input-output controllability as defined by Skogestad and Postlethwaite (2005) is used.

Definition 1. **(Input-output) controllability** *is the ability to achieve acceptable control performance; that is, to keep the outputs (y) within specified bounds or displacements from their references (r), in spite of unknown but bounded variations, such as disturbances (d) and plant changes (including uncertainty), using available inputs (u) and available measurements (y_m and d_m).*

The ability of the system to reach performance and robustness requirements with the control can be evaluated quantitatively by calculating minimum achievable peaks of different closed-loop transfer functions. These peaks are related to physical limitations of a the system in terms of controllability and they are dependent on the location of poles and zeros of the open-loop system.

3.1 Transfer functions

We assume a linear model in the form $y = G(s)u + G_d(s)d$ with a feedback controller $u = K(s)(r - y - n)$ in which d represents disturbances and n is the measurement noise. The resulting closed-loop system is

$$y = Tr + SG_d d - Tn, \tag{39}$$

where $S = (I + GK)^{-1}$ and $T = GK(I + GK)^{-1} = I - S$ represent the sensitivity and the complementary sensitivity transfer functions, respectively. The control input to the closed-loop system is

$$u = KS(r - G_d d - n). \tag{40}$$

In addition to the transfer functions introduced above, the transfer function SG is related to the effect of input disturbances on the control error $r - y$. The closed-loop transfer functions S, T, KS and SG can also be regarded as the measures of robustness against different types of uncertainty. We prefer to keep them as small as possible to achieve better robustness properties of the control system. For instance, the sensitivity transfer function S is also the sensitivity to inverse relative uncertainty, which is a good indication of uncertainty in the pole locations (Skogestad and Postlethwaite (2005)). Therefore, the lowest achievable peaks of the closed-loop transfer functions S, T, KS, SG, KSG_d and SG_d provide information regarding both achievable performance and possible robustness issues.

Table 1. Parameters values used in simulations

Symb.	Description	Values	Units
R	universal gas constant	8314	$J/(kmol.K)$
g	gravity	9.81	m/s^2
μ	viscosity	3.64×10^{-3}	$Pa.s$
ρ_L	liquid density	760	kg/m^3
M_G	gas molecular weight	16.7	gr
T_a	annulus temperature	348	K
V_a	annulus volume	64.34	m^3
L_a	annulus length	2048	m^3
P_{gs}	gas source pressure	140	bar
V_t	tubing volume	25.03	m^3
S_{bh}	cross-section below injection point	0.0314	m^2
L_{bh}	length below injection point	75	m
T_t	tubing temperature	369.4	K
GOR	mass gas oil ratio	0	–
P_{res}	reservoir pressure	160	bar
$\overline{w}_{res}$	average mass flow from reservoir	18	kg/s
D_t	tubing diameter	0.134	m
L_t	tubing length	2048	m
PI	productivity index	2.47e-6	$kg/(s.Pa)$
K_{gs}	gas-lift choke cons.	9.98×10^{-5}	–
K_{inj}	injection valve cons.	1.40×10^{-4}	–
K_{pr}	production choke cons.	2.90×10^{-3}	–

By the "peak" we mean maximum value of frequency response or $\mathcal{H}_\infty$ norm, $\|M\|_\infty = \max_\omega \|M(j\omega)\|$, that is simply the peak value of the transfer function. The bounds are not dependent on the controller K, and they are physical properties of the system itself. The bounds are, however, dependent on a systematic and correct scaling of the system. Scaling of the system will be explained later in this Section.

The lowest achievable peaks in sensitivity and complementary sensitivity transfer functions, denoted $M_{S,min}$ and $M_{T,min}$, are closely related to the distance between the unstable poles (p_i) and zeros (z_i). Considering SISO systems, for any unstable (RHP) zero z:

$$\|S\|_\infty \geq M_{S,min} = \prod_{i=1}^{N_p} \frac{|z + p_i|}{|z - p_i|}. \tag{41}$$

Note that the bound approaches infinity as z approaches p_i. For systems with only one unstable zero, the bound holds with equality.

Formulae for calculating bounds on minimum achievable peaks of the other closed-loop transfer functions are given by Skogestad and Postlethwaite (2005), also by Storkaas and Skogestad (2007).

3.2 Mixed Sensitivity Controllability Analysis

The above controllability measures were also considered by Sivertsen et al. (2009), Storkaas and Skogestad (2007). However, these measures considering only one of transfer functions at any time, may give conflicting results. To get a single measure (γ), we consider an $\mathcal{H}_\infty$ problem where we want to bound $\overline{\sigma}(S)$ for performance, $\overline{\sigma}(T)$ for robustness and to avoid sensitivity to noise and $\overline{\sigma}(KS)$ to penalize large inputs. These requirements may be combined into a stacked $\mathcal{H}_\infty$ problem (Skogestad and Postlethwaite (2005)).

$$\min_K \|N(K)\|_\infty, \quad N \triangleq \begin{bmatrix} W_u KS \\ W_T T \\ W_P S \end{bmatrix} \tag{42}$$

where W_P and W_T determine the desired shapes of sensitivity S and complementary sensitivity T. Typically, W_P^{-1} is chosen to be small at low frequencies to achieve good disturbance attenuation (i.e., performance), and W_T^{-1} is chosen to be small outside the control bandwidth, which helps to ensure good stability margin (i.e., robustness). Solution to this optimization problem is a stabilizing controller K corresponding to S, T and KS which satisfy the following loop shaping inequalities:

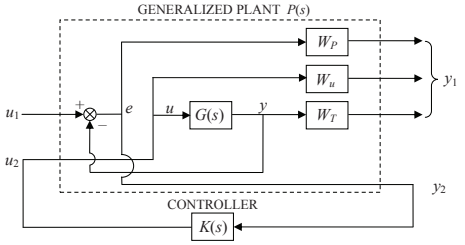

Fig. 3. Closed-loop transfer function for mixed sensitivity control design

$$\begin{aligned} \overline{\sigma}(KS(j\omega)) &\leq \gamma \underline{\sigma}(W_u^{-1}(j\omega)) \\ \overline{\sigma}(T(j\omega)) &\leq \gamma \underline{\sigma}(W_T^{-1}(j\omega)) \\ \overline{\sigma}(S(j\omega)) &\leq \gamma \underline{\sigma}(W_P^{-1}(j\omega)) \end{aligned} \tag{43}$$

To have the same cost function in all simulation tests for the measurement selection, all the candidate control variables shown in Fig. 1 are included in the y_1 port and the control variable(s) for test is in the port y_2 of the generalized plant in Fig. 3. The value of γ in equation (43) should be as small as possible for good controllability.

3.3 Scaling

One important step before controllability analysis is scaling of inputs, outputs and disturbances of the model. In *Definition 1*, the bound that the control variable must be kept within is not the same for different control variables shown in Fig. 1. For a correct comparison between candidate control variables, they must be scaled based on their maximum allowed variations, in a way that maximum allowed variation for all of them in the scaled model become (-1,1). The scaling factors D_y for different measurements are given in Table 2. Disturbances in the scaled model are also expected to vary in the range of $(-1, 1)$. The maximum expected value of the both disturbances (P_{res} and P_{gs}) is 3 *bar* variation around their nominal values. Therefore, the scaling matrix of the disturbances:

$$D_d = \begin{bmatrix} 3 & 0 \\ 0 & 3 \end{bmatrix}.$$

Controllability analysis is performed at the operating point $u_1 = 0.6$ and $u_2 = 0.4$. Valves can go to filly-open or fully-closed condition, therefore the maximum possible change for the both manipulated variables is 0.4, this means

$$D_u = \begin{bmatrix} 0.4 & 0 \\ 0 & 0.4 \end{bmatrix}.$$

4. CONTROLLABILITY ANALYSIS RESULTS

4.1 Bounds on Minimum Achievable Peaks

Minimum achievable peaks for different closed-loop transfer functions are given in Table 2 and Table 3. Minimum peaks of $|S| = |T|$ for P_{tt}, $\rho_{mix,t}$ and $\alpha_{L,t}$ in Table 2 are larger than 1, and it is expected to have difficulty using these measurements as control variables.
The reason for large values of $|S| = |T|$ is RHP-zeros in transfer functions. Location of RHP-poles of the system and RHP-zeros of P_{tt} for $u_2 = 0.4$ and different production choke openings u_1 are shown in Fig. 4. The system has a pair of complex conjugate poles on the imaginary axis for $u_1 = 0.3$. These two poles move to the RHP and the system becomes unstable for $u_1 > 0.3$; this is in agreement with the stability map in Fig. 2. P_{tt} shows two RHP-zeros for all u_1 values. One of the RHP-zeros does not move so much and it is always close to pole locations. As the production valve opening u_1 increases, RHP-poles get closer to the smaller (important) RHP-zero. According to equation (41), the closer poles and zeros are, the larger the peak of sensitivity transfer function becomes.

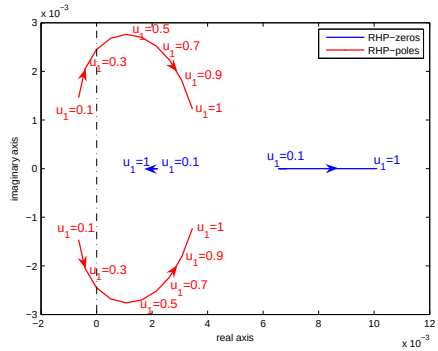

Fig. 4. Location of RHP-poles of system and RHP-zeros of tubing top pressure for $u_2 = 0.4$ and different values of u_1

The pressure at top of the tubing, P_{tt}, is not recommended to be used as a single control variable, but the large peak of sensitivity does not occur when it combines with other measurement. The minimum achievable peak of sensitivity transfer function for the paired measurements becomes 1 in Table 2, because the system becomes non-square and zeros disappear.
The bottom-hole pressure P_{bh} shows the best controllability properties. It has the largest element in the output pole vector that makes it suitable for stabilization of the unstable system. Moreover, P_{bh} has the largest steady-state gain $G(0)$ and the smallest values for all of the closed-loop transfer functions. In the second place, the pressure at the bottom of the annulus shows good controllability properties. The third good candidate is the pressure at top of the annulus, P_{at}.

4.2 Mixed Sensitivity Controllability Analysis

The γ values are given in Table 2 and Table 3. Control structures with small value of γ are able to reach performance, robustness and input requirements easier. The bottom-hole pressure shows the smallest γ among the single measurements; it is consistent with the other controllability data. Moreover, combination of the bottom-hole pressure and the tubing top pressure results in the smallest γ for the both single manipulated variable and the related MIMO case.
Using two control variables and one manipulated variable,

Table 2. Controllability data using u_1 as manipulated variable

Measurement	Value	D_y	$G(0)$	Pole vector	$\|S\| = \|T\|$	$\|KS\|$	$\|SG\|$	$\|KSG_{d1}\|$	$\|KSG_{d2}\|$	$\|SG_{d1}\|$	$\|SG_{d2}\|$	γ_1	γ_2
$w_{gin}[kg/s]$	0.86	0.05	0.76	0.0004	1.00	3.04	0.00	0.23	1.987	0.00	0.00	89.55	–
$P_{at}[bar]$	81.16	1	5.22	0.0031	1.00	0.44	0.00	0.23	0.10	0.00	0.00	14.85	–
$P_{tt}[bar]$	20.89	1	5.72	0.0028	3.06	0.38	10.49	0.25	0.11	0.69	0.42	19.16	–
$P_{ab}[bar]$	90.35	1	5.81	0.0034	1.00	0.40	0.00	0.23	0.10	0.00	0.00	13.54	–
$P_{bh}[bar]$	88.56	1	6.95	0.0089	1.00	0.11	0.00	0.23	0.09	0.00	0.00	3.60	–
$w_{out}[kg/s]$	18.51	2	0.88	0.0024	1.00	0.49	0.00	0.30	0.11	0.00	0.00	19.35	–
$\rho_{mix,t}[kg/m^3]$	186.96	20	1.61	0.0013	3.11	1.24	3.77	0.56	0.29	0.71	0.38	38.08	–
$\alpha_{L,t}[-]$	0.23	0.23	0.17	0.0001	3.11	10.83	0.43	0.57	0.30	0.08	0.04	289.88	–
P_{ab} w_{out}	–	–	–	0.0034	1.00	0.26	0.00	0.13	0.05	0.00	0.00	8.89	19.35
P_{ab} ρ_{mix}	–	–	–	0.0034	1.00	0.36	0.00	0.20	0.08	0.00	0.00	12.20	13.17
P_{ab} $w_{G,in}$	–	–	–	0.0034	1.00	0.40	0.00	0.12	0.10	0.00	0.00	13.42	22.13
P_{at} P_{bh}	–	–	–	0.0089	1.00	0.11	0.00	0.12	0.05	0.00	0.00	4.52	3.45
P_{at} P_{tt}	–	–	–	0.0031	1.00	0.26	0.00	0.12	0.05	0.00	0.00	8.65	11.58
P_{at} w_{out}	–	–	–	0.0031	1.00	0.27	0.00	0.13	0.05	0.00	0.00	9.17	19.35
P_{at} ρ_{mix}	–	–	–	0.0031	1.00	0.39	0.00	0.20	0.08	0.00	0.00	13.12	13.96
P_{at} $w_{G,in}$	–	–	–	0.0031	1.00	0.44	0.00	0.12	0.10	0.00	0.00	14.70	22.13
P_{bh} w_{out}	–	–	–	0.0089	1.00	0.10	0.00	0.13	0.05	0.00	0.00	3.39	19.35
P_{bh} ρ_{mix}	–	–	–	0.0089	1.00	0.11	0.00	0.20	0.09	0.00	0.00	3.53	10.96
P_{bh} $w_{G,in}$	–	–	–	0.0089	1.00	0.11	0.00	0.12	0.10	0.00	0.00	3.60	22.13
P_{tt} P_{bh}	–	–	–	0.0089	1.00	0.10	0.00	0.12	0.05	0.00	0.00	7.25	3.39
P_{tt} w_{out}	–	–	–	0.0028	1.00	0.30	0.00	0.14	0.06	0.00	0.00	15.41	19.35
P_{tt} ρ_{mix}	–	–	–	0.0028	1.00	0.34	0.00	0.21	0.10	0.00	0.00	16.97	12.23
P_{tt} $w_{G,in}$	–	–	–	0.0028	1.00	0.37	0.00	0.12	0.12	0.00	0.00	18.64	22.13
w_{out} $w_{G,in}$	–	–	–	0.0024	1.00	0.47	0.00	0.13	0.12	0.00	0.00	19.35	22.13

Table 3. Controllability data using u_1 and u_2 as manipulated variables (MIMO controller)

Measurement	Pole vector	$\|S\| = \|T\|$	$\|KS\|$	$\|SG\|$	$\|KSG_{d1}\|$	$\|KSG_{d2}\|$	$\|SG_{d1}\|$	$\|SG_{d2}\|$	γ_1	γ_2	γ_3
P_{ab} w_{out}	0.0034	1.00	0.12	0.00	0.08	0.03	0.00	0.00	7.55	13.20	15.31
P_{ab} $\rho_{mix,t}$	0.0034	1.50	0.14	2.00	0.11	0.05	0.34	0.12	10.39	12.16	16.53
P_{ab} $w_{G,in}$	0.0034	1.00	0.16	0.00	0.09	0.07	0.00	0.00	11.43	10.98	12.40
P_{at} P_{bh}	0.0089	1.00	0.07	0.00	0.08	0.03	0.00	0.00	3.94	3.20	14.47
P_{at} P_{tt}	0.0031	1.59	0.13	11.00	0.08	0.03	0.96	0.62	7.36	7.76	8.16
P_{at} w_{out}	0.0031	1.00	0.13	0.00	0.08	0.03	0.00	0.00	7.83	12.30	15.33
P_{at} $\rho_{mix,t}$	0.0031	1.52	0.15	1.87	0.11	0.05	0.32	0.11	11.23	12.89	16.74
P_{at} $w_{G,in}$	0.0031	1.00	0.18	0.00	0.09	0.07	0.00	0.00	12.59	12.20	13.63
P_{bh} w_{out}	0.0089	1.00	0.07	0.00	0.08	0.04	0.00	0.00	3.15	13.30	75.80
P_{bh} $\rho_{mix,t}$	0.0089	1.02	0.07	7.71	0.11	0.06	1.05	0.52	3.28	10.07	32.09
P_{bh} $w_{G,in}$	0.0089	1.00	0.07	0.00	0.09	0.09	0.00	0.00	3.35	3.20	3.58
P_{tt} P_{bh}	0.0089	1.20	0.07	16.73	0.08	0.04	1.04	0.64	5.19	3.15	5.22
P_{tt} w_{out}	0.0028	2.05	0.19	0.00	0.09	0.04	1.04	0.64	11.37	13.30	12.33
P_{tt} $\rho_{mix,t}$	0.0028	2.15	0.20	19.48	0.12	0.06	1.69	0.95	12.18	11.35	13.09
P_{tt} $w_{G,in}$	0.0028	2.69	0.25	19.38	0.09	0.09	1.14	1.09	14.15	8.78	16.56
w_{out} $w_{G,in}$	0.0024	1.00	0.30	0.00	0.10	0.09	0.00	0.00	13.30	11.32	21.55

it is impossible to get tight control on the both control variables at the same time. Similar to a cascade controller, we can have tight control with a constant set-point only on one of control variables.

In Table 2, we calculated γ_1 when tight control was required on the first control variable of the pair, and γ_2 when tight control was on the second one in the pair.

Uisng two manipulated variables, it was possible to have tight control on the both control variables in the pairs; γ_3 values in Table 3 were calculated for this condition. γ_1 and γ_2 in Table 3 can be compared to those in Table 2, but the cost function related to the $\mathcal{H}_\infty$ problem for calculating the γ_3 values is different.

5. CONTROL STRUCTURE SELECTION

Based on the controllability data provided in Table 2 and Table 3, we can decide about choosing the control structure. For a SISO control structure, pressure at bottomhole P_{bh} is the best control variables in our results. It is in accordance with previous works in which always P_{bh} has been favored. P_{bh} usually is not directly measurable, but as suggested by Eikrem et al. (2004) and Aamo et al. (2005), it can estimated using an observer. Simulation result of using this measurement is shown in Fig 5. Simulation results of using P_{tt} and P_{at} are shown in Fig 6 and Fig 7, respectively. The both P_{tt} and P_{at} demonstrate poor performance when they are used for SISO control. All of the simulations are based on scaled variables, and the ideal is to keep the control variables in the range of (-1,1).

Looking at paired control variables with u_1 as the manipulated variable in Table 2, all parings including P_{bh} with tight control on P_{bh} result in small γ values. However, there is no significant improvement in γ values compared to using the single control variable P_{bh}; simulation result of combing P_{bh} and w_{out} is shown in Fig. 8. The next suitable combination is the pair of P_{at} and P_{tt} (two top-side pressures) with tight control on P_{at}. The simulation result for this case is given in Fig. 9.

We did controllability analysis also by using u_2 as the

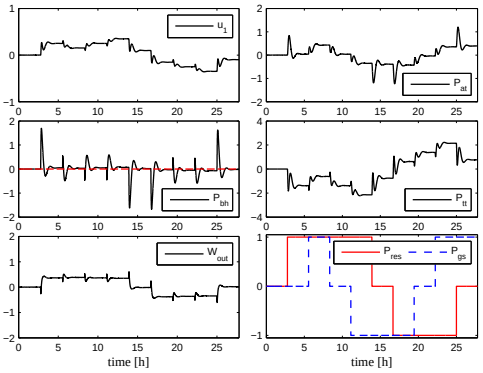

Fig. 5. Simulation result of $\mathcal{H}_\infty$ control using P_{bh} as control variable and u_1 as manipulated variable

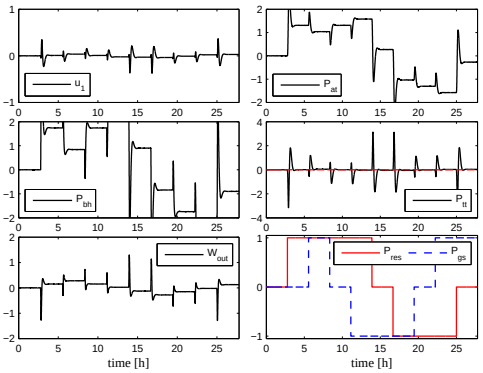

Fig. 6. Simulation result of $\mathcal{H}_\infty$ control using P_{tt} as control variable and u_1 as manipulated variable

single manipulating variable, but the results using u_2 were not satisfactory and we did not add another large table for sake of the space limitation. The simulation result using relatively the best pair of control variables for this case, resulted in $\gamma_2 = 14.1$, is shown in Fig. 10.

Looking at Table 3, the pairs with P_{bh} show small γ values, but compared to the γ values in Table 2, there is no substantial improvement. The simulation result of using the two top-side pressure measurement, P_{at} and P_{tt}, using two manipulated variables is shown in Fig. 11.

The pressures at top can be easily measured with good accuracy and a control structure using their combination (Fig. 9) is recommended. However, by comparing simulation results in Fig. 9 and Fig. 11, one should notice that adding the secondary manipulated variable does not enhance the control performance.

The choice of the suitable control structure is dependant on proper scaling of the control variables. For example for this case, first we chose a small scaling factor for the mass flow rate and we wanted to control it in a tight bound.

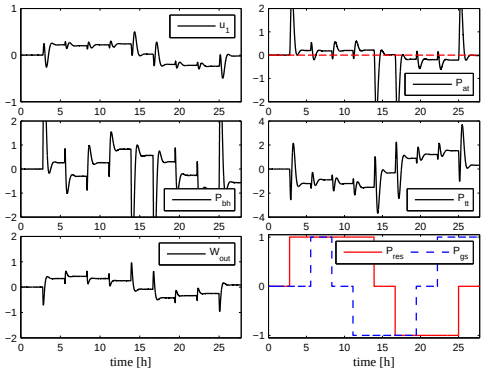

Fig. 7. Simulation result of $\mathcal{H}_\infty$ control using P_{at} as control variables and u_1 as manipulated variable

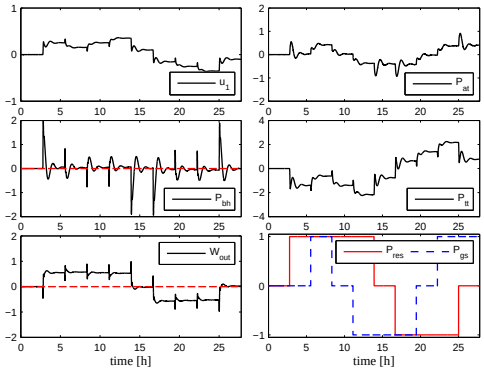

Fig. 8. Simulation result of $\mathcal{H}_\infty$ control using P_{bh} and w_{out} as control variables and u_1 as manipulated variable

As a result, gain of the system with this control variable increased and the control structures using the flow rate resulted in better performance compared to those using the pressures. In order to control the flow rate in a tight range, we must be able to measure it accurately. However, this is unlikely for two-phase flow in practice. Therefore, we chose a wider scaling factor for the flow rate. On the other hand, pressure can be measured more reliably, thus a small scaling factor was used for pressures. Consequently, the control structures using pressure measurements are shown to be superior for this case study.

6. CONCLUSION

An improved dynamical model for the casing-heading instability in gas-lifted oil wells was proposed, then the proposed model was fitted to a rigorous model in the OLGA simulator. Minimum achievable peaks of the different closed-loop transfer functions with each of the candidate control variables and their combinations were calculated.

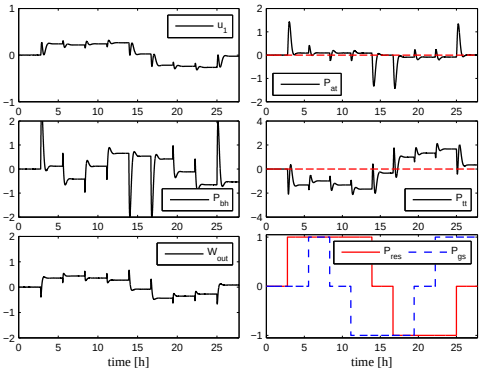

Fig. 9. Simulation result of $\mathcal{H}_\infty$ control for P_{at} and P_{tt} as control variables and u_1 as manipulated variable

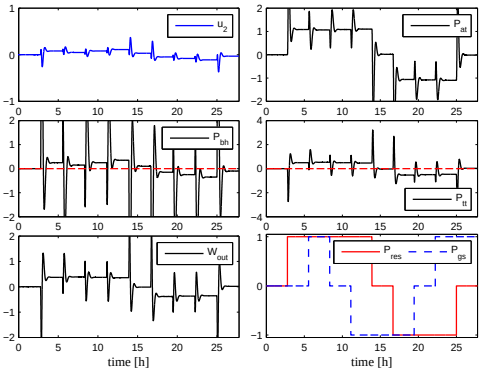

Fig. 10. Simulation result of $\mathcal{H}_\infty$ control using P_{bh} and P_{tt} as control variables and and u_2 as manipulated variable

Performance, robustness and input usage requirements were integrated in a mixed-sensitivity control problem and a single number (γ) was represented to evaluate quality of alternative control structures. We found out that adding the secondary manipulated variable does not improve stabilization of the gas-lifted oil wells significantly.

The bottom-hole pressure is the best control variable for this system in terms of controllability. Nevertheless, this variable often is not directly measurable.

Finally, a control structure using a pair of top-side pressure measurements was shown to be effective for preventing the casing-heading instability.

Further, it was found that accuracy of the sensors must be taken into account for scaling of different control variables correctly.

ACKNOWLEDGEMENTS

Financial support for this research was provided by Oil and Gas Division of SIEMENS.

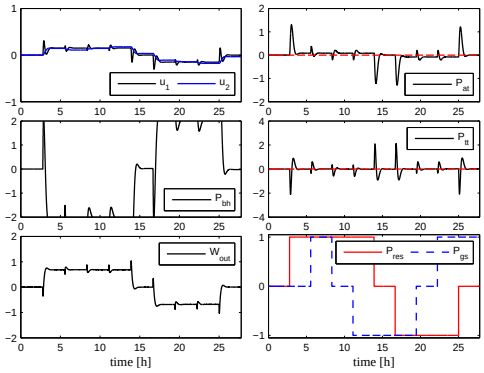

Fig. 11. Simulation result of $\mathcal{H}_\infty$ control for P_{at} and P_{tt} as control variables using MIMO controller

REFERENCES

Aamo, O., Eikrem, G., Siahaan, H., and Foss, B. (2005). Observer design for multiphase flow in vertical pipes with gas-lift - theory and experiments. *Journal of Process Control*, 15(3), 247 – 257.

Ahmed, T. (2006). *Reservoir Engineering Handbook, Third Edition*. Elsevier, Oxford, UK.

Dvergsnes, S. (1999). Modeling and control of gas-lifted oil wells. *Masters thesis. Department of Engineering Cybernetics, NTNU*.

Eikrem, G.O., Imsland, L., and Foss, B. (2004). Stabilization of gas lifted wells based on state estimation. In *IFAC International Symposium on Advanced Control of Chemical Processes*. Hong Kong, China.

Haaland, S.E. (1983). Simple and explicit formulas for the friction factor in turbulent pipe flow. *Journal of Fluids Engineering*, 105(1), 89–90. doi:10.1115/1.3240948.

Imsland, L. (2002). *Topics in Nonlinear Control - Output Feedback Stabilization and Control of Positive Systems*. Phd thesis, Norwegian University of Science and Technology.

Jahanshahi, E. and Skogestad, S. (2011). Simplified dynamical models for control of severe slugging in multiphase risers. In *18th IFAC World Congress*, 1634–1639. Milan, Italy.

Jansen, B., Dalsmo, M., Nøkleberg, L., Havre, K., Kristiansen, V., and Lemetayer, P. (1999). Automatic control of unstable gas lifted wells. In *SPE Annual Technical Conference and Exhibition*. Houston, Texas.

Sivertsen, H., Alstad, V., and Skogestad, S. (2009). Medium-scale experiments on stabilizing riser-slug flow. *SPE Projects, Facilities & Construction*, 4(4), 156–170, SPE no. 120040.

Skogestad, S. and Postlethwaite, I. (2005). *Multivariable Feedback Control: Analysis and Design*. Wiley & Sons, Chichester, West Sussex, UK.

Storkaas, E. and Skogestad, S. (2007). Controllability analysis of two-phase pipeline-riser systems at riser slugging conditions. *Control Engineering Practice*, 15(5), 567–581.